ON THE EVALUATION OF LOW VELOCITY FRICTION COMPENSATION METHODS IN ROBOTICS

by

John Douglas Betts Adams

B.Eng. (Electrical Engineering)
Ryerson Polytechnical Institute, 1992

A THESIS SUBMITTED IN PARTIAL FULFILLMENT
OF THE REQUIREMENTS FOR THE DEGREE OF
MASTER OF APPLIED SCIENCE
in the School
of
Engineering Science

SIMON FRASER UNIVERSITY
December 1996

ISBN 0-612-16768-2

APPROVAL

Name: John Douglas Betts Adams

Degree: Master of Applied Science

Title of thesis: On the Evaluation of Low Velocity Friction Compensation Methods in Robotics

Examining Committee: Dr. John Bird
Chair

Dr. Shahram Payandeh
Senior Supervisor

Dr. Kamal Gupta
Committee Member

Dr. Bill Gruver
Examiner

Date Approved: December 4, 1996

PARTIAL COPYRIGHT LICENSE

I hereby grant to Simon Fraser University the right to lend my thesis, project or extended essay (the title of which is shown below) to users of the Simon Fraser University Library, and to make partial or single copies only for such users or in response to a request from the library of any other university, or other educational institution, on its own behalf or for one of its usrs. I further agree that permission for multiple copying of this work for scholarly purposes may be granted by me or the Dean of Graduate Studies. It is understood that copying or publication of this work for financial gain shall not be allowed without my written permission.

Title of Thesis/Project/Extended Essay

"On the Evaluation Of Low Velocity Friction Compensation Methods in Robotics"

Author: _____
(signature)

_____
(name)

November 6, 1996
(date)

Abstract

Friction between surfaces sliding relative to each other at low velocities, possesses a high degree of uncertainty. These uncertainties are known to put an upper limit on the positioning accuracy that the mechanism is capable of. Many robotic tasks involve motion at these velocities, and so adequate compensation for friction at these velocities is necessary. Compensation must address the robotic joint mechanisms, as well as any tasks which involve the end effector in sliding contact with a surface.

Different methods of compensation of low velocity friction are studied. There have been many methods proposed in the literature. There seems lacking however, any form of a comparison of these methods with respect to each other. This thesis evaluates four methods of robot joint manipulation through position control. Two of the selected methods are designed specifically with the intent of compensating for friction at low velocities. The methods studied are intended for use with manipulators undergoing free motion.

The applicability of these methods when the end effector of the robot is in contact with a rigid surface during constrained motion is then investigated. This involved the upgrade of the manipulator from a 2 DOF planar type to a 4 DOF SCARA type assembly cell. The merits and demerits of each controller are explored and discussed throughout the investigation. Influences of various control parameters specific to individual control schemes are discussed. Both simulations and experiments are used in this investigation to explore the different characteristics.

Acknowledgments

The work contained herein is a result of not only my own efforts, but also of the assistance provided me by many others. I would like to extend my gratitude to the School of Engineering Science and the graduate secretary Bridgitte Rabold, who together have enabled a smooth and productive journey through the course of my Master's degree. I would also like to acknowledge the support received from the engineering support staff, during the upgrade of the robot manipulator. This project was also the result of many hours spent by the machinists in the science machine shop, whose talent and advice produced an attractive and highly functional two degrees of freedom mechanical subassembly, to be fitted onto the manipulator. Finally, I would like to extend my appreciation to my senior supervisor Dr. Shahram Payandeh, for his support and guidance throughout my tenure as a graduate student.

Contents

List of Figures

Glossary of Terms

Static Friction/Stiction The friction acting between two surfaces in contact, when there is no relative motion between them.

Viscous Friction The friction acting between two surfaces in contact and moving relative to each other when there is a lubricating medium present.

Stribeck Effect The rapid decrease in the friction between two contacting surfaces shortly after motion commences.

DOF **D**egrees **O**f **F**reedom. A number normally referring to the number of joints on a robot manipulator.

PD **P**roportional plus **D**erivative. A linear time invariant method of control.

PID **P**roportional plus **I**ntegral plus **D**erivative. A linear time invariant method of control.

Lyapunov's Direct Method A method for proving the stability for systems, generally used with nonlinear systems satisfying certain conditions.

Negative/Positive (Semi)Definite Function An indication of the range of values permissible by a function. The ranges are either positive or negative, which may then include or not include zero.

Asymptotic Stability A measure of a system's stability. The system is stable and tends towards its equilibrium as time increases.

Decrescent Decrescentness describes a function of more than one variable, which will remain bounded while one of its variables is unbounded.

Lipschitz Condition A condition describing a function which is smooth and has continuous derivatives.

Dini Derivative A method used to facilitate the calculus needed for Lyapunov functions, when a differential equation with a discontinuous right hand side occurs.

Constrained Motion Motion of a manipulator which is restricted along one or more of its degrees of freedom.

Hybrid Control A control system which performs both position and force control on a robot manipulator.

Preface

This thesis investigates the performance of control systems used for the purpose of low velocity friction compensation in robotics. Four controliers are selected; two nonlinear controllers and two linear control systems. Simulations and experimental methods are used to investigate the performance of the control systems. The controllers selected are intended for use with manipulators undergoing free motion. They are examined on a manipulator in free motion, then implemented when under constrained motion to see how well they perform in such a scenario.

The experimental work involved with the investigations includes the upgrade of a 2 DOF planar manipulator to a 4 DOF SCARA type assembly cell. This procedure is also presented in the thesis.

Chapter 1

Introduction

Any two materials in contact and moving relative to each other experiences the effects of friction. The characteristics friction displays varies depending on the relative velocities of the bodies in contact. It *is* known that there are various regimes of friction, depending on the relative velocity between the two rigid bodies. While it is widely believed that as the relative velocities of the bodies increase, there is a linear increase in the coefficient of friction, there is still no universally accepted description of what happens at velocities close to zero, commonly reffered to as the sticking regime. In this region, it is known that the behavior of friction is highly non-linear, and there are certain characteristics that have been established: bodies in contact which are at rest possess what is referred to as a *coefficient of static friction* (or *stiction*, or *coulomb friction*). This sticking force increases as the force at which the materials press against each other increases. Once motion commences, the coefficient of friction decreases rapidly to some lower bound, referred to as the *Stribeck effect*, after which it increases linearly with velocity. These characteristics are illustrated in figure 1.1. W is the mass of the object moving with velocity *vel* on top of the rough surface. There is a normal force N acting on the body due to its mass, which corresponds to a static friction value of f. When the velocity changes sign, there is a corresponding change in direction (sign) of static friction, and is commonly believed to be a discontinuity in the frictional relationship with velocity.

Robotic tasks often involve joints moving at low velocities. Applications which

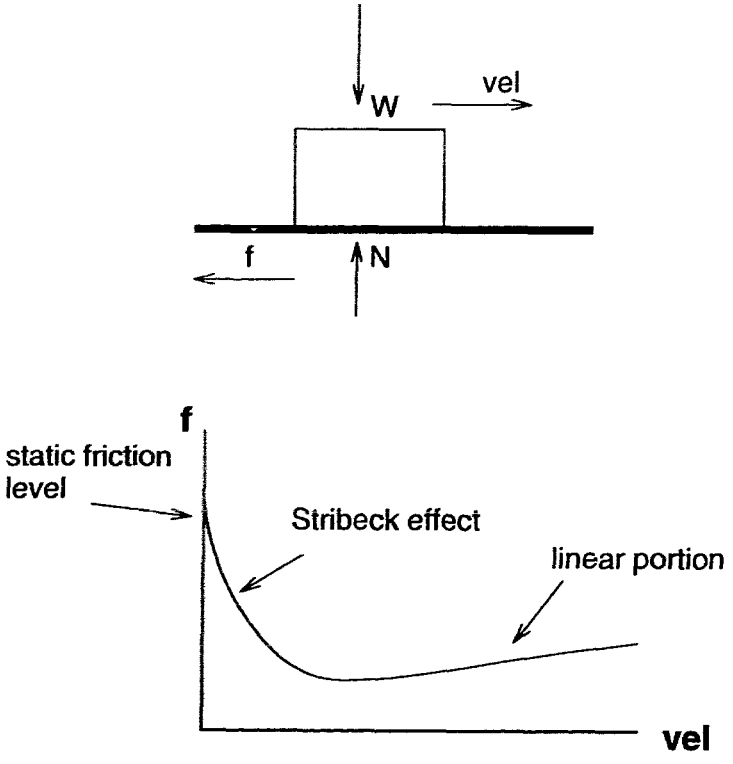

Figure 1.1: A general description of the frictional characteristics on the contacting surfaces of two bodies moving relative to each other.

involve micro-positioning, such as manufacturing and medical applications, have this requirement. It has been shown that improper compensation of joint stiction in robots can lead to anything from limit cycles, to instability . While much work has been invested in compensation methods and stiction modeling, little was found that include hardware implementation, and even less that provides a comparison of any of the proposed methods. Theoretical studies are important to provide a mathematical framework on the problem, as well as to give some prediction of a system's behavior. However a mathematical approach alone is unable to foresee all the problems that arise when a control system is implemented on an actual manipulator. There are many robotic tasks which involve motion while in contact with the environment (*constrained motion*), such as assembly operations. It was found that work done involving constrained motion either down-played or neglected friction, or made assumptions that would be impractical in practice.

The work undertaken in this thesis is an extension of previous work published by the author [1] [2]. It investigates the performance and applicability of various control schemes used for low velocity robotic applications. It then extends the results to investigate their effectiveness when a robot's end effector is in contact with a rigid surface. Each control scheme is simulated to verify expected theoretical performance measures. Thus their characteristics can be anticipated when implemented on an experimental platform. Each control scheme is then implemented experimentally on a 2 DOF manipulator for free motion, and then a 4 DOF manipulator for constrained motion. This serves to provide greater insight into the performance of these control systems when used with actual mechanisms, than theoretical analysis and simulations alone can reveal.

1.1 Literature Review

There are many processes and mechanisms which rely on the relative motion of contacting bodies at low velocities. In these situations, nonlinear frictional effects degrade their performance, and as such, effective compensation techniques must be devised. Most compensation techniques for nonlinear systems rely on some form of model of the

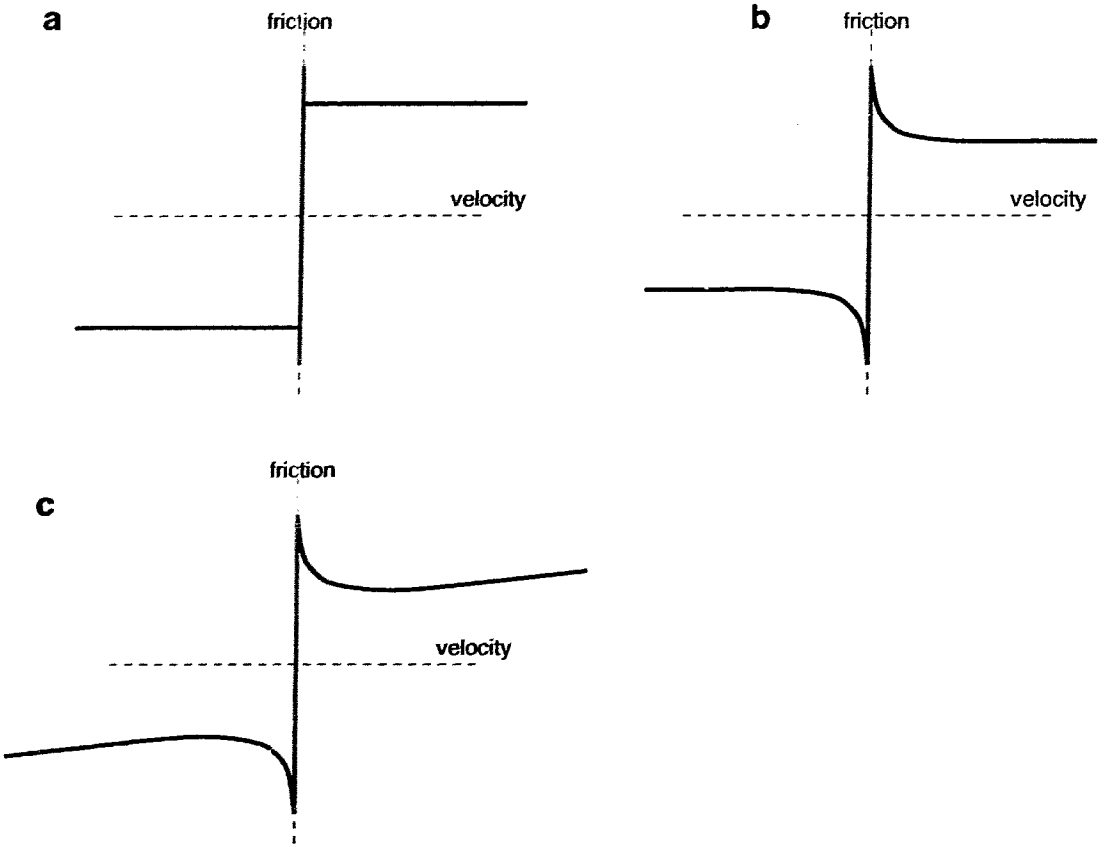

Figure 1.2: Some common friction models found in the literature

system. This has prompted many researchers to attempt to come up with a reliable model of friction at low velocities, or identify factors which affect it at these velocities. However, due to the complexity of friction models for individual mechanisms, researchers in robotics typically use an aggregate friction model for each robot joint. Some common friction models are presented in figure 1.2.

Before a friction model can be created, there has to be some theoretical groundwork on which to base the model. This work is more the concern of tribologists and physicists. A good starting point for the investigation of friction from a theoretical point can be found in Martins, Oden and Simoes [3]. A more mathematically detailed presentation is provided by Shaw [4], which reveals more subtle effects of nonlinear friction. Models found in controls literature are usually derived from experimental work done in the field of tribology. For instance the different factors that affect the friction between

two surfaces such as velocity, load, lubrication, e.t.c.. Control literature is found to be more focused on identifying these parameters for various applications, or predicting their behavior in such applications, for the purpose of devising control methodologies.

There is very little available literature in the area of experimental friction modeling. Armstrong [5] developed an experimental model based upon a geared brush type DC motor, where he was able to show the occurrence of the Stribeck effect at low velocities. Johnson and Lorenz [6] used Spacial Synchronous Averaging with DSP technology to experimentally identify nonlinear frictional parameters.

The adverse effects of the nonlinear friction characteristics in robotics have been presented in the robotics literature. For example, its effects on the machining process were examined by Chin and Chen [7]. Newman, Glosser, Miller, and Rohn [8] outlined the detrimental effects in space applications, where the absence of gravity causes disturbances in the acceleration due to the slipping motion, having adverse effects on a manipulators stability. Literature on the control of machines under the influence of low velocity friction is abundant. Both experimental works mentioned previously also propose methods for control. Cai and Song [9] use a nonlinear control system to compensate for low velocity friction, Southward, Radcliffe, and McCluer [10] also use nonlinear control. Tomizuka and Ciliz [11] use Neural Networks to identify and compensate for frictional uncertainties. Tung, Anwar, and Tomizuka [12] use repetitve control to teach a manipulator the control which eliminates errors caused by stiction. There has been only recently a comprehensive literature review on the subject, covering everything from tribological results to control methodologies and their significance; this was published by Armstrong-Helouvry, Dupont, and Canudas de Wit in 1995 [13].

1.2 Contribution

The work herein presents a realistic evaluation of some of the methods proposed in robotics and controls literature, for the compensation of low velocity friction in robotic mechanisms undergoing unconstrained motion. Experimentation on an actual manipulator will reveal subtleties that do not appear in theoretical analyses or simulations.

Implementation of each controller on the same hardware platform provides consistency in the conclusions that are drawn from the investigation. An attempt is made in each case, to explain any discrepancies between the claimed performance and the performance when implemented on hardware. This includes a full theoretical analysis of the control systems under investigation, which highlights assumptions made that do not apply well in reality. It thus provides one interested in using a control system in a mechanism with dry friction, a basis with which to make a decision on which would best be suitable.

In addition to the above analysis, the work is extended to see how well the control systems perform without the benefit of unconstrained motion. For this task the manipulator was upgraded from a 2 DOF planar manipulator to a 4 DOF SCARA type assembly cell. Although this was not the intent of the control systems presented in the literature, it was considered an interesting exercise as indeed, literature is scarce on low velocity friction compensation methods which incorporate the problem of constrained motion.

1.3 Thesis Layout

The outline of this thesis is as follows: chapter 2 investigates the use of selected controllers under unconstrained motion, when no contact with the environment is considered, hence only joint friction needs to be addressed. It first discusses the nature of the controllers under investigation, then proceeds through the theoretical framework of the various techniques, outlining stability proofs and expected performance measures. Simulations are then run to verify these results. These controllers are then implemented on a 2 DOF planar manipulator, where their actual performance is observed and compared to the theoretical analysis, as well as to each other's. The details of the upgrade from a 2 DOF planar manipulator to a 4 DOF SCARA assembly cell are then presented in chapter 3. Chapter 4 will study the implementation of these control systems when constrained motion is considered, with the 4 DOF system. The thesis will conclude with some discussions and ideas for future work on the topic, in chapter 5

Chapter 2

On Friction Compensation in Free Motion

The control methodologies under study will be investigated to see how well they perform when controlling the position of a manipulator undergoing unconstrained motion. This will incorporate a theoretical overview of the proposed methods including their stability, simulation of each control system to verify theoretical claims, and finally their performance on an actual manipulator. The chapter will conclude with a discussion of the results from the simulations and experiments.

For analytical purposes, a model of friction was chosen which incorporates static friction, viscous friction, and the Stribeck effect (figure 2.1). This model can be described for each joint as:

$$\tau_f = \tau_{slp}(\dot{q}) \cdot (\lambda(\dot{q})) + \tau_{stk}(\dot{q}) \cdot (1 - \lambda(\dot{q})) \tag{2.1}$$

where

$$\lambda(\dot{q}) = \begin{cases} 1 & \dot{q} > \alpha \\ 0 & \dot{q} \leq \alpha \end{cases}$$

τ_f is the joint friction. α is the zero bound assigned to the velocity to prevent instability with numeric simulation [14]. Any velocity within α is taken as zero. τ_{slp} is the function describing the friction at nonzero velocities, while τ_{stk} describes the friction when the velocity is zero (within α). $\dot{q}$ is the derivative of the joint angle.

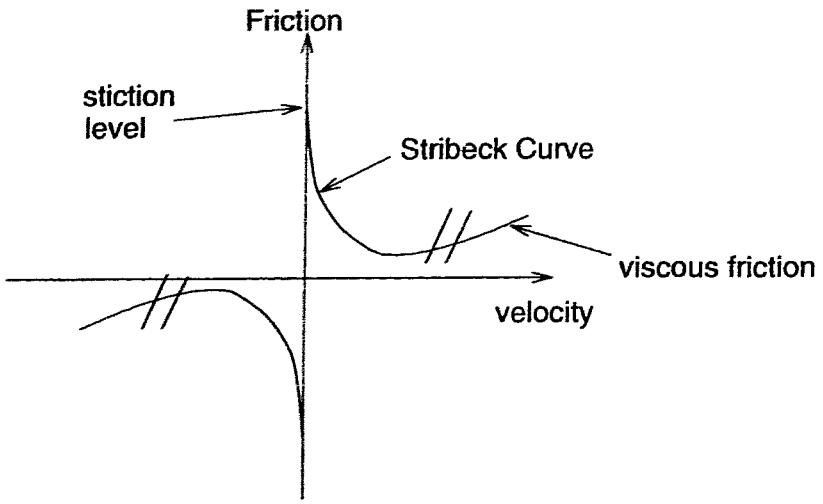

Figure 2.1: Friction model used for theoretical work and simulations

There are many models used to describe stiction and viscous friction. They will be described here mathematically using the model in [10] as:

$$\tau_{stk} = \begin{cases} \tau & \tau \leq \tau_{stk} \\ \tau_{stk} & \tau > \tau_{stk} \end{cases} \tag{2.2}$$

$$\tau_{slp} = sgn(\dot{q})(\tau_{stk} + [\tau_{slp_0} - \tau_{stk}][1 - \exp^{-a\dot{q}}]) + b\dot{q} \tag{2.3}$$

which is a nonlinear function, discontinuous at zero velocity, falling off exponentially to some lower bound τ_{slp_0}, then increasing linearly with nonzero velocity. b is the *damping coefficient*, the rate at which the viscous friction increases with respect to velocity. The signum function is modeled mathematically as:

$$sgn(\dot{q}) = \begin{cases} 1 & \dot{q} > 0 \\ 0 & \dot{q} = 0 \\ -1 & \dot{q} < 0 \end{cases}$$

2.1 System Description

For the purpose of simulations the dynamics of the experimental platform must be formulated mathematically. The experiments are to be conducted on a 2 DOF planar

manipulator, using only the distal link for motion. This in effect creates a 1 DOF system without gravitational effects. The use of the 1 DOF system as opposed to the complete system will facilitate an easier understanding of the results obtained from the simulations and experiments. The complete system equation for the 2 DOF manipulator are formulated as:

$$\mathbf{I(q)\ddot{q} + C(q,\dot{q})\dot{q} = \tau - \tau_f} \tag{2.4}$$

with $\mathbf{I(q)}$ being the system inertial matrix, and $\mathbf{C(q,\dot{q})}$ the vector of coriolis and centrifugal terms. where:

$$\mathbf{I(q)} = \begin{bmatrix} p_1 + 2p_3cos(q_2) & p_2 + p_3cos(q_2) \\ p_2 + p_3cos(q_2) & p_2 \end{bmatrix}; \qquad \mathbf{C(q,\dot{q})} = \begin{bmatrix} -\dot{q}(2\dot{q}_1 + \dot{q}_2)p_3sin(q_2) \\ \dot{q}_1^2 p_3 sin(q_2) \end{bmatrix}$$

$$\tau \in \Re^2 = \begin{bmatrix} \tau_1 \\ \tau_2 \end{bmatrix}$$

The terms p_1 to p_3 are constants defined by the dynamics of the system.

$$p_1 = I_1 + I_2 + I_3 + I_{3_c} + I_4 + L_1^2(M_3 + M_4) + M_2L_3^2 + M_4L_4^2$$

$$p_2 = I_3 + I_4 + M_4L_4^2$$

Appendix 2.4 describes and gives values for the various system inertias (I) and masses (M). q_1 and q_2 are the angular position of the proximal and distal joints respectively.

For the 1 DOF system, we assume q_1 and all its derivatives remain at zero reference. Thus the equation of motion can be written as:

$$p_2\ddot{q}_2 = \tau - \tau_f \tag{2.5}$$

where p_2 consists of the link link inertia and also the motor rotor inertia. For the rest of the paper, p_2 will be considered to be the inertia of the system and denoted I, τ_2 to be the applied torque τ, and q_2 as the joint variable q. We thus have a set of scalar equations which describe the dynamics of the system:

$$I\ddot{q} = \tau - \tau_f \tag{2.6}$$

τ_f is the disturbance due to friction, nonlinear in general.

2.2 Linear Methods

This section will outline two linear control methods used in robot motion control, and examine the effect that friction has on their performance. In general, The two methods, namely PD and PID offer ease of design and simplicity in tuning.

2.2.1 PD control

Proportional plus derivative is a linear time-invariant method of control in manipulators. It has also been shown to be globally asymptotically stable by Vidyasagar [15].

The main drawback of PD type control when the system dynamics include dry friction, is the existence of a steady state error throughout the trajectory. It is well known that increasing the proportional gain can reduce these errors, but the required accuracy may well be beyond the capacity of the actuators. Increasing proportional control also results in increased oscillatory behavior.

It has been shown by Hahn [16] using a mass-spring model, that the discontinuity associated with dry friction when proportional control is present, will cause multiple stable equilibrium points. These equilibrium points occur when trajectories at zero velocity, are within certain limits of the position error, and any trajectory within these limits at zero velocity will get stuck.

Consider a friction model that is modeled by the signum function $\tau_f = \alpha sgn(\dot{q})$, where $\dot{q}$ is the velocity of the 1 DOF system under test. Let q, K, M represent the position, proportional gain, and mass of the system, respectively. The equations of motion are:

$$\ddot{q} = \frac{-Kq}{M} - \frac{\alpha sgn(\dot{q})}{M}$$

The system will reach an equilibrium of $\dot{q} = \ddot{q} = 0$ at a position between $\frac{-\alpha}{K} \leq q \leq \frac{x+\alpha}{K}$.

For the system described in (2.6), the closed loop dynamics with a PD controller become:

$$\tau = -k_p(q) - k_d(\dot{q}) \tag{2.7}$$

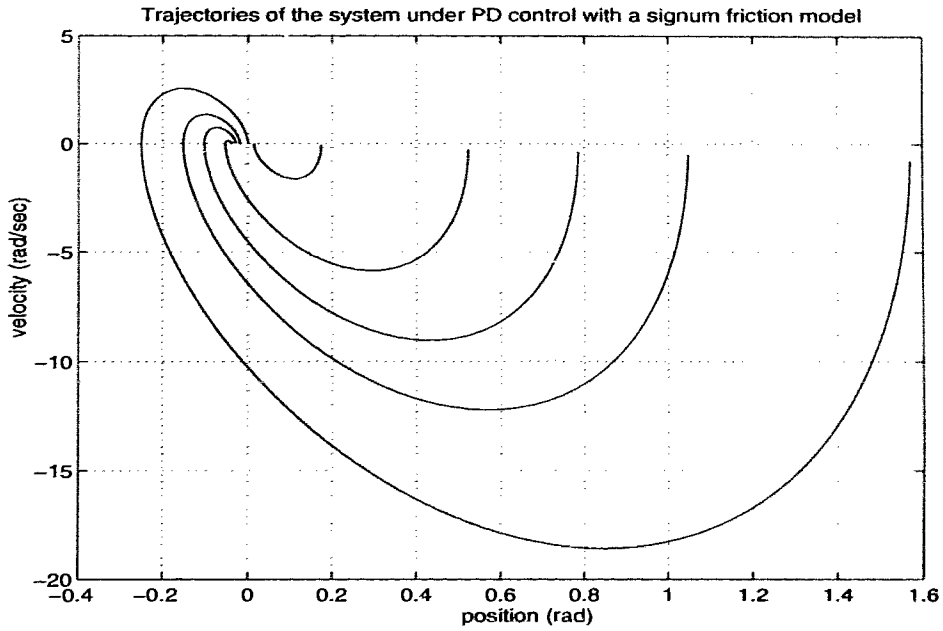

Figure 2.2: Simulations showing the multiple equilibria for a PD controlled system with static friction

$$\ddot{q} = -\frac{1}{I}(k_p(q) + k_d(\dot{q}) - \tau_f) \tag{2.8}$$

The system was simulated to show the existence of these equilibria. The friction model of equation (2.1) is used for this simulation. Figure 2.2 shows the convergence of the state trajectories q and $\dot{q}$ for the system with dry friction. For a given set of parameters, the reference point was set further and further away from the origin. The parameters used in this simulation were:

$$\begin{aligned} k_p &= 50 \\ k_d &= 4 \\ \tau_{stk} &= 2 \ Newtons \\ \tau_{slp_0} &= 1 \ Newtons \\ b &= 1 \ viscous \ friction \ damping \\ I &= 1 \ inertia \ of \ the \ distal \ link \end{aligned} \tag{2.9}$$

The termination of the trajectories was bounded within $\|0.04\|$, as specified in [16]

2.2.2 PID Control

PID control is another linear time-invariant method of control. The advantage of PID control is that it leaves no steady state error. Cancelation of the steady state error is due to the presence of integral control action.

The PID control law is defined as,

$$\tau = k_p(q) + k_d(\dot{q}) + k_i \int_{t_0}^{t} q \cdot dt \tag{2.10}$$

Substituting the PID control law into the system open loop dynamics (eq. (2.6)), the system dynamics become:

$$\ddot{q} = -\frac{1}{I}(k_p(q) + k_d(\dot{q}) + k_i \int_{t_0}^{t} q \cdot dt - \tau_f) \tag{2.11}$$

Integral action in a control law with dry friction present has been shown to be capable of producing limit cycles. A limit cycle is a periodic equilibrium point. They are characterized by trajectories circling the origin at a constant radius in the state-plane. Both describing function analysis [17] and the contraction mapping theorem [18], [19] have been used to show its existence.

A manipulator under PID control can be made unstable when the link of the manipulator comes under the effect of stiction and the control gains are too high. As time proceeds, the output of the integrator attempting to move the joint from its stuck configuration, becomes so high that the joint overshoots the origin and is brought to rest at a position further away from it than it originally was. This will cause larger integral action due to a larger setpoint error, and the effect cascades. This is demonstrated by taking the system described by (2.11) and simulating it with a large integral gain and initial conditions which place the system inside a sticking region.

Figure (2.3) shows trajectory behaviors and indicate the existence of limit cycles for the friction model described in eq.(2.1). Figure (2.3a) shows the trajectory for the default parameters of the friction model (eq.(2.9)). In Fig.(2.3b) the proportional gain is doubled. As expected the amplitude of the limit cycle decreases substantially. Fig.(2.3c) shows the trajectory when the integral gain is increased by a factor of 5; the

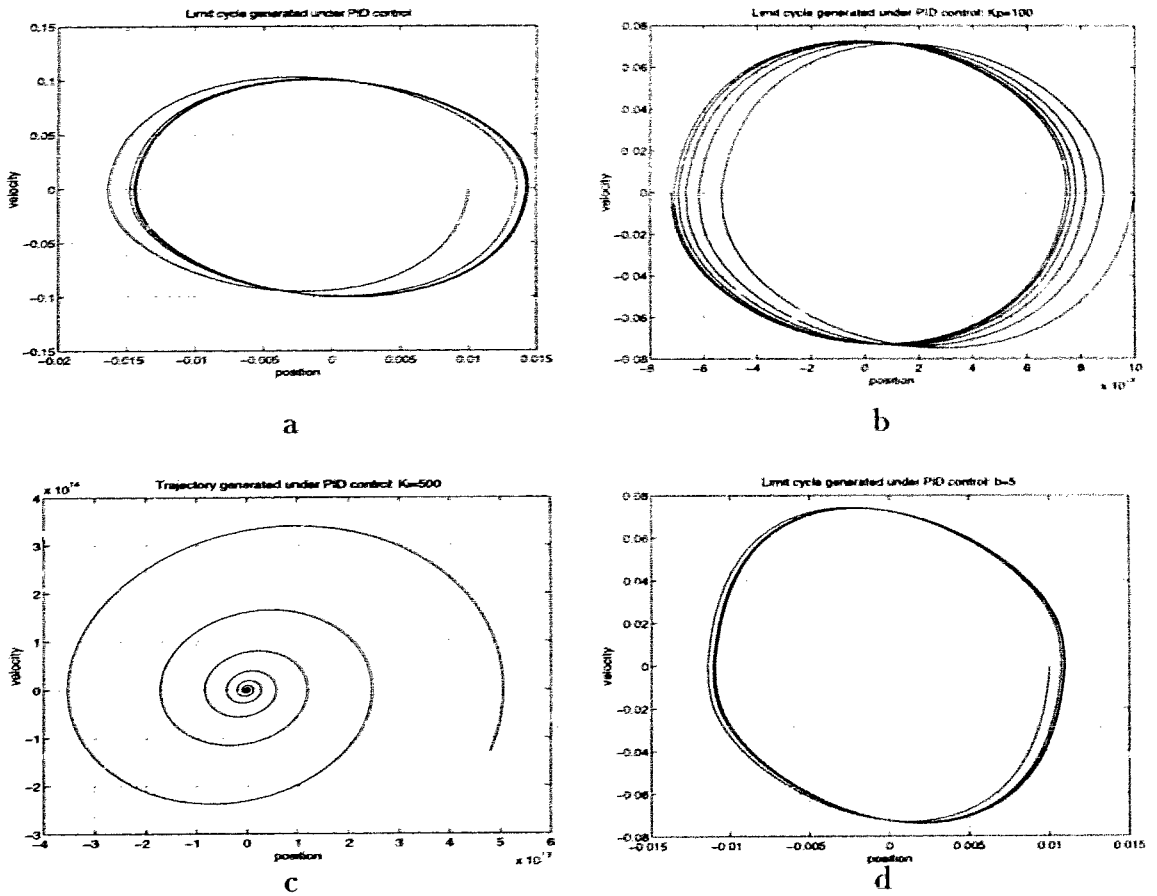

Figure 2.3: Simulation Results for PID controller: a) default gains, b) Kp = 100, c) Ki = 500, d) b = 5.

spiral is a source and extends outwards indicating an unstable system. The damping coefficient was then increased by a factory of 5 shown in Fig.(2.3d), the limit cycle amplitude remained constant as the system is dampened.

2.3 Nonlinear Methods

This section presents an analytical overview of two robust nonlinear controllers presented in the literature by Cai and Song [9] and Southward, Radcliffe, and McCluer [10]. Both controllers use a nonlinear compensation scheme to supplement a PD control law. The methods differ with respect to which the compensating controller is implemented. In Southward *et al* [10], a piecewise linear function is generated which is a function of the sticking limits similar to those shown by Hahn [16]. The other nonlinear compensator implements a *tanh ()* function which is continuous and twice differentiable. It should also be mentioned that each of these control systems is robust in the sense that one needs not know an exact value for the level of stiction in a mechanism, just

an upper limit.

Bounded stability of both controllers is demonstrated. Lyapunov's direct method is used in [9], whereas a modified version of Lyapunov's direct method employing the notion of the dini-derivative is used in [10] to account for the fact that the controller is *discontinuous* at the origin. In [9], La Salle's theorem is exploited to show asymptotic convergence of the solution trajectories, as well as error bounds within which the trajectories will converge. A mathematical treatment of these proofs are presented in appendix A.

In the sections to follow, an analytic overview of these methods will be presented, with proofs of their stability.

2.3.1 Smooth Continuous Nonlinear Compensation

The control law presented by Cai *et al* [9] uses a nonlinear part to supplement a PD controller. The additional control is a *tanh*() function of setpoint error. This forces an extra control torque to be output until the error is within the proximity of zero, the accuracy of which is controlled by a parameter in the *tanh*() function.

The proposed control law is defined as:

$$\tau = -k_p q - k_d \dot{q} - \tau_c(q) \tag{2.12}$$

$$q = \textit{position}$$

$$\tau_c(q) = \tau_{mstk} \tanh(\alpha q) \tag{2.13}$$

$$\tau_{mstk} = \tau_{stk} + \epsilon \tag{2.14}$$

$$\tau_{stk} = \textit{maximum stiction torque}$$

The maximum stiction torque can be experimentally determined. This is accomplished by increasing the output torque to an axis initially at rest, until motion is detected. The torque at which this occurs is then recorded. This maximum stiction torque is then supplemented by a small positive constant ϵ to guarantee the stiction levels are always exceeded. The constant α is used to adjust the slope of the *tanh*() function in the vicinity near zero error. A steeper slope corresponds to a smaller

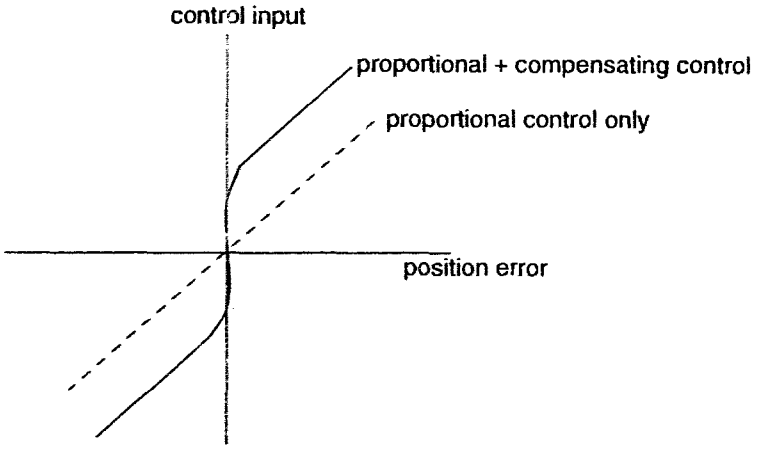

Figure 2.4: Smooth Continuous Nonlinear Controller

allowable steady state error. This in turn adjusts the steady state error achievable. This controller is illustrated in figure 2.4. The controller adds an extra compensating torque equal to the magnitude of τ_{mstk}, which always exceeds the magnitude of the sticking torque of the joint. This forces the trajectory to a unique equilibrium point closer to the origin.

Using the 1 DOF system equation (2.6), and control law described by (2.12), the closed loop system becomes:

$$I\ddot{q} = -k_d\dot{q} - k_p q - \tau_c(q) + \tau_f \tag{2.15}$$

The system (2.15), is globally asymptotically stable with the nonlinear term given by (2.13). To show this, the following Lyapunov function candidate is selected,

$$V = \frac{1}{2}I\dot{q}^2 + \frac{1}{2}k_p q^2 + \frac{\tau_{stk}}{\alpha}\ln(\frac{e^{\alpha q} + e^{-\alpha q}}{2}) \tag{2.16}$$

which is positive definite and satisfies a Lipschitz condition. Its derivative is negative semidefinite, and La Salle's Theorem [20] has been used to prove it's stability.

An integral part of La Salle's Theorem, the concept of the Invariant Set, has been used to reveal bounds that exist on the steady state error. It can be shown that the steady state error is bounded by

$$q \leq \frac{1}{2\alpha}\ln(1 + 2 \cdot \frac{\tau_{mstk}}{\alpha}) \tag{2.17}$$

The details leading up to each of these claims are set out in appendix A section A.1.

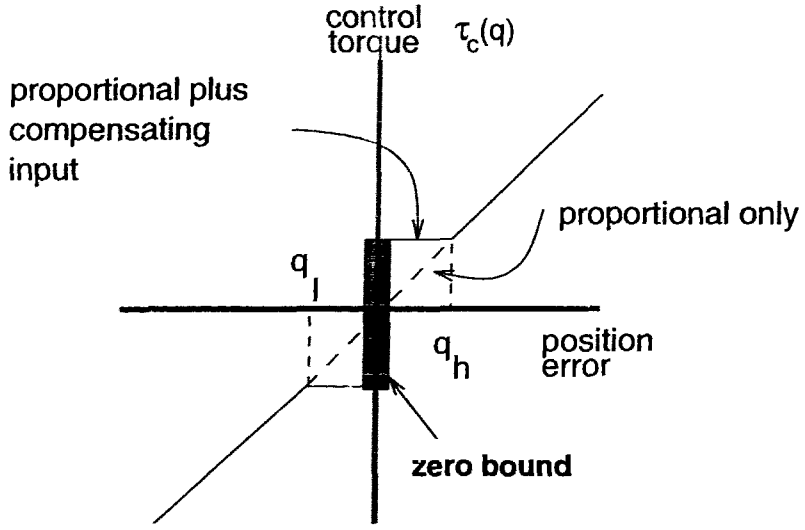

Figure 2.5: Discontinuous nonlinear controller

2.3.2 Discontinuous Compensation

This controller uses the sticking limits q_h and q_l given in in figure 2.5, to provide bounds within which extra compensating torque will be applied. Unlike the previous method, this compensating input is only applied when the position error is so small, the proportional gain due to this error is unable to overcome the forces of static friction, and sticking occurs (see figure 2.5). The added input ceases when the position error is zero. For numerical robustness, any error within a certain region around zero, was taken as zero [14]. This is depicted as the zero bound in figure 2.5.

The control law is defined as follows:

$$\tau = -k_p q - k_d \dot{q} - \tau_c(q) \tag{2.18}$$

$$\tau_c(q) = k_p q_c = \textit{compensating control}$$

$$q_c(q) = \begin{cases} 0 & q > q_h \\ (q_h - q) & 0 < q \leq q_h \\ 0 & q = 0 \\ (q_l - q) & q_l \leq q < 0 \\ 0 & q < q_l \end{cases} \tag{2.19}$$

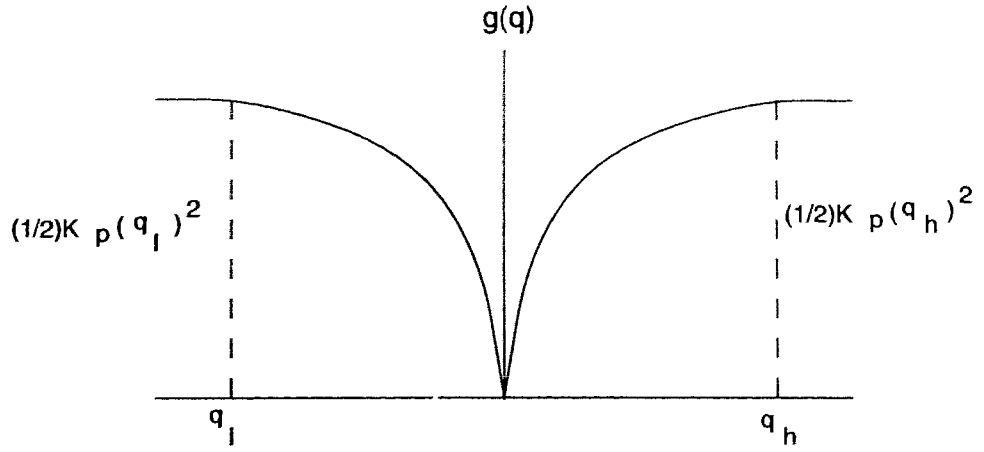

Figure 2.6: Nonlinear addendum for the discontinuous controller

Stability is proven using a modified version of Lyapunov's direct method involving the notion of the "Dini-Derivative" [21] [22], for the discontinuous trajectories in the controller. The energy function is similar to that used in the smooth continuous controller, except for the nonlinear addendum. The Lyapunov function candidate is formulated as follows:

$$V = \frac{1}{2}I\dot{q}^2 + \frac{1}{2}k_p q^2 + g(q) \tag{2.20}$$

where,

$$g(q) = \begin{cases} \frac{1}{2}k_p(q_h)^2 & q > q_h \\ k_p(q_h q - \frac{1}{2}q^2) & 0 \leq q \leq q_h \\ k_p(q_l q - \frac{1}{2}q^2) & q_l \leq q \leq 0 \\ \frac{1}{2}k_p(q_l)^2 & q < q_l \end{cases} \tag{2.21}$$

This nonlinear addendum is shown graphically in fig(2.6). The details of the proof are outlined in appendix A section A.2.

2.4 Experimental Setup for Experiments

Each controller discussed has been implemented on a planar 2DOF manipulator, with the base link held stationary while the elbow followed a trajectory.

The trajectory for the joint is a 90^o clockwise rotation following a smooth (inverted cosine curve) velocity profile. A smooth acceleration profile commencing at 0 (sine curve) was chosen so as not to cause extreme setpoint error at the start and end of motion. The entire trajectory has been parameterized as follows:

$$\begin{aligned} accn &= amax \cdot \sin(\frac{2\pi t}{T}) \\ vel &= -amax \cdot \frac{T}{2\pi} \cdot \cos(\frac{2\pi t}{T}) + amax \cdot \frac{T}{2\pi} \\ dist &= -amax \cdot (\frac{T}{2\pi})^2 \cdot \sin(\frac{2\pi t}{T}) + amax \cdot \frac{T}{2\pi} \cdot t \end{aligned}$$

To further parameterize this profile, the maximum velocity and rotation angle is specified as:

$$\begin{aligned} amax &= \frac{\pi \cdot vmax}{T} = \frac{2\pi \cdot dist}{T^2} \\ T &= \frac{2 \cdot dist}{vmax} \\ amax &= \frac{\pi \cdot vmax^2}{2 \cdot dist} \end{aligned}$$

where we have defined:

$accn$:	angular acceleration, $rad \cdot sec^{-2}$
vel :	angular velocity, $rad \cdot sec^{-1}$
$dist$:	radians to rotate,
$amax$:	maximum angular acceleration,
$vmax$:	maximum angular velocity.

The manipulator uses brushless DC motors that have high torque capabilities. The motor responsible for the distal joint has a maximum torque output capability of 39 N.m, and has a resolver that gives 153,600 counts per revolution. This is read by a quad decoder on a data acquisition card using a PC as the workstation. The control algorithm was executed at the manipulator's default sample rate of 1 msec. and is run on a DSP processor, to which the data acquisition board is connected.

The data sampled consists of link position, output torque, and commanded position, from which are calculated the actual velocity, commanded velocity, and positioning error.

The stiction level of the joint was found experimentally by applying a linearly increasing torque to the joint motor untill motion is detected. This was found to be around 2N, and ϵ used for the smooth nonlinear controller (eq.(2.14)) is taken as 0.5 N.m. With this data, the experiment was conducted implementing each of the controllers.

The dynamic parameters of the 2 DOF manipulator are as follows,

I_1 = base motor rotor inertia = 0.267 $Kg.m^2$
I_2 = base link inertia = 0.334 $Kg.m^2$
I_3 = elbow motor rotor inertia = 0.0075 $Kg.m^2$
I_{3_c} = elbow motor stator inertia = 0.04 $Kg.m^2$
I_4 = elbow link inertia = 0.063 $Kg.m^2$
M_1 = Base motor mass = 73 Kg
M_2 = Base link mass = 9.78 Kg
M_3 = Elbow motor mass = 14 Kg
M_4 = Elbow link mass = 4.45 Kg
L_1 = length of link 1 = 0.359 m
L_2 = length of link 2 = 0.24 m
L_3 = Distance of COG of link 1 from axis of rotation = 0.136 m
L_4 = Distance of COG of link 2 from axis of rotation = 0.102 m

2.5 Results and Discussion

In comparison with the PD controller (Fig.2.7 - 2.10), it is apparent that both nonlinear controllers (Fig. 2.15 - 2.18), and the PID scheme (Fig. 2.11-2.14) offer superior performance.

As demonstrated in the experiments, the amplitudes of the limit cycles associated with the PID controller are far less than the steady state error level of a PD controller even when the proportional gain is increased (compare figures 2.10 and 2.12).

The velocity lag at the beginning of motion is seen with the PD and PID controllers (Fig. (2.7), (2.9), and (2.13)). This is due to the inherent stiction level. Before any

motion can commence, both the integral and proportional gains must be large enough to counteract this effect. The rate of increase of the integral control being proportional to time and position error, and that of the proportional control increasing only with position error.

The nonlinear controllers however don't exhibit this lag (Fig. (2.17) and (2.15)), and also offer better tracking performance. This is due to the nature of the nonlinear compensators. There is no latency period for the gains to build up to a level large enough to counteract the stiction; once the error is small enough, the additive compensation is activated and there is enough torque to overcome stiction. Once this initial lag is finished however, the tracking performance of PID controller is not much inferior to the two nonlinear controllers.

The drawback of the nonlinear controllers is with their oscillatory response and their jerky torque profiles. The oscillations exhibited by the nonlinear controllers appear to be more than just the oscillation of a link in motion, as it appears to be with the linear controllers . In effect, these nonlinear controllers are simply error dependent high proportional gain controllers; as a result, whenever more control input is needed the proportional gain increases and so does the oscillations and erratic torque outputs. There is no additional damping added in either of the nonlinear terms. A look at the torque profile for the smooth continuous controller in fig. (2.18) shows this. This controller adds extra stiction compensating torque at all points on the trajectory, not just when needed, as a result the effective proportional gain of the smooth nonlinear controller is always higher than that of the discontinuous one and the linear controllers. To illustrate this, only the proportional term of each of the control methods are superimposed and shown in figure (2.19).

A comparison between Fig's. (2.17) and (2.15) will show that the discontinuous controller has afr fewer oscillations at the end of its trajectory than does the controller in other nonlinear controller. The oscillations at the beginning of motion are due to the fact that when the nonlinear compensation of both controllers is dominant, which is due to a small setpoint error and stiction being in effect, there is a proportional control that acts with relatively little damping. The inertia of the moving link towards the end its trajectory keeps the link in motion. Stiction is therefore not a factor

and so the nonlinear additive is unnecessary. The smooth controller however, has a high proportional gain approaching the end of the trajectory, which may lead to an underdamped oscillatory response. On the other hand, the discontinuous controller has a normal PD gain approaching the reference point and so tends not to excite the system as much.

Equation (2.17) of section (2.3.1) sets a theoretical bound within which the setpoint error of the smooth continuous controller should lie. A value of 10^8 was used for α in the experiments. Reference to 2.17 reveals that the setpoint errors do not lie within the bounds predicted theoretically. The derivation of this bound is outlined in Appendix A section (A.1). This was done using conditions of the invariant set that show this controller to be stable. The time constant of the theoretical system is much too large to be realized by any real system implementing setpoint control, i.e. a new setpoint will be generated long before the convergence time of the theoretical system; thus this error bound is not readily achievable in practice.

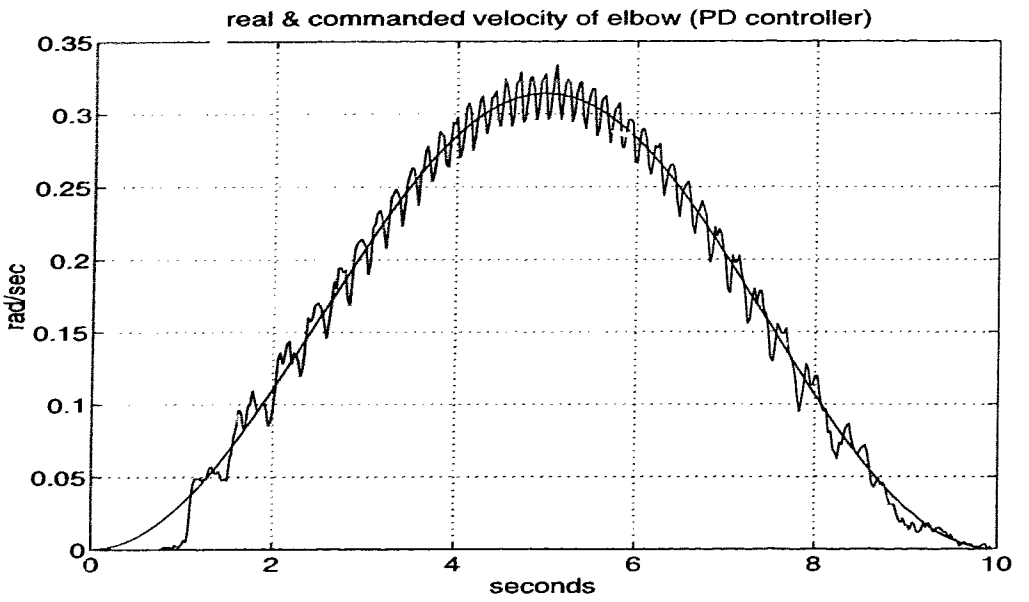

B: Velocity profile

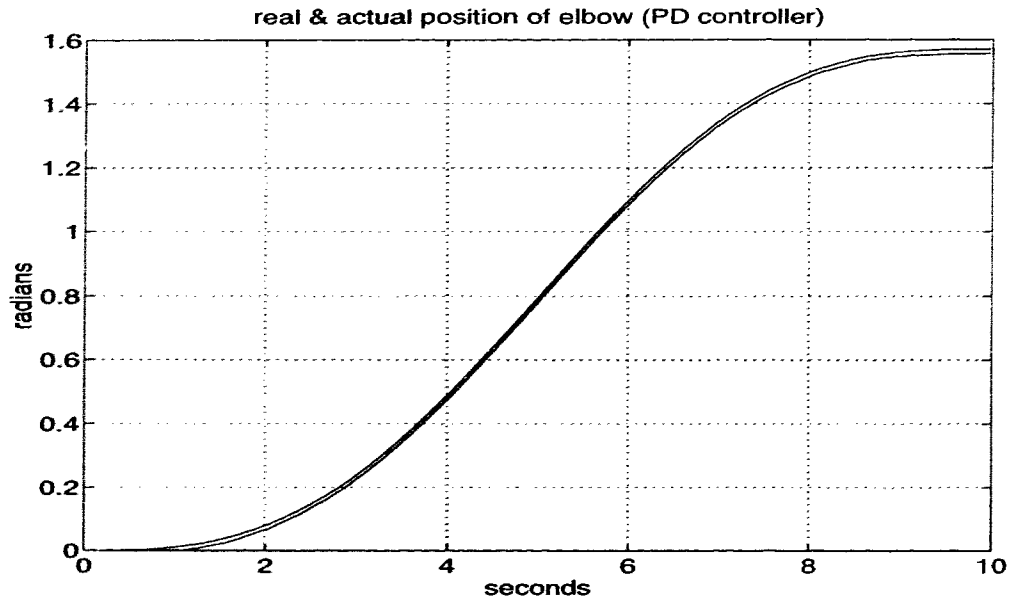

A: Position tracking

Figure 2.7: Experimental Results for PD controller

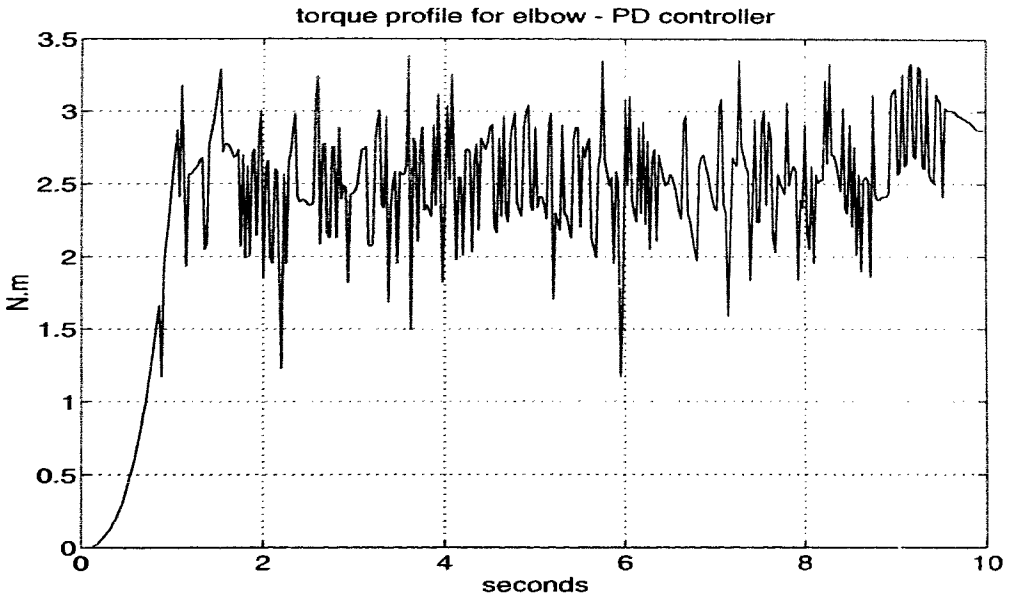

B: Torque profile

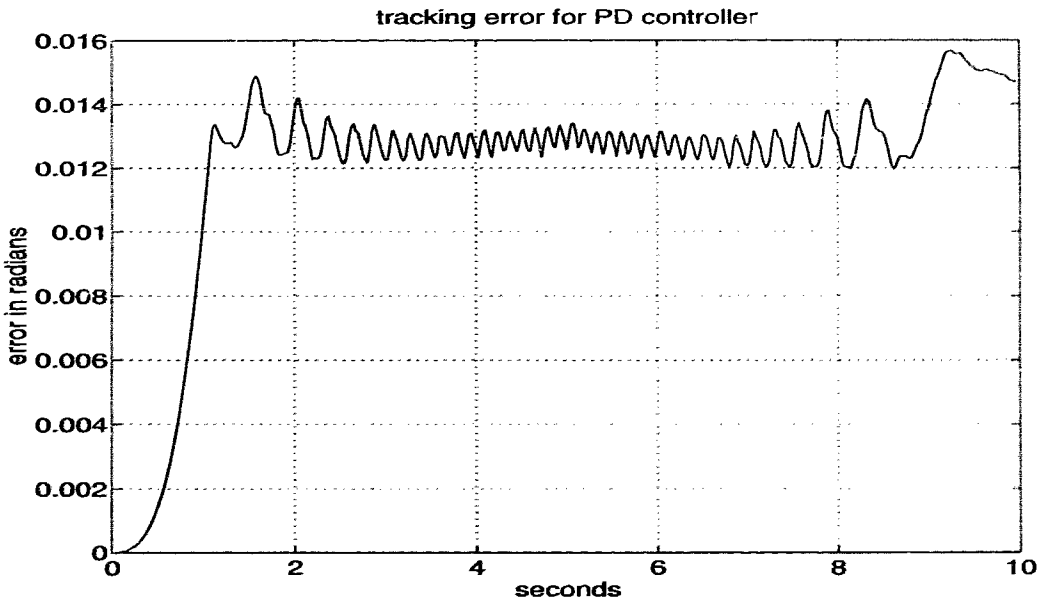

A: Tracking error

Figure 2.8: Experimental Results for PD controller

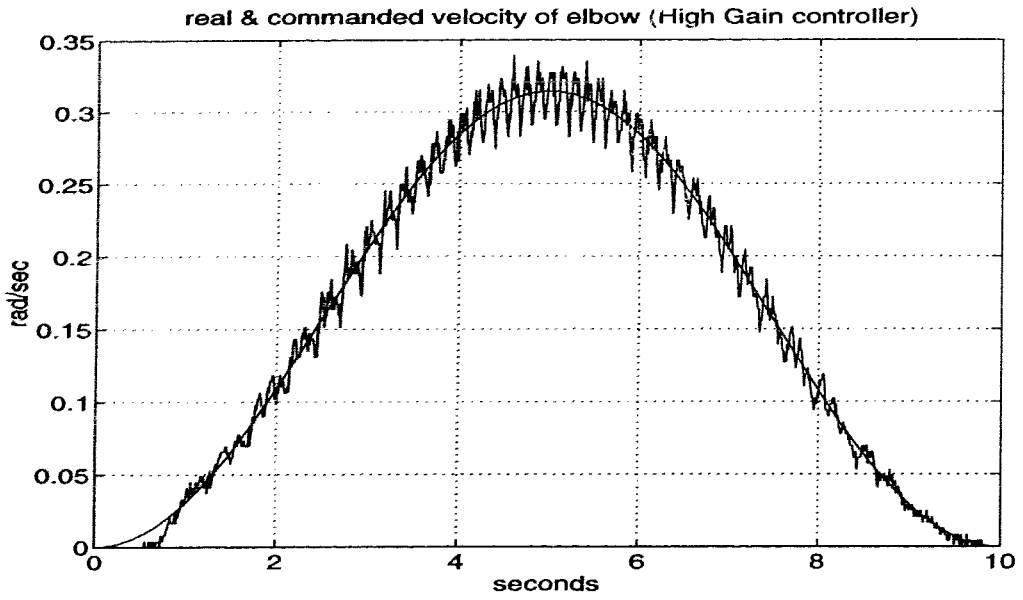

B: Velocity profile

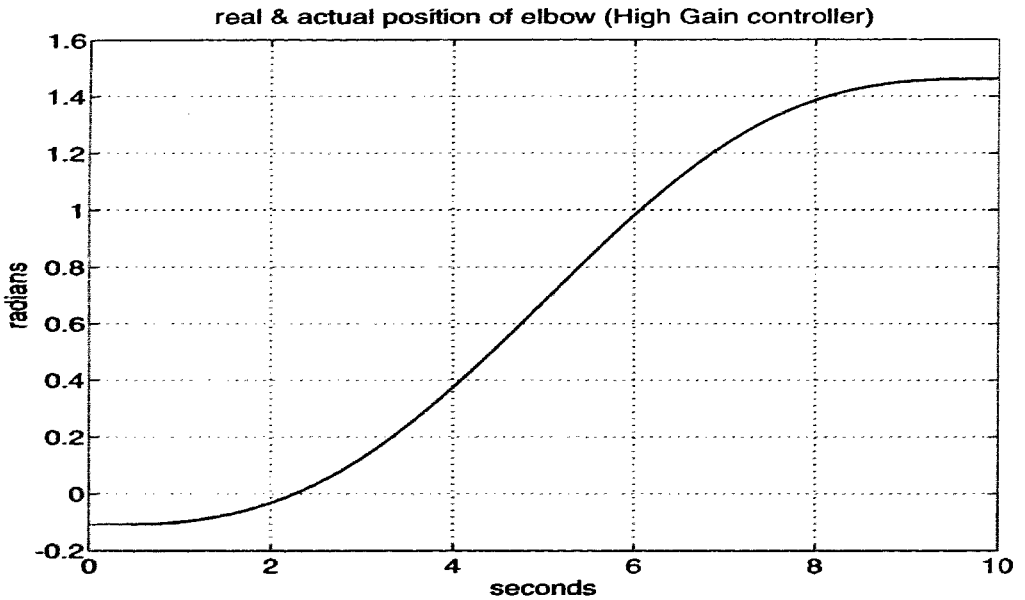

A: Position tracking

Figure 2.9: Experimental Results for high gain PD controller

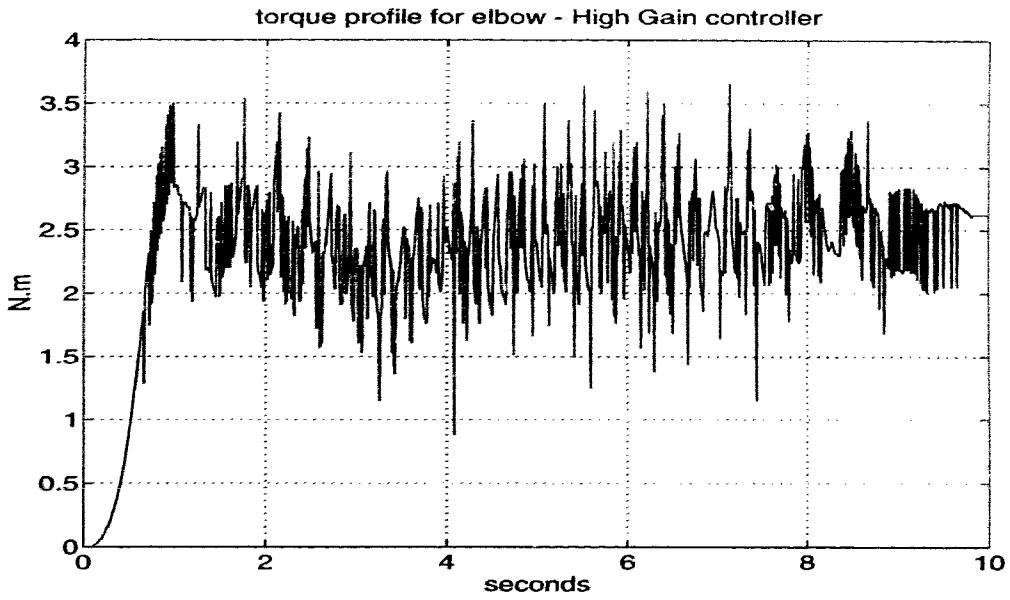

B: Torque profile

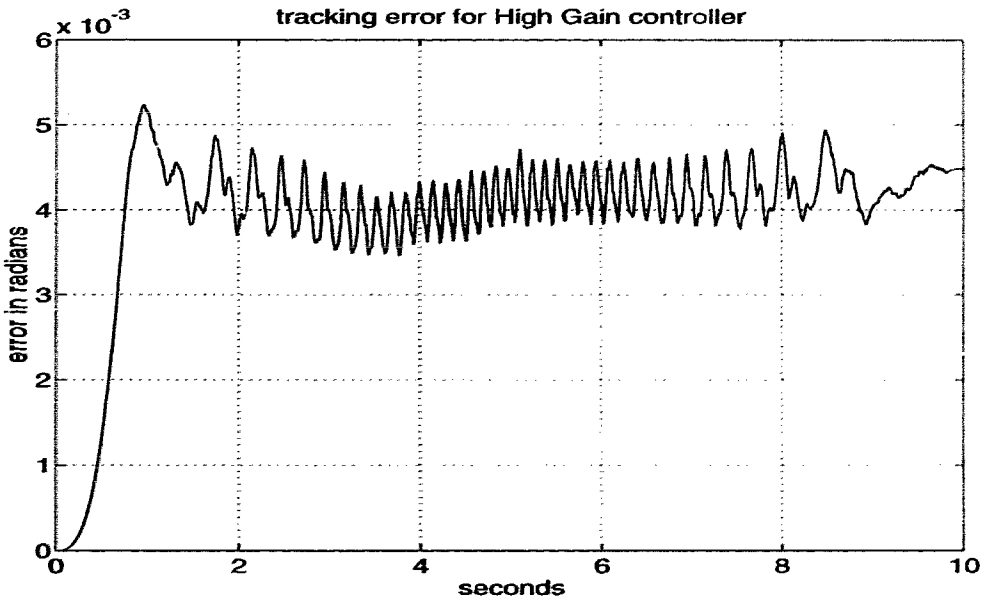

A: Tracking error

Figure 2.10: Experimental Results for high gain PD controller

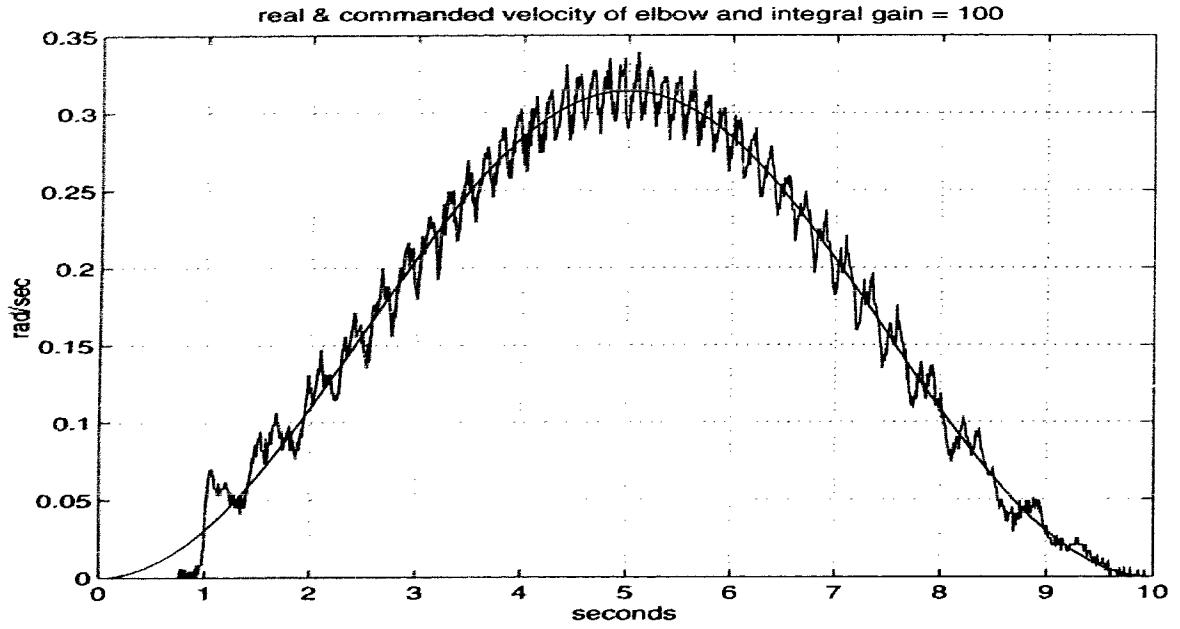

B: Velocity profile

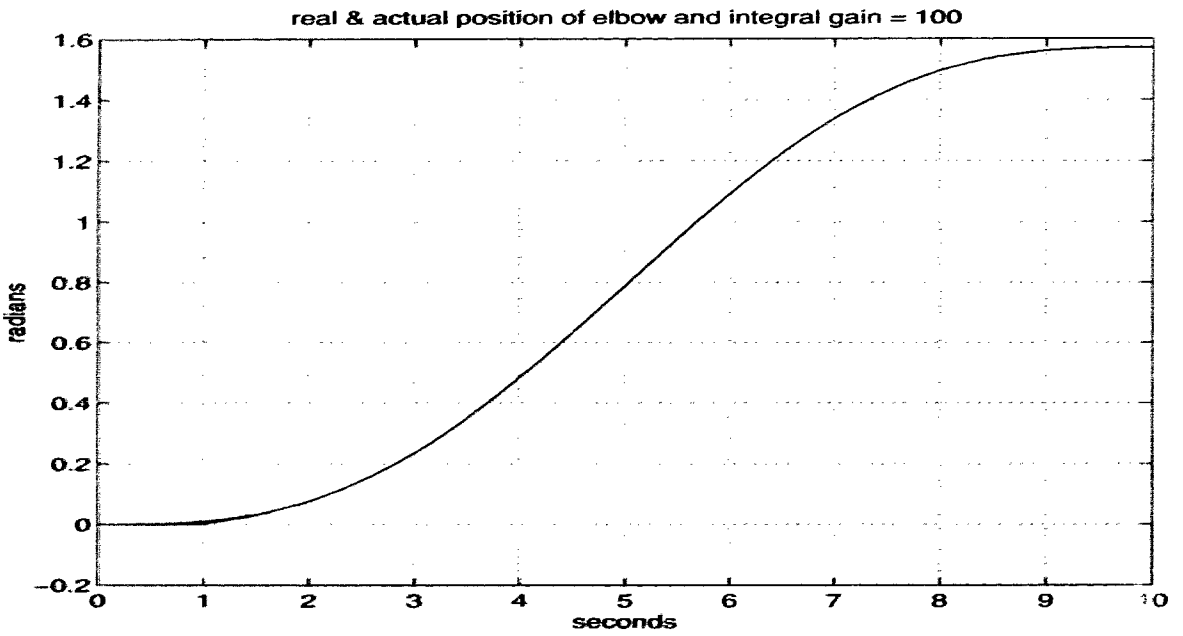

A: Position tracking

Figure 2.11: Experimental Results for PID controller

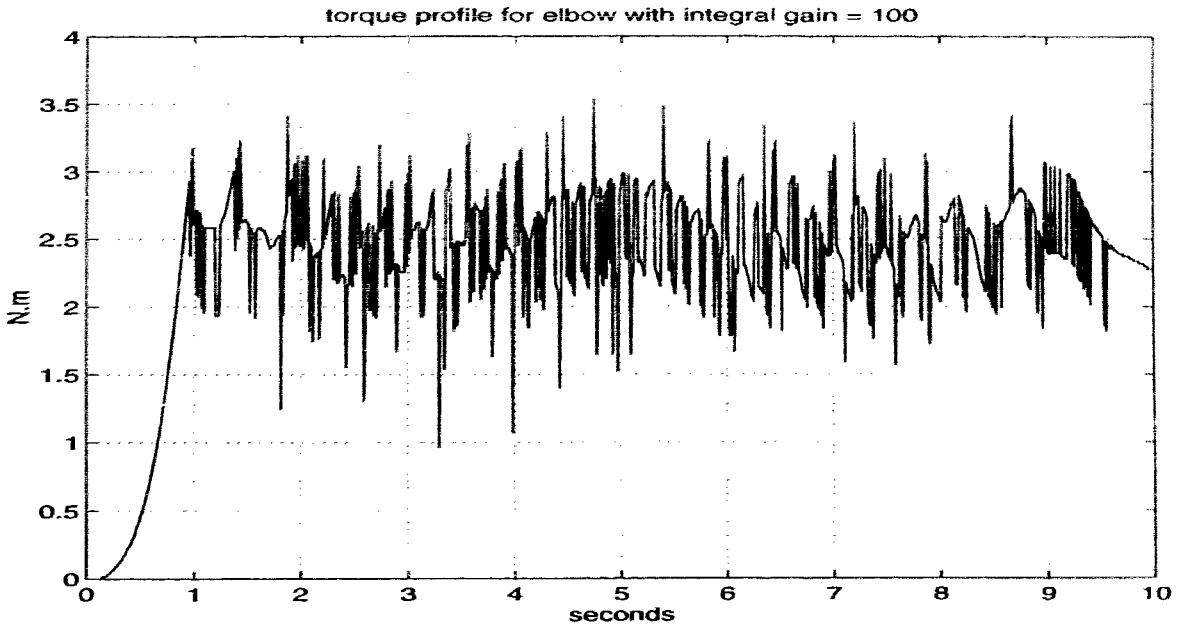

B: Torque profile

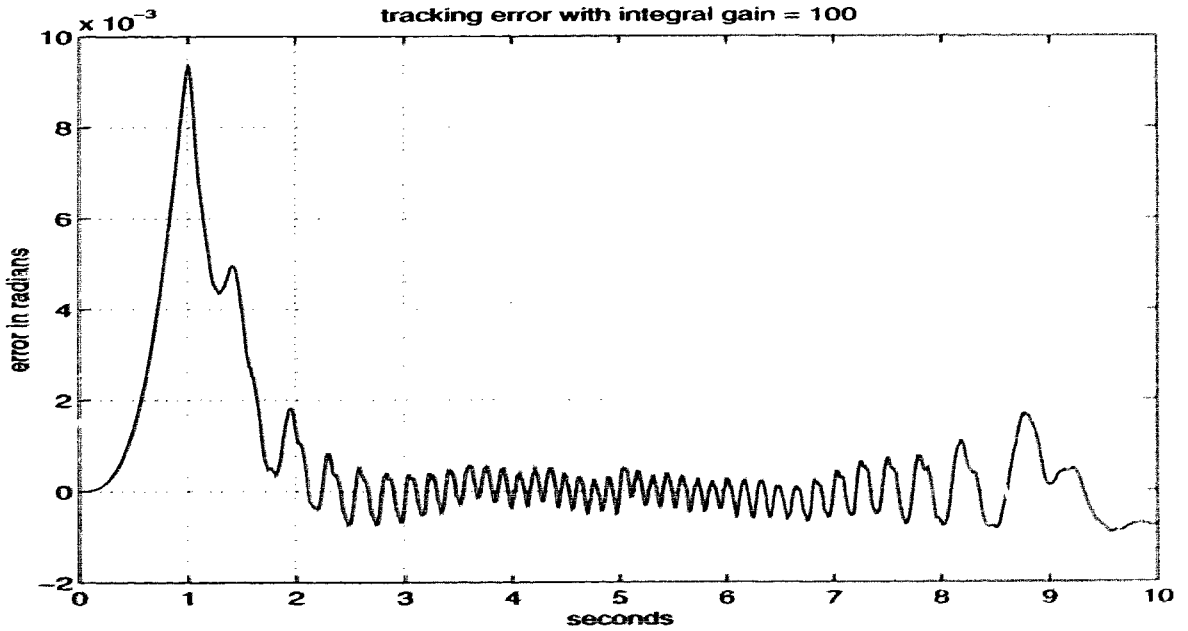

A: Tracking error

Figure 2.12: Experimental Results for PID controller

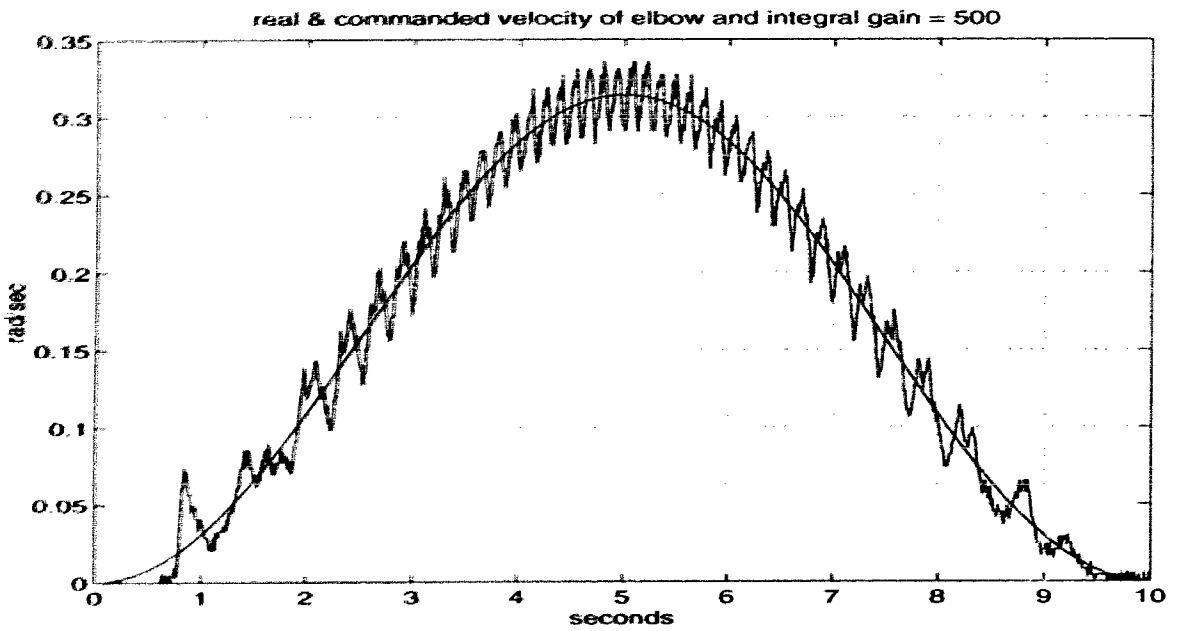

B: Velocity profile

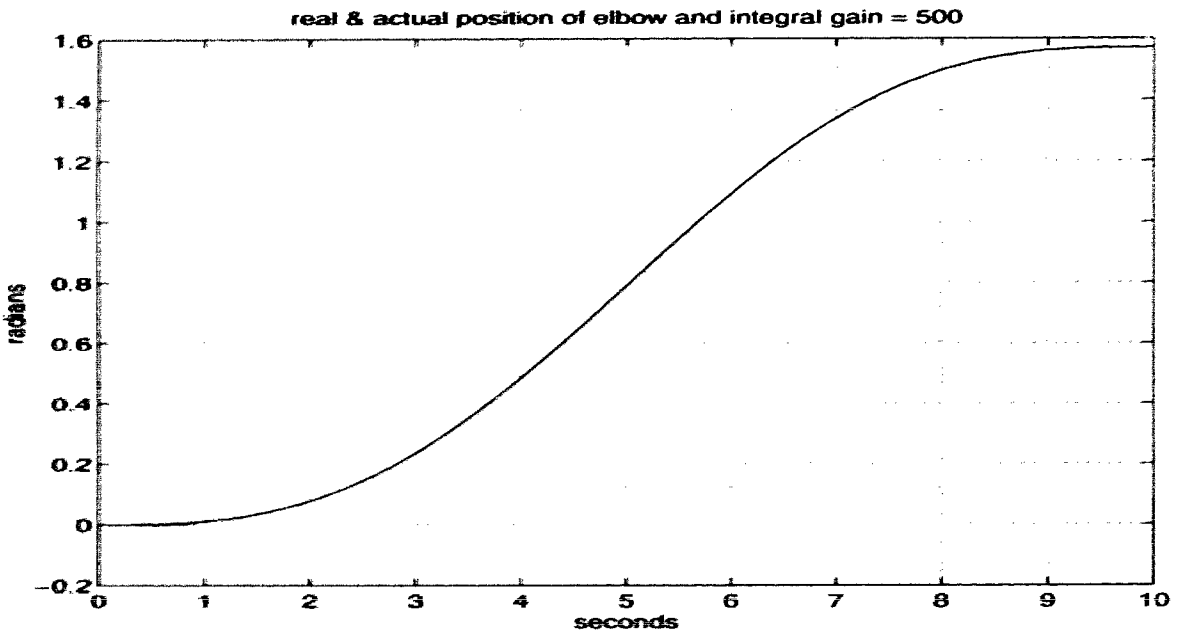

A: Position tracking

Figure 2.13: Experimental Results for PID controller with increased integral action

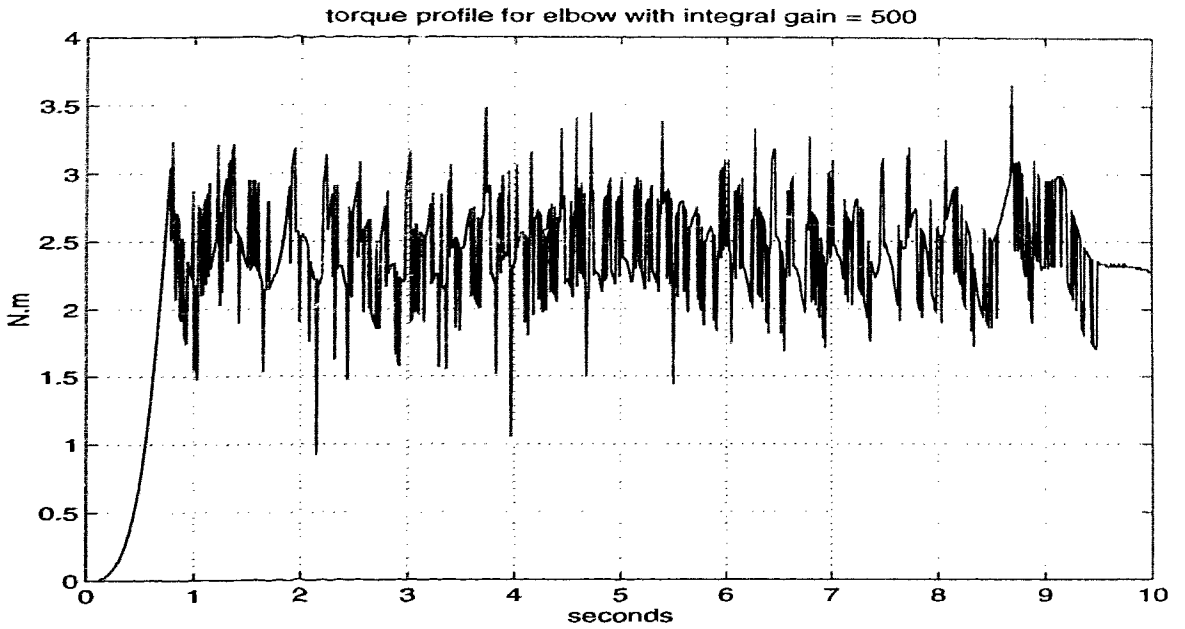

B: Torque profile

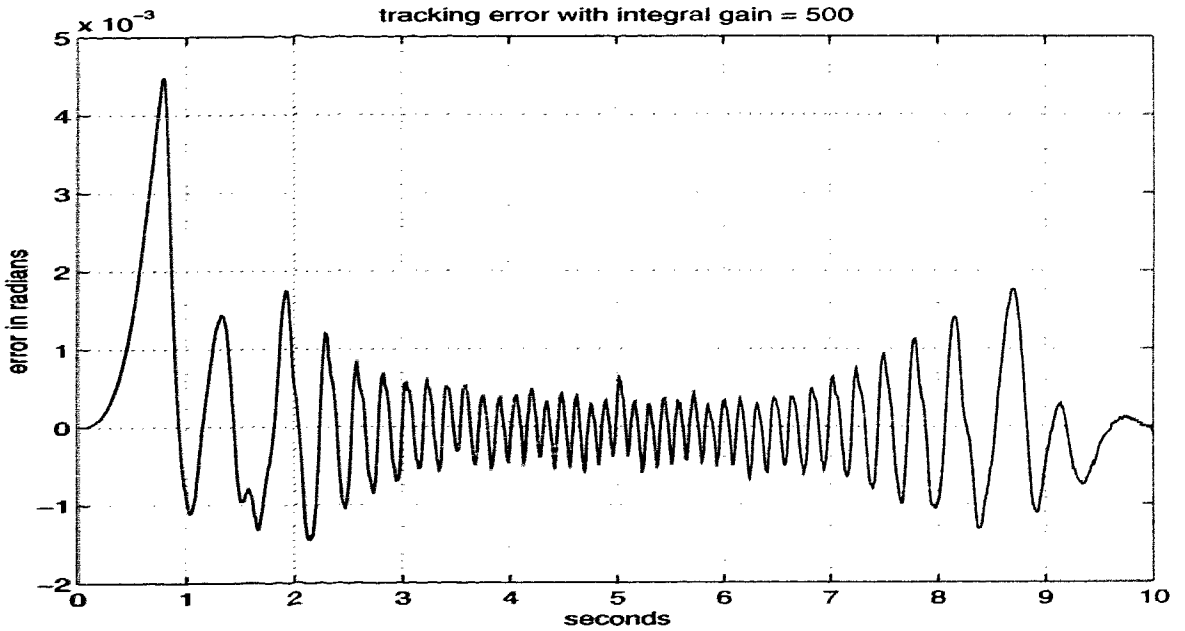

A: Tracking error

Figure 2.14: Experimental Results for PID controller with increased integral action

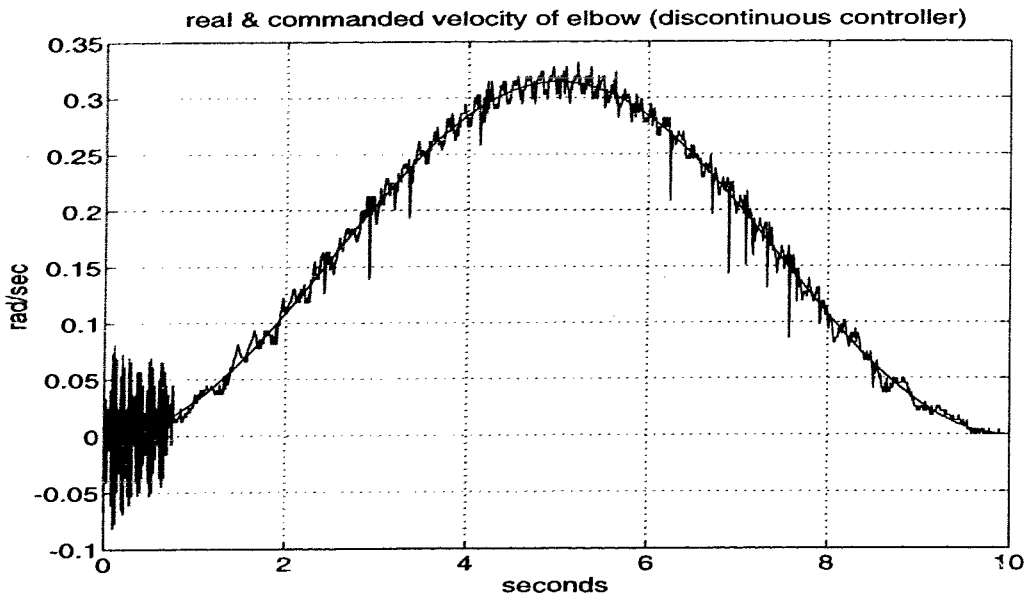

B: Velocity profile

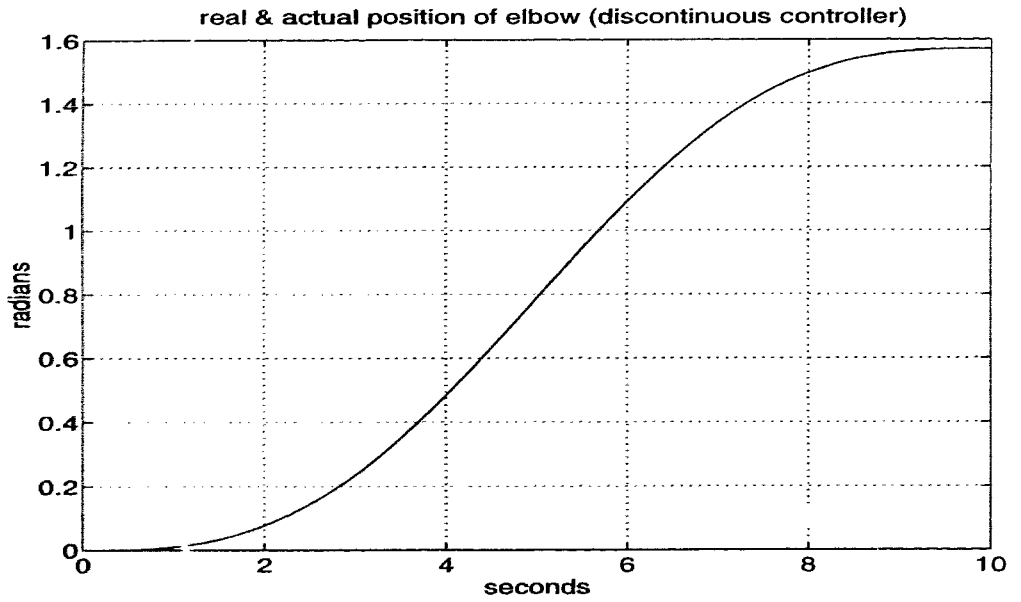

A: Position tracking

Figure 2.15: Experimental Results for discontinuous controller

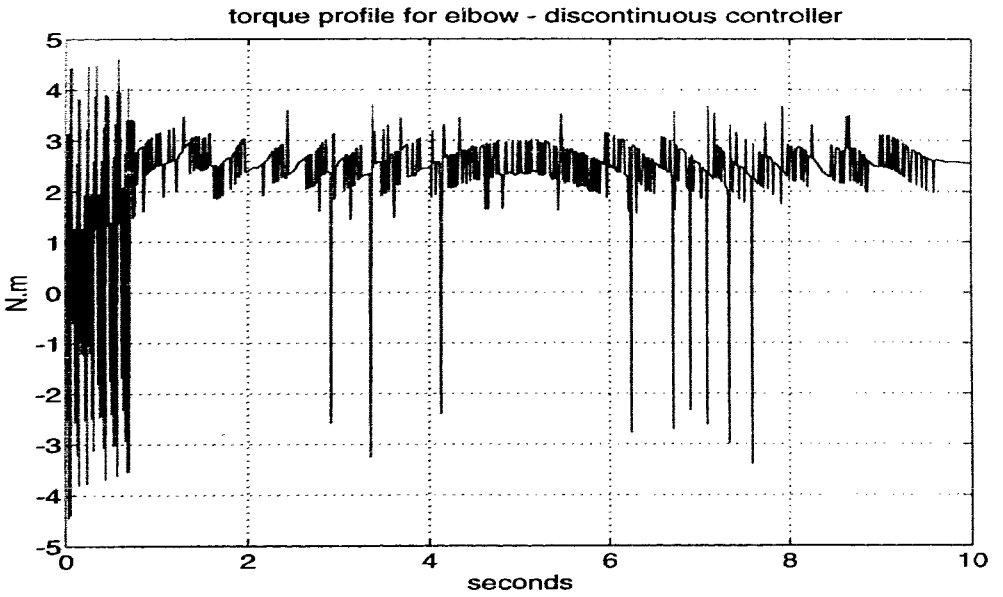

B: Torque profile

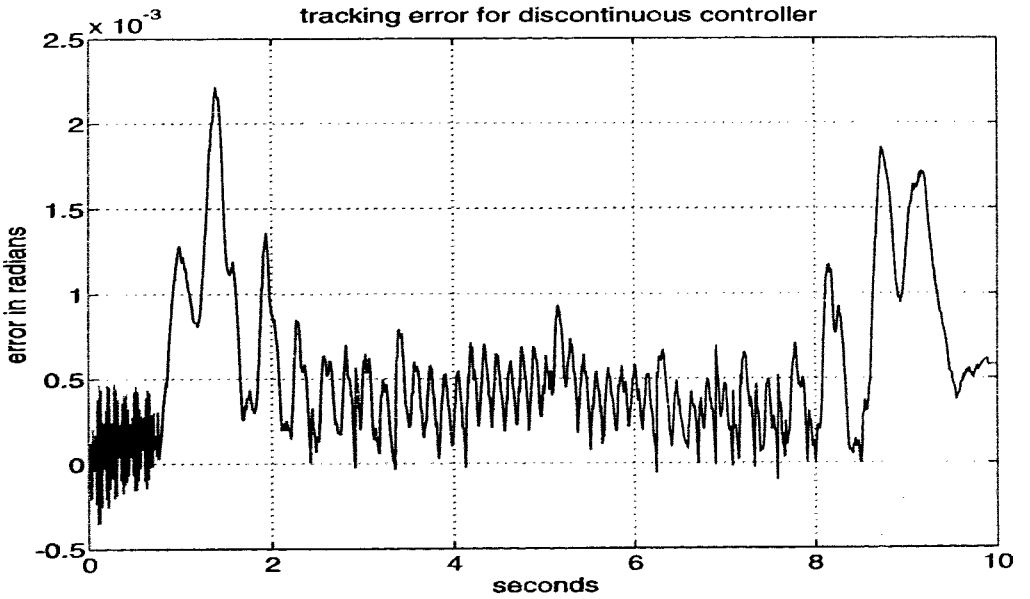

A: Tracking error

Figure 2.16: Experimental Results for discontinuous controller

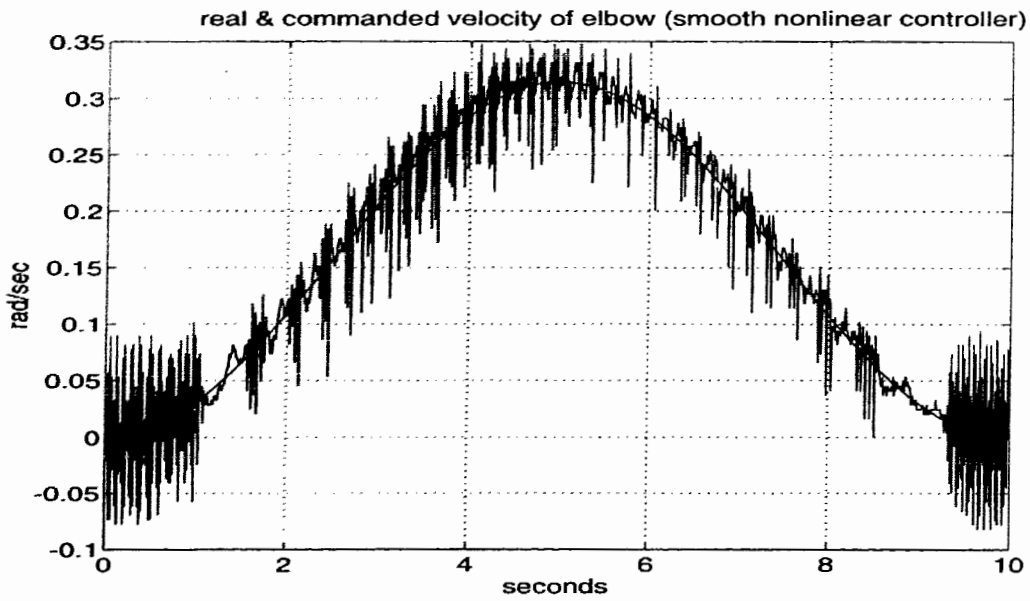

B: Velocity profile

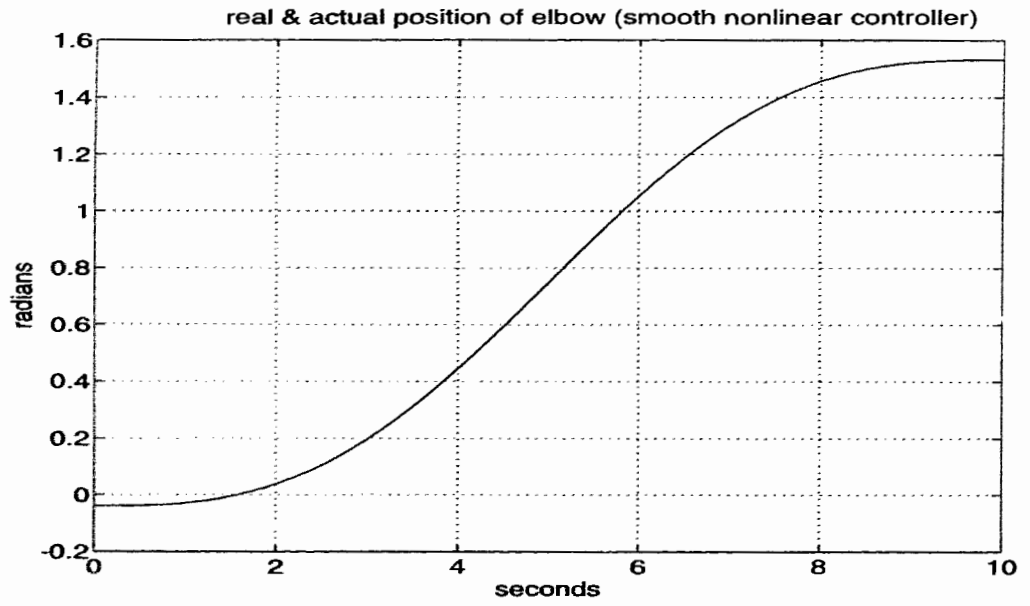

A: Position tracking

Figure 2.17: Experimental Results for smooth continuous controller

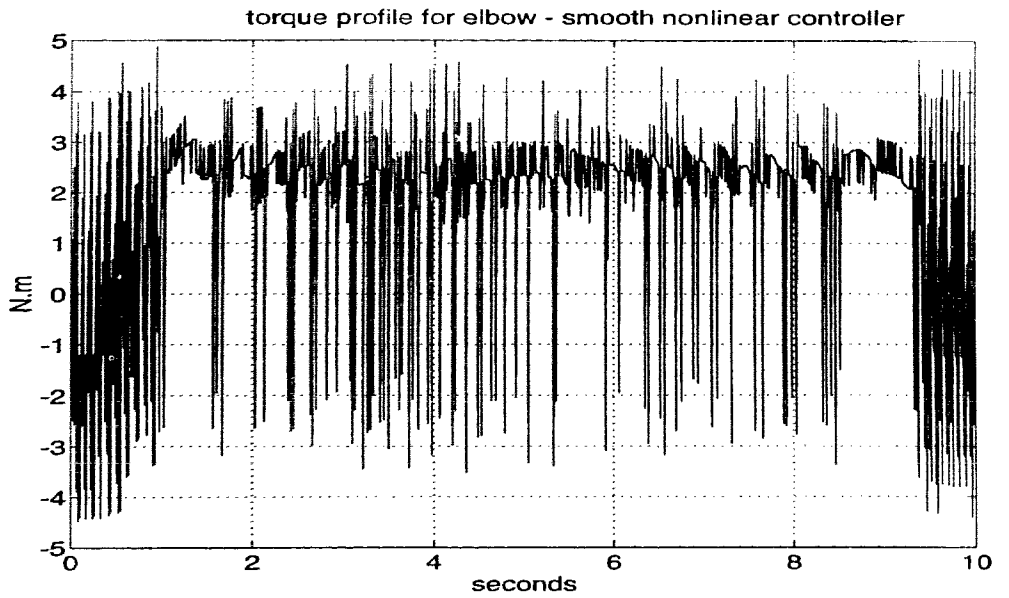

B: Torque profile

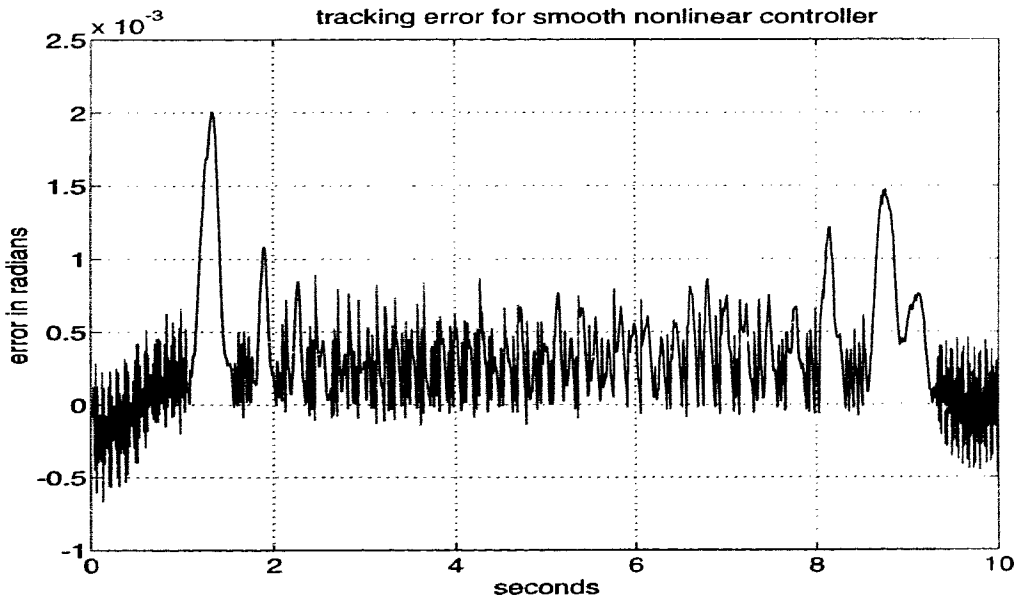

A: Tracking error

Figure 2.18: Experimental Results for smooth continuous controller

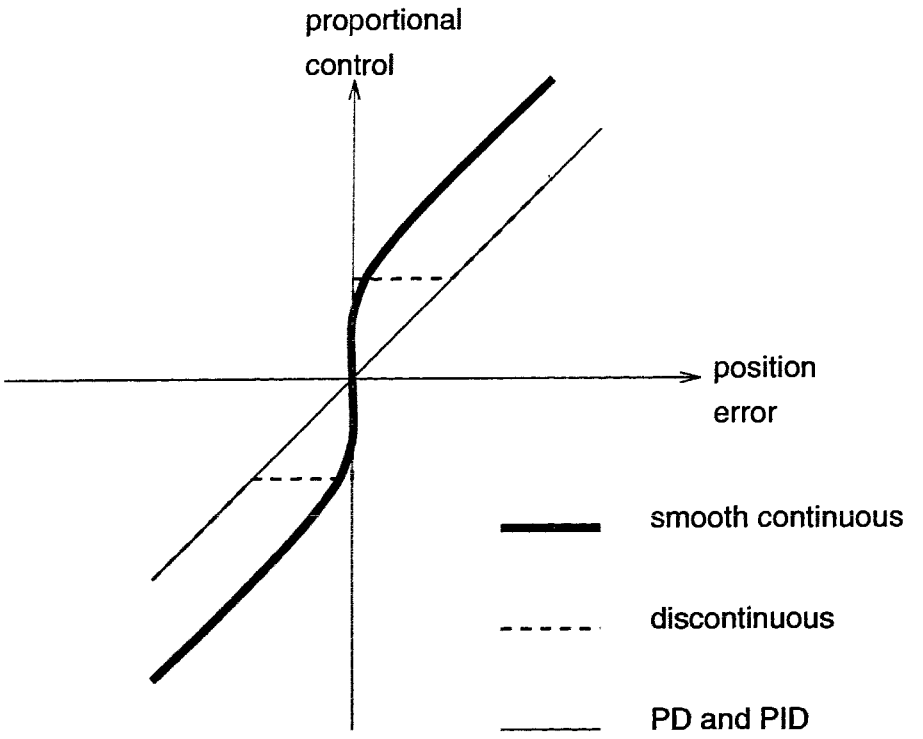

Figure 2.19: Super-imposition of the proportional gains of the different controllers

Chapter 3

Upgrading a 2 DOF planar manipulator to a 4 DOF SCARA type assembly cell: Procedure and Recommendations.

3.1 Introduction

A 2 DOF planar manipulator is modified for use as a manufacturing cell for force guided assembly tasks. The control subsystem is run on a real time kernel exploiting DSP architecture. The main task involves designing a mechanical assembly, which will convert the the 2 DOF planar configuration into a 4 DOF SCARA type assembly cell. This configuration is to pick and place objects as well as regulate the interaction force between the gripper mechanism and its environment. In addition, an electronic interface is designed and developed to provide a reliable communication channel between the assembly cell and the control subsystem for feedback and control signals to propagate.

Reprogramming of the real time kernel to accommodate the extra 2 DOF's must also be addressed. Low level I/O functions will be used to develop a command base

to facilitate a proper user interface for the development of control routines. Due to the enormous torque capabilities of the motors used with the cell, a robust real-time control architecture must be developed for proper fault detection and compensation abilities.

3.2 Mechanical Assembly Design

This section will describe the mechanical design and construction of the upgrade procedure.

3.2.1 Objectives

The purpose of this mechanism is to allow a manipulator that possesses only two degrees of freedom (DOF) in a planar configuration to enjoy an extra two DOF's in a SCARA type setup. Thus the mechanism must travel vertically at the tip of the first two DOF's, as well as rotate in the horizontal plane while traveling vertically. It should also be mentioned that the actuation device for the wrist should be capable of regulating the position of the wrist that is subject to external forces acting on it. Attached to this rotation mechanism must be a force sensor capable of measuring six force components.

3.2.2 Design Constraints

The first concern in deploying this mechanism is space. At the distal tip of the first two DOF's, there is only 39 cm of vertical travel available. This vertical space must also be shared by a force sensor, gripper, and a motor as well. This severely limits the configuration options for implementing a mechanism to be responsible for vertical motion. One alternative would have been to raise the base of the 2DOF manipulator in order to allow for more vertical travel. Due to the size and torque capabilities of the base motor, whatever was implemented to raise the base of the manipulator would have to be sufficiently rigid to withstand the inertia generated by occasional instability of a controller responsible for the base motor. This places restrictions on the method used

to raise the base, as well as what sort of materials are used to accomplish this task. With all these conditions to be met, it was decided to adopt a configuration which did not require the manipulator to be raised from its present position. To accomplish this, a mechanism employing a worm gear for 90 degree actuation was deployed. It has the same functionality as a mechanical jack, only its intention was not to increase the power capability but to enable a 90 degree actuation configuration in order to save vertical space.

The conceived system is presented in figure 3.1. With a general guide now available for the location of each component, it is necessary to focus on each subsystem and ensure its integrity with the rest of the still to be proposed system. Most constraints in the design procedure have been due to the use to which he manipulator will be put, as well as natural constraints of the mechanical assembly. However, due to the concurrency which accompanies this design, some constraints have to be fabricated in order to proceed. These will be revealed as necessary.

There will be a motor and housing assembly sitting atop the tip of the second link. The design of the housing assembly must take this into account, as must the size of the motor. This puts an upper limit on the weight of the motor, as well as the entire assembly. The motor must also be able to lift the third link (vertical travel) and all the hardware attached to the end of it. This puts a lower limit on the torque capability of the motor. There will be what amounts to a lumped mass at the end of the second link. This will adversely affect the dynamics of the manipulator and attempts at modeling it. Attempts must be made to make this assembly as symmetrical as possible.

Consideration must now be given to the wrist mechanism and its actuator. Ideally the mechanism would be as flat as possible for space saving considerations, but the type of object to be grasped must also be considered when designing it. The same applies to the actuator for the wrist, but again, the type of motions that the wrist is expected to produce must also be taken into account. The wrist will not need to rotate at high speeds, but rather it should rotate accurately at low speeds with enough torque to regulate its commanded position against external force disturbances, coming from an object within the gripper's grasp, sliding along a surface. Thus, we have a pseudo constraint on both the actuator's size and torque characteristics.

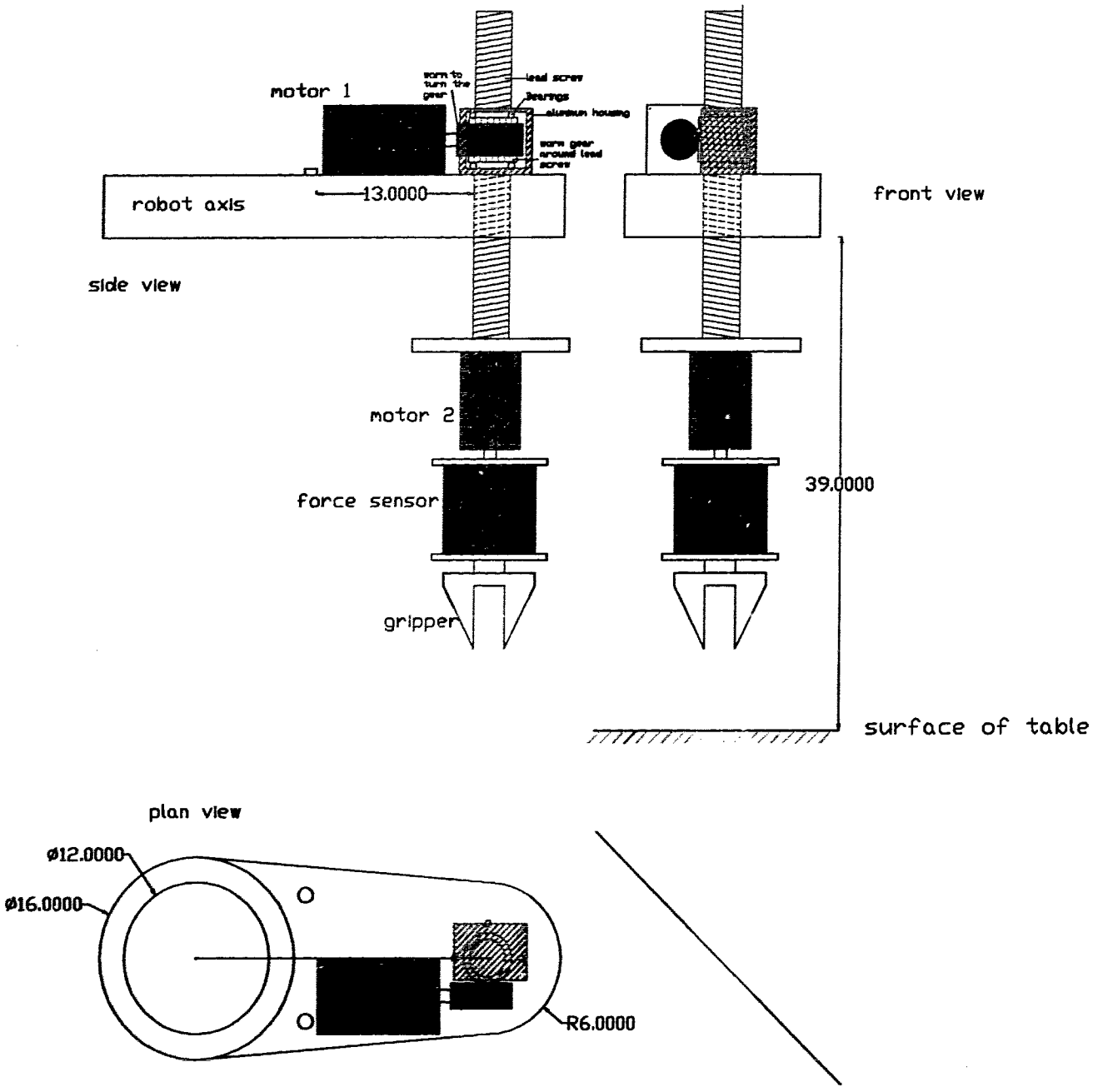

Figure 3.1: Configuration of the extra 2 degrees of freedom to the tip of the elbow link.

In order for a grasped object to slide along a surface without slipping within the gripper mechanism itself, a firm grip is required to hold the object in place. The gripping mechanism is to be pneumatically operated. A two way mechanism is chosen as opposed to a one way, spring return.

3.2.3 Hardware Selection

With the various constraints placed on the hardware as described in the previous section, the actual components may now be chosen based on these constraints. Due to the interdependency of the subcomponents on each other, an iterative procedure is necessary in choosing the components. Cross validation must constantly be performed when choosing components to ensure that none will prevent another from performing as required by the mechanism as a whole. Concurrency must be maintained.

It was decided that the vertical operation would first be addressed, since this would probably pose the greatest mechanical challenge. Vertical motion is accomplished by fixing a worm gear to the flange of a lead screw assembly. The worm-gear/flange assembly would be fixed inside a housing and allowed to rotate, but not move laterally or vertically. Thus when the worm attached to the shaft of the motor turns the worm-gear/flange, the lead screw is forced up and down.

Due to the diameter of the flange, the worm gear required to be fitted around it would need to have a large bore. This meant a large gear and in turn a large worm. This would cause an excessive amount of friction to exist in the mating of the worm and gear, impeding the motion of the lead screw. The other impediment caused by this setup is the extra inertia added to the end of the motor shaft, by the large worm attached to its tip. The adoption of this design necessitates a high speed, high torque motor for actuation. The torque is needed to overcome the load inertia (worm) and the friction generated from the mating of the large worm and gear set [1]. Another factor to consider is the fact that this assembly will be sitting at the tip of the second link, so the motor used for this operation may not be excessively large. It was also

[1] The friction between the flange and lead screw is negligible since there are ball bearings separating them.

not possible to machine down the diameter of the flange in order to fit a smaller gear, since its ball bearings protrude its outer surface.

Thus before this design could proceed, it would first have to be determined if there were any motors available that would accomplish the fore-mentioned tasks. Torquing a motor for this operation was thus necessary. In order to do this, several parameters need to be determined: what velocities are required for vertical motion and what torques will be required at these velocities. The former depends on the application and on the judgment of the designer. The latter however will require some calculations, and more importantly, estimations due to uncertainties. The parameters needed for this calculation are: the weight of the lead screw and the gripper/force-sensor assembly that would be attached below it, the inertia of the worm on the motor shaft, and the friction due to mating of the worm-gear and worm. Since no components have been chosen to this point, there are no numbers to work with.

A ball screw with a diameter of 0.5 inches was decided upon. This enables the use of an existing hole through the tip of the second link. The diameter of the ball screw cannot be too thin. Rigidity will be necessary when moving the load of the gripper assembly up and down, if wobbling is to be minimized. The lead of the ball screw also needs to be determined. This dictates the relative ease of vertical motion associated with the ball screw, as well as the speeds at which this vertical motion will occur. It was decided that a small lead screw would be used, which facilitates easier lift but gives up traveling velocity for a given motor shaft rotation speed. Vertical velocity is not of paramount importance in this application. It was decided that a vertical velocity of 1 inch per second would suffice. The worm gear must be chosen to fit around the screw. Thus its bore must be greater than 0.5 inches.

Specifying the worm motor

The vertical motion will be geared down in two stages. The first is through the lead associated with the ball screw, the second is the lead associated with the worm gear. The following choices were made after studying the available hardware and their specifications:

Ball screw:	0.2 inch lead, 0.5 inch diameter
Worm gear:	0.875 inch bore, 20 teeth.
Worm:	9°5' lead angle, double thread. Pitch Dia. = 1.25 in, Bore = 0.75 in.

From the above specifications, the worm ratio is 10:1. A 0.2 inch lead means that it takes the flange 5 revolutions to move the ball screw 1 vertical inch, which implies a desired angular velocity of the flange to be 31.4 rad/sec, and thus that of the worm to be 314 rad/sec.. It now remains to be calculated, how much torque will be required to accomplish this velocity at some given acceleration.

The opposing forces that the shaft of the motor will have to overcome in lifting the screw vertically are as follows:
- Worm inertia
- Worm/Worm gear coupling friction
- Relevant components of the weight of the ball screw and gripper assembly attached to it.

The inertia of the worm is calculated by assuming that it is a hollow cylinder. With inner and outer radius of R_1 and R_2 respectively, the inertia is found using the formula $I = \frac{1}{2}M(R_1^2 + R_2^2)$. The mass of the worm was not provided in the literature, so a mass of 0.3 Kg. was assumed. Using the well known formula for calculating the required torque, $\tau = I\alpha$, the required acceleration is needed. It is decided that the ball screw assembly should be able to accelerate upwards at a rate of $1 in/sec^2$, which translates to 314 rad/sec^2. With this information, the required torque at the shaft *just for turning the worm* τ_g is 16.3 mN.m. As a precaution, the units are checked for compatibility. This is illustrated as:

$$I = Kg.(m^2 + m^2) = Kg. \cdot m \cdot m$$

$$\alpha = \frac{rad}{(sec \cdot sec)}$$

Radians are unit-less, so $I\alpha$ is in effect $\frac{kg.\cdot m \cdot m}{sec^2}$. Newtons are $\frac{kg.\cdot m}{sec^2}$, so in effect we do indeed have units of Newton meters.

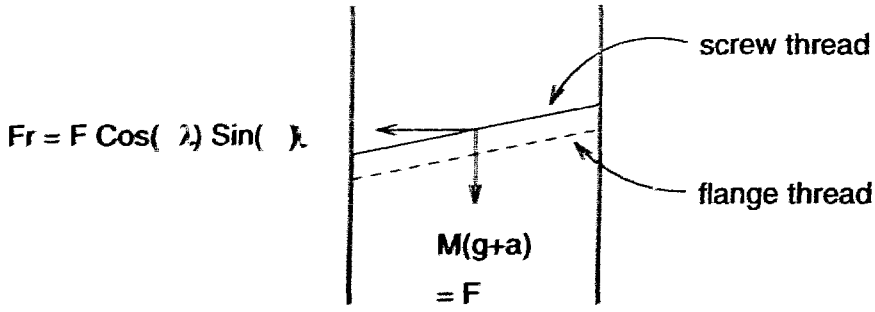

Figure 3.2: Resolving forces on the ball screw for vertical acceleration

The next requirement is the torque needed to accelerate the assembly upwards at 314 rad/sec^2. This is done with the aid of the diagram in figure (3.2). For the ball screw to move upwards at a rate of a, the vertical force required is $F = M(g + a)$ N. Assuming minimal friction (μ of 0.9 used) between the threads of the screw and those of the flange [2], this translates into an equivalent horizontal force of $F_r = F\cos(\lambda)\sin(\lambda)$. λ is the lead angle of the screw, which can be found from the specifications given earlier to be $\lambda = \frac{lead}{circumference} = \frac{0.2}{2\pi(0.25)} = 7.25^o$. It was assumed that with the gripper assembly attached to the end of the screw, the total mass (M) should not be more than 7 Kg. The value of F_r is thus calculated to be

$$F_r = \frac{7(9.8 + 0.0254)\cos(7.25)\sin(7.25)}{0.9} = 9.567N.$$

A 10:1 gear ratio and a ball screw radius of 0.25 in. means the required torque at the motor shaft τ_i is 6.1 mN.m.

For the above worm/gear combination, the friction specified by the manufacturer's literature corresponds to an efficiency η of 75 %. Thus the total torque required from the motors is $\frac{\tau_i + \tau_g}{0.75}$, which is 30 mN.m; a 30 % safety factor is added, so the torque required from the worm motor is 40 mN.m. Thus a motor is needed that produces this torque at a shaft speed of 314 rad/sec.

To accomplish this task, a Pittman brushless DC servomotor was chosen [39]. The motor has dimensions of 6.4 × 5 × 5 cm and provides 180 mN.m at 500 rad/sec. The servo has a back EMF constant of 45.6 mV/rad/sec and a torque constant of 45.6 mN.n/amp. Thus it needs 4 A at 24 V to operate.

[2] which is a valid assumption due to the ball bearings between the two.

Specifying the wrist motor

This task was considerably simpler. This motor is used directly to control the orientation of the wrist. It is known that this motor will be required to provide high torque without necessarily rotating at high speed. Thus a gear motor seems fitting for the task. A hypothetical situation is now conjured for the purpose of determining the torque required from this motor.

For constrained motion experiments, tasks involve moving the end effector against an environment while maintaining a certain force on that environment. To get an idea of the torque require of the motor, it was decided that the gripper would hold an rectangular object that was 10 cm. long, at the center, while it was moved along the surface with a normal force F_n of 5 N pushing down on it . Assuming a coefficient of friction μ of 0.6, the torque τ to maintain the orientation of the object is, $\tau \geq \mu \cdot F_n \cdot 0.05 = 150$ mN.m. This is the torque needed to keep the gripper and object oriented while being the object is being dragged along the surface. If the orientation of the object slips for some reason, extra torque will be required to realign it. Assuming a 45 deg slip in orientation that must be corrected in 0.2 seconds, what amount of torque will this require ? The force sensor is known to weigh 0.5 Kg, the gripper will be assumed to weigh no more than 1 Kg. The radius of the gripper design will be assumed to be no more than that of the force sensor (9 cm). Thus the inertia I of the entire gripper assembly (assuming a cylindrical shape) is $0.03375 Kg.m^2$. The acceleration of the correcting motion is now required. This is the assumed $\frac{\pi}{4}$ slip angle, divided by the desired 0.2 sec correction time; $4 rad/sec^2$. Thus the correction torque $\tau_c = I\alpha = 135$ mN.m. Thus the total torque required to drag the object and also correct for any slippage in the motion is 135 + 150 = 285 mN.m = 40.3 oz.in. A 30% safety factor is added so the wrist motor needs to provide at least 52.4 oz.in of torque.

The motor used for the wrist is a spur gear motor [40] with a gear ratio of 6.3:1 and a torque constant of 2.92 oz.in/amp. Thus it needs to be able to carry 2.88 (say 3) amps in order to fulfill its role in a constrained motion task. It's peak current of 4.2 amps is more than capable of performing the required tasks.

Supporting peripherals

In order for the motors to operate properly, the amplifiers need to be chosen correctly. Both motors operate with Pulse Width Modulated (PWM) amplifiers. The amplifier used for the wrist motor is operated as a basic voltage to current converter, due to the simplicity of operation of the gear-motor. The worm motor however, being a brushless DC servo motor, requires a more complex driver unit with three phase windings and hall sensors. The 300 series amplifier from Copley Controls was used to drive the gear motor. It is rated at 6 Amps continuous. The 513 series from the same manufacturer was used to tend to the more complex task of driving the worm unit. This driver features three phase wye or delta windings and hall sensors operating at 60 or 120 degrees. It is rated at 13 Amps continuous. The limited selection forced the current to be overrated.

Attached to each motor is a three channel optical encoder for positioning information. These encoders provide resolutions of 2000 counts/rev. In order to provide a homing mechanism for the extra 2 DOF's, two proximity sensors were acquired. One will be placed in a position which indicates the home position of the lead assembly, the other provides the same function for the wrist.

gripper

For simplicity, the gripper used for this design was identical to the gripper on a puma 560 robot. It is actuated pneumatically with an embedded double acting piston. A two way air valve was thus used to control the actuation of the gripper.

3.3 Description of DSP Subsystem

This section will describe the operation of the hardware which controls the manipulator, as well as introduce the software structure on which it runs.

The digital control of the entire manipulator is governed by a DSP card inside a host PC. The card uses a TMS320C30 [41] floating point DSP chip to execute real-time control algorithms. The control signals propagate between the manipulator and the

DSP card through the use of up to four I/O cards (henceforth referred to as DS2 cards, as per the manufacturer's convention [42]). Each DS2 board is capable of controlling two axes by way of I/O signals.

To use the DSP card, a control algorithm is written in the C programming language. This algorithm is translated into C30 code by a cross compiler residing on the host machine. There are primitive functions that may be used in the C code, which are specific to the C30 card, that allow more functional control routines to be realized. There are also a library of functions which are specifically used by the C30 card to perform various operations (such as data I/O) on the DS2 boards. These are useful when another card is being added to the system to accommodate extra degrees of freedom, such as the case is here. This requires writing a new set of low level functions that allow the new card to be controlled by the DSP board (see section 5). For each DS2 board linked to the DSP board, there is a specific section of memory in the DSP card set aside for the data communicated between each board (The expansion boards are memory mapped). There is no I/O done directly between the DSP board and the manipulator, all of it is done through the DS2 boards.

The two DS2 boards and the DSP board are connected in parallel with each DS2 board distinguishing itself by way of dip switches, which define different addresses in the DSP memory space. Each DS2 board is equipped with two A/D and two D/A converters, giving each the ability to control two axes. Also, they each have a quad decoder built onto them, as well as four undedicated digital I/O lines. These features serve to make these cards ideal for motor control. A block diagram describing the system is given in fig. 3.3.

3.4 Electronic Interface

One DS2 board has already been configured by the manufacturers of the manipulator. The second board must be configured and interfaced to the rest of the system. When interfacing the second card to the newly added hardware, many of the connections could be directly attached to the DS2 board; there were some exceptions however, that

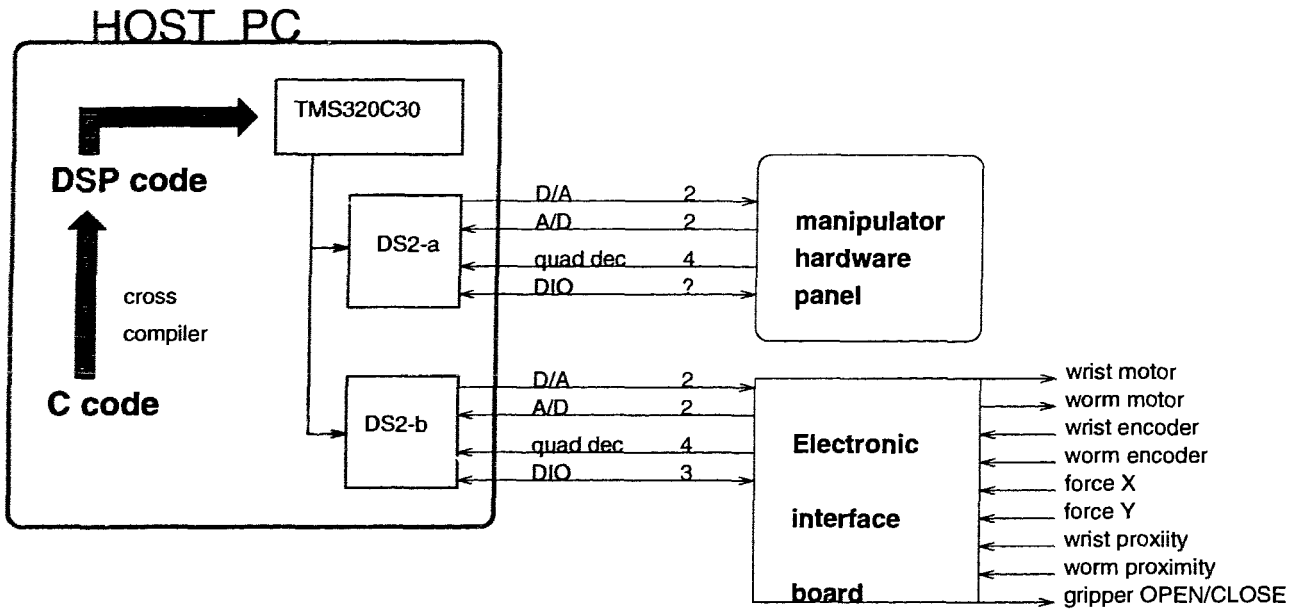

Figure 3.3: Complete System Block diagram

required the use of additional circuitry.

The first components that required additional circuitry were the proximity sensors. These operate on 12 volts and so they issue 0/12 V signals. These simply had to be stepped down to 0/5 V since the DIO lines on the DS2 cards use TTL logic. This was accomplished with the use of a voltage divider resistor pair.

The second component that required additional circuitry was the pneumatic valve which is responsible for the operation of the gripper. This valve is rated at 12V 2.4W. It thus needs a 12V power supply that is capable of supplying 0.2 amps. The PC bus has 12V connections, but is unable to supply 200 mA. Thus the power supply used for the motors will also need to tend to the job of powering the relay for the air valve. This supply is 24 V however, so this will also need to be brought down. It must be remembered that due to the relatively large amounts of current going through the divider, power resistors must be used. The resistance of the relay coil was found to be 64 Ohms, thus a 57 Ohm 5 W resistor was used for the task, and put in series with the relay. This causes approximately a 12V drop across each of the resistor and the relay coil. Once the 12 V is attained, the valve will need to be turned on and off. This is accomplished through the use of a transistor, controlled by one of the DIO lines

on the DS2 card. When the transistor is turned on, current flows through the relay coil down through the transistor to ground. Once the transistor is turned off, there is energy stored in the relay that needs to be released, or the next time the transistor is turned on, the relay may be damaged. To accommodate this, a diode is placed in parallel with the relay. Once the transistor is turned off, the current will flow through the diode and dissipate itself as heat. A current limiting resistor is placed between the DIO control line and the input to the transistor. This is all illustrated in fig. 3.4.

Besides a 0.5 amp fuse to protect the coil, this is all the circuitry that is needed for the interfacing, all other signals could be wired directly to the DS2 card. For consistence however, and ease of maintenance, all the lines from the DS2 card were attached to the interface board through the use of a 37 pin ribbon cable. The lines from the peripherals were directly connected to the interface board. The schematic for the interface board is shown in fig. 3.5. A single sided design was opted for since only a few jumpers were required and it costs less to fabricate. A section for prototyping was also integrated on the PCB. Presently, only 4 analog signals (force sensor) can be read (2 on each DS2 board); since the force/torque sensor outputs 6 axes of data, it may be necessary at some point to implement a multiplexer/demultiplexer circuit, in order to be able to read 4 analog signals on the PCB. The other 2 can be read by the initial DS2 board.

3.5 Reprogramming of the DSP Subsystem

With the interface board built, and the connections made between the DS2 and interface boards, as well as the interface board and the peripherals, the next step is to write a new set of low level routines, which control the actions of the DS2 board.

The initial code written to control the first 2 axes is unavailable to the end user. It thus cannot be modified to accommodate another 2 degrees of freedom. In order to accommodate a new DS2 card, it is first necessary to know the inner workings of the DSP servo software.

It is required that each controller written in C have two functions, *init-control()*

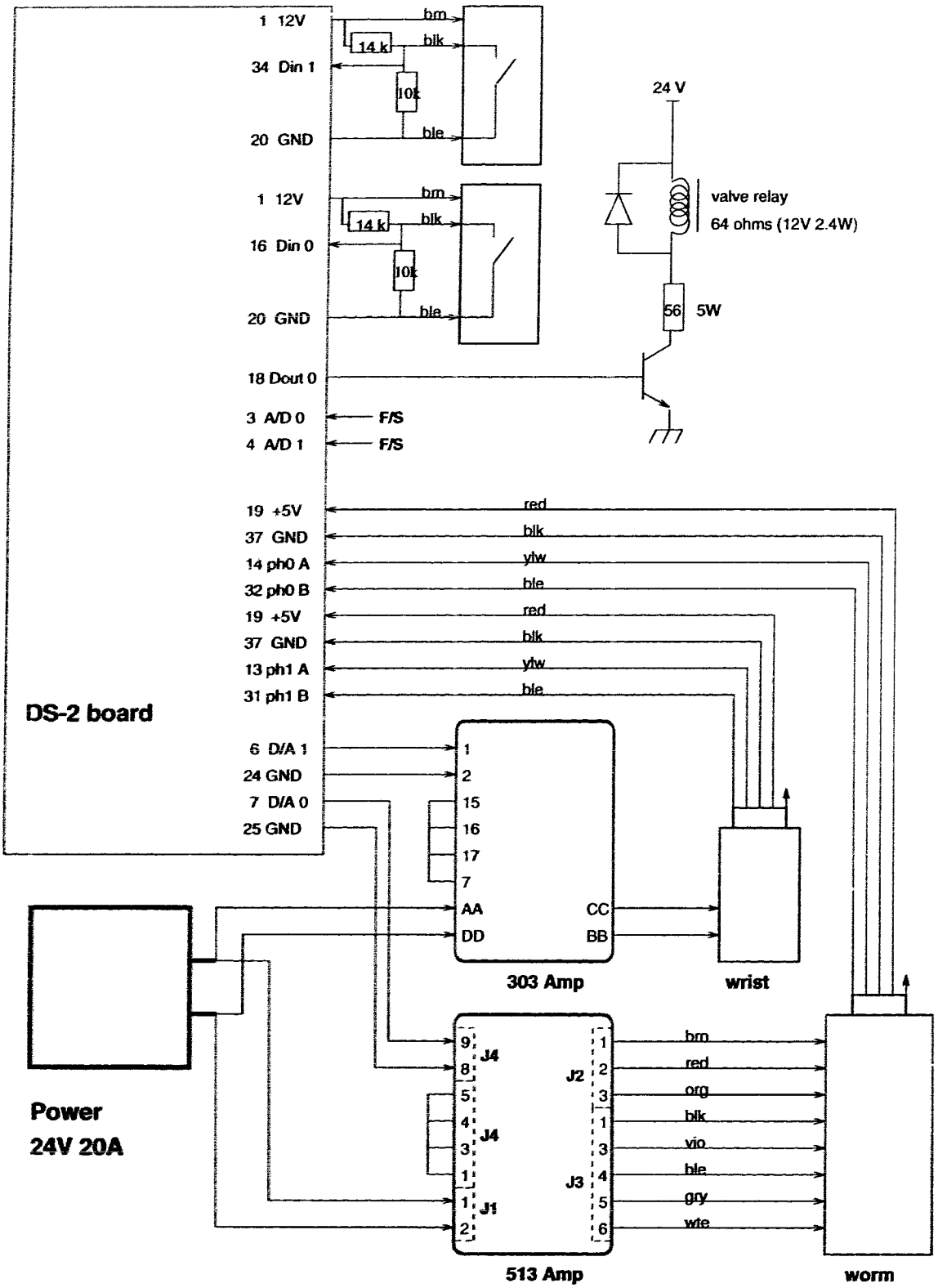

Figure 3.4: Functional Wiring Diagram

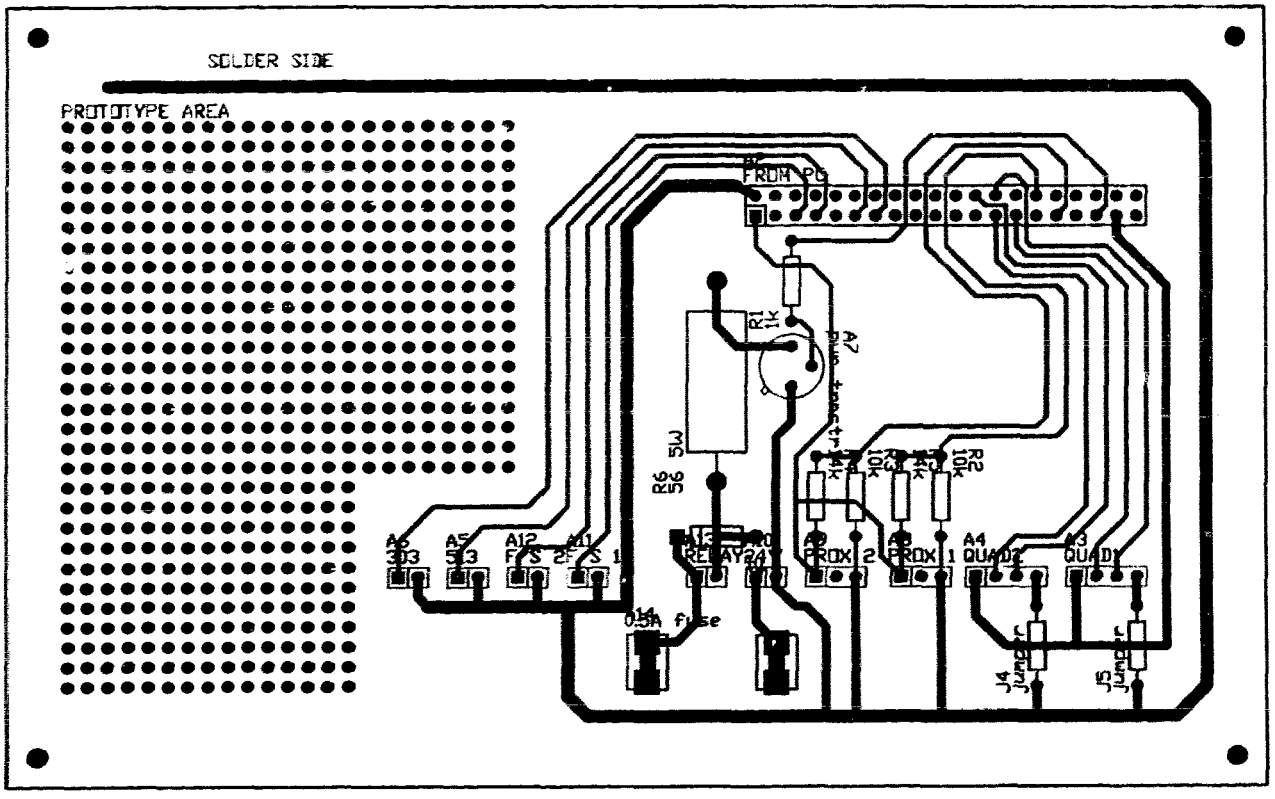

DISCRETE Check Plot

Figure 3.5: Actual Schematic Used

and *control()*. These functions reside elsewhere on the system and are unavailable to the user. *init-control()* is responsible for initializing the first DS2 card that came with the system. The function must be called even if it is empty. Once the algorithm is enabled, the first function to get executed is *init-control()*. Then at every sample period the code residing within the *control()* function in the C code gets executed. In order for the new code to work just like the existing code, and for it to be transparent to the user, it was decided to make three major functions which would incorporate all the routines necessary to make the second DS2 card as functional as the first, and just call them from within the appropriate routine. This way the end user need not concern themselves with the intricacies of how information is processed, they simply need to read certain variables, or set certain variables within the *control()* routine as desired.

Once the control algorithm is downloaded, there is a routine called *init-control()* which automatically gets executed before anything else. If there are variables that the user would like to initialize BEFORE the controller is activated, this is where they are initialized. Initializing the variables that are associated with the second DS2 card is necessary. These variables include setting the initial lead length and wrist angle, and initializing the DAC's on the board. Thus a routine was created, called *initialize-card2()*, which does all these functions. It is called from within the *init-control()* routine so that the card is initialized and ready before the control routine is activated.

When the *control()* routine is active, there are several variables that get processed automatically at each sample period, invisible to the user. Position data is updated automatically and stored in variables called *pos1* and *pos2*, in terms of encoder counts. The values of variables called *u1* and *u2* are output to the D/A converters, and are the torque values output to the motors in counts. There are no variables available to the user, but the proximity sensors that accommodate the first 2 DOF's are also read at each sample interval, and the manipulator halted if they are activated.

The new DS2 board will have similar responsibilities of its own. Outputting a value of certain reserved variables to the D/A converters for the purpose of updating the command signal to the motors, and reading the values of the optical decoders attached to each of the motors are some. There are also proximity sensors for each of the extra

2 DOF's which need to checked at every sample period. The state (*on* or *off*) of the proximity sensor can be read by the user at each ccontrol sample. There is also a gripper which needs to be controlled and monitored. There exists a reserved variable which controls the action of the gripper (*open* or *closed*), and is sent to the appropriate DIO line every sample period. The routine to maintain all this housekeeping is called *update-card2()*. It is placed within the *control* routine at the very top, so that the first thing that happens in this routine after the elbow and base links are updated, is the updating of the second 2 DOF's. The variables used in this routine are: *lead* for the distance traveled from the top of the lead in centimeters, *wrist-angle* for the angle of the wrist in radians, *worm-sensor-status* and *wrist-sensor-status* for the status of the respective proximity sensors, and the values contained in reserved variables *u-worm* and *u-wrist* are used to update the D/A converters for the command torque to the respective motors.

As with the initial configuration, the user must call a separate function from within the *control()* routine in order to read the A/D converters (which is attached to the force/torque sensor). Another routine was written which reads the A/D converters on the second DS2 card. This is called *ra2d2()* and puts analog (in this case force) data in reserved variables *analog0* and *analog1*.

3.6 Discussion

The design procedure has been outlined for the upgrade of a 2DOF planar manipulator into a 4 DOF SCARA type assembly cell. The functionality of the design has been revealed through experiments carried out in the new configuration. The manipulator is now fully capable of carrying out pick and place operations as well as force guided assembly tasks. All the design criteria were met and the overall performance satisfactory.

Due to time limitations, there are certain aspects of the manipulator that could be improved, or were not investigated at all. This work can be done in the future, or undertaken as an undergraduate project. An attempt has been made henceforth to outline some of these possibilities.

Each DS2 card has two A/D channels on them. As a result, only four analog channels can be read. The force/torque sensor however, is capable of producing 6 axes of data (three forces and three torques). Presently, the four axes that are read are XYZ forces, and one direction of torque. As figure 3.5 indicates, provisions have been made on the interface board for additional circuitry. The main intent of this was to provide for the addition of a multiplexing/demultiplexing circuit on the interface board. This would allow the two A/D channels on the DS2 board to read four analog signals, with the help of the DIO lines. In this configuration, the first DS2 board could read say X and Y data, while the second board could read Z data and the three torque axes.

The second issue which may require more attention in the future is the wrist assembly. At present, the design requires that the force/torque sensor not be fitted on to the support bracket too tightly or the rotation will be difficult. If the support nuts are too loose, vibration in motion will loosen them further, and loose nuts will block the rotation of the wrist. This design was completed with the assistance of the facility that actually machined the mechanism, and its specifics are not entirely known. Perhaps an improved design would be an interesting project for an undergraduate student interested in mechanics.

The second feature of the wrist assembly which needs some attention is the fixation of this assembly onto the shaft of the motor. If there is sufficient vibration in the wrist motor,the nuts that are against the shaft of the motor will be jarred loose, and backlash occurs in the wrist motion. If there is sufficient torque acting against the wrist motor, slipping will occur. AS mentioned previously, the specifics of the design are not known, but further investigation could lead to a solution to the problem.

It was well anticipated during the design stage that there would be a large damping effect within the worm gear assembly. This puts bounds on the performance capable of being realized for vertical motion. It was experimentally determined that there is a maximum vertical velocity of 3 cm/sec, which is consistent with the 1 inch/sec requirement in the design stage. Any attempt at higher speeds will induce cogging in the mechanism. Figure 3.6 depicts the velocity profile for the leadscrew which is close to the maximum possible before cogging starts. The graph also indicates an

acceleration which is way in excess of the 1 inch/sec required by the design procedure. This cogging is due to the high level of friction within the worm gear assembly. It is

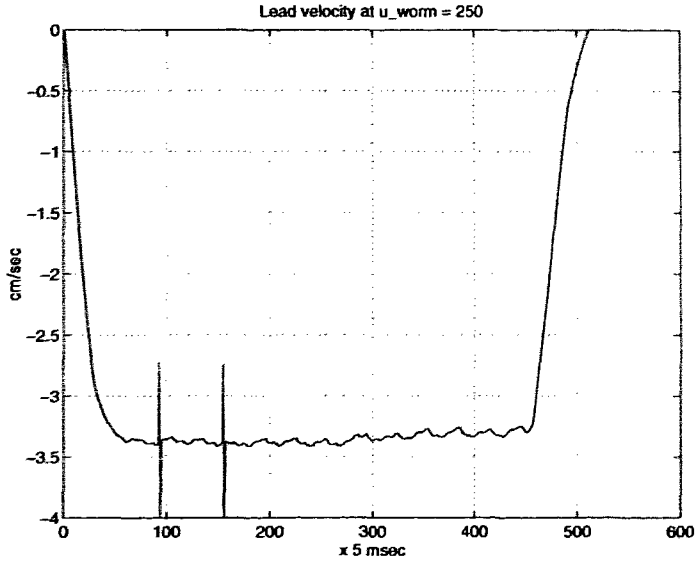

Figure 3.6: Velocity profile of the lead screw assembly

unknown at this point whether or not slipping occurs about the motor shaft as well. Future work on this mechanism could include adding a lubricant within the worm gear housing in an attempt to lower the friction level. It is presently anticipated that this would be the single most effective adjustment that would improve the performance of the lead screw/worm gear assembly. It would also reduce the backlash slightly within the mechanism. The extent of the improvement has not been gauged; thus it is not known if the overall improvement in performance (specifically, the responsiveness of the lead to a change in motor torque) would make the lead assembly any more functional than it is at present.

The fore-mentioned improvements would result in a manipulator that is much improved over the current version. As an example, due to the lack of responsiveness by the worm assembly, doing force regulation in the Z axis is impractical. The bandwidth of the worm assembly is much too small to match that of the actuating motor. The Z component of the force/torque sensor suffices only as an indicator that contact is made. The wrist would also be better able to regulate its design torque rating if

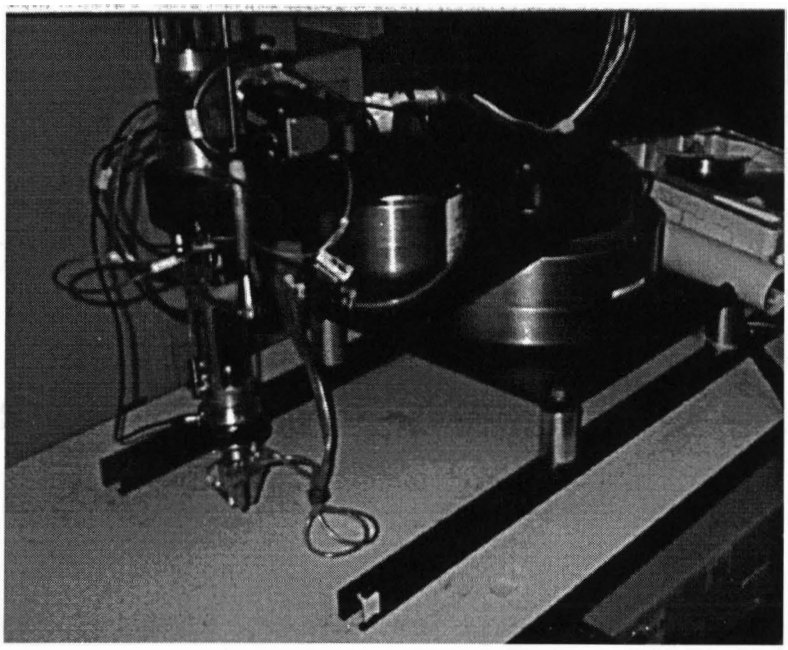

Figure 3.7: 4 DOF Manipulator assembly.

slipping did not occur. As it stands however, the manipulator functions well for its intended purpose,and it is recommended that any attempts at improving it should be done when extended periods of downtime are acceptable.

A photograph of the completed assembly is presented in figure 3.7.

Chapter 4

Extension to Constrained Motion

This chapter extends the work undertaken in chapter 2 to a manipulator under constrained motion. Constrained motion involves regulating the force of the manipulator on an environment along a desired direction, while tracking a trajectory profile along the unconstrained direction. For this purpose, the controller must be able to perform both force and position control. The intent of this chapter is to implement a hybrid controller, using the previously studied control schemes for friction compensation. The intent of this chapter is not to present a thorough analysis of constrained motion, and how to adapt these control systems for such use; the controllers are implemented on an "as is" basis, with observations made on the effect of varying the various parameteres, as opposed to any solid conclusions.

This chapter will begin by outlining a method of describing the dynamics of a robot under constrained motion. The performance of the controllers within a hybrid scheme are first looked at through simulations. This indicates how well these control schemes can be expected to perform when implemented on the manipulator. Here one can investigate the effects of differing values for pertinent parameters and gains. The control schemes are then ported to the actual manipulator, where their performance on hardware can be assessed.

The scope of this thesis precludes the investigation of the force regulation, or hybrid control in any great detail. PID control is used top regulate the force, with the gains adjusted as necessary.

4.1 Constrained Dynamics

Chapter 2 outlined the dynamics of the manipulator under free motion. It has been shown to be insufficient to use these same dynamics in an attempt to investigate a manipulator under constrained motion [23] [24]. The constraints imposed by the rigid surface must also be taken into account. What this means is that the interaction forces of the end effector in contact with the environment must be accounted for in the formulation of the manipulator dynamics. Several authors have outlined a method by which this may be done [25], [26]. The main difference between the dynamics for unconstrained motion, as described in chapter 2, and constrained motion is the requirement of the dynamic equations of motion to include these constraint forces. Friction at the contact surface implies that the constraints used for the dynamic equations are no longer holonomic, and must be reformulated using non-holonomic constraints. The method for generating the equations of motion for the constrained system is outlined in appendix B.

The next section will present the control architecture used. Following that, the results of the simulations will be presented and discussed. Then the experimental results will be examined.

4.2 Hybrid Control

Hybrid position/force control (or just hybrid control), is the scheme used in robotics to simultaneously control the force and position of a manipulator along different trajectories. A generic hybrid control scheme is presented in figure 4.1. **J** corresponds to the manipulator Jacobian, and **S** is the selection matrix [27] for the trajectory. The control scheme for the work in this chapter is shown schematically in figure 4.2. Note the absence of a selection matrix **S** in this hybrid control system. This is possible since the physical setup for the experiments and the simulations uses a contact surface that is allways parallel to the trajectory, and the trajectory is along the X axis (see figure 4.3)).

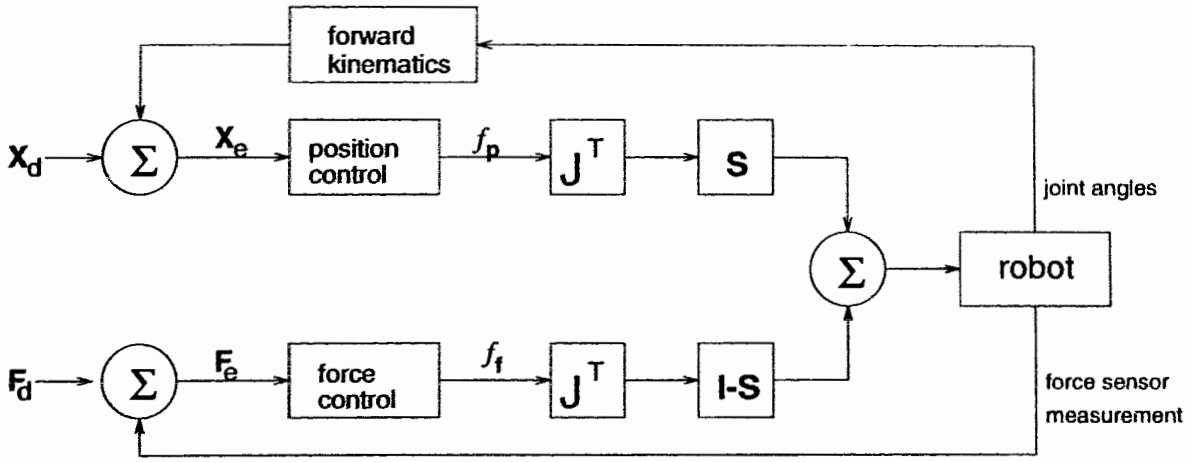

Figure 4.1: Block diagram of generic hybrid control system.

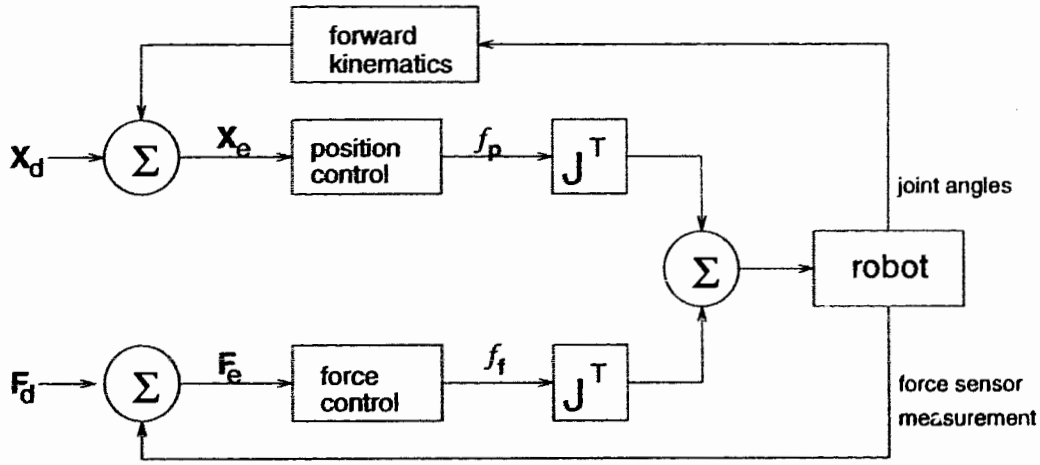

Figure 4.2: Schematic of control system used for hybrid control

4.3 Simulations

The system is simulated to examine the effect of different classes of controllers and the effect of their parameters on a manipulator undergoing constrained motion with friction. The system simulated is described mathematically as,

$$\mathbf{I}(\mathbf{q})\ddot{\mathbf{q}} + \mathbf{C}(\mathbf{q},\dot{\mathbf{q}})\dot{\mathbf{q}} + \tau_{\mathbf{f}}(\dot{\mathbf{q}}) + \mathbf{J}^{\mathbf{T}}(\mathbf{F}_{\mathbf{f}}(\dot{\mathbf{y}},\mathbf{f}_{\mathbf{y}})) = \tau \tag{4.1}$$

where $F_f(\dot{y}, f_y)$ is the friction experienced by the end effector as it slides along the surface in the Y direction. The closed loop system dynamics is completed by substituting any of the controllers of the previous chapter, (2.7), (2.10), (2.12 and 2.13), (2.18 and

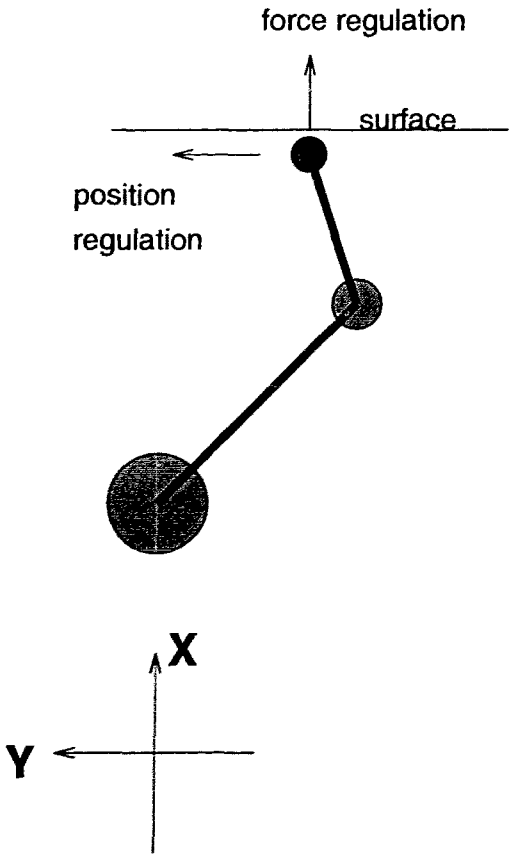

Figure 4.3: 2 DOF planar manipulator for hybrid control

2.19), for τ. The model is the same as that used for free motion with the following additions:

- The trajectory of the end effector is now a straight line in the global Y direction.
- The end effector exerts a force in the global X direction throughout its trajectory. This force is modeled as a spring (spring constant $k = 10^5$) on the environment.
- The friction model used for the surface is similar to that used for joint friction, with the exception that there is no viscous effect (as in figure 1.2 a), and that the stiction level is proportional to the normal force. Dry friction only was used since the contacting surfaces had no lubricating medium between them. The values for the coefficients of dry friction were taken from [28].

The simulation responses will present trajectories resulting from each of the different control methods, PD, PID, continuous nonlinear, and discontinuous nonlinear. Each set of plots includes the trajectory followed by the end effector along the X axis, the position error while tracking this trajectory, the contact force on the surface, and the velocity profile. The simulation was run so that at one second force control commences; position control starts one second later. Thus regulation along the Y axis between second one and second two is accomplished by the force control attempting to exert zero resultant force along this axis.

PD and PID control are characterized by oscillatory behavior while breaking away from static friction, and a smooth trajectory thereafter until the end of motion. The PID controller offered superior position tracking (fig. 4.7) over its counterpart without an integrator. The PID controller peaks at an error of about 2 millimeters and then resides to zero thereafter. The PD controller's position error (fig. 4.5) increases to a peak of 8 millimeters throughout the trajectory. Force regulation for each controller was smooth once the static friction was overcome.

The first feature that is apparent with the nonlinear controllers is their oscillatory behavior (fig's. 4.8 - 4.13). This is believed to be due to the proportional position gain that characterize them. None of the gains or parameters specific to either of these control systems could be tuned to recede this behavior. Even though the position errors are extremely small, the regulation of the force was unable to be accomplished effectively. One reason for this is the same as the case for free motion, underdamped dynamics due to dominant proportional control. This however is amplified by the nature of force control not to react gently to proportional input. Even though the proportional control on the force controller was tiny, there is a considerable contribution from the position controller. This causes the force regulation to start oscillating, which in turn is amplified to the rest of the system.

The extra torque generated by the discontinuous control system is applied until the position error is within the vicinity of zero. This is all in the form of extra proportional input. The nature of the discontinuous control system thus prevents any action from being taken to lessen the effect of its nonlinear input. Decreasing the value of q_h of (2.19) (fig. 2.5) in an effort to decrease the extra input would make the value of the

compensating torque less than that of the static friction, thus defeating the purpose of the control system. The α parameter (which affects the gradient of the slope of the control output in the vicinity of the origin) of the smooth nonlinear controller was changed to see how this would affect the response of this control method. It was found that reducing the value of α to 1000 reduced the oscillations encountered dramatically, while giving up only minor positioning accuracy.

To help illustrate this, two sets of plots are presented for the smooth nonlinear controller. One set has α set to 100,000, while the other has it set to 1000. Consider the nonlinear function $(tanh(\alpha q))$; for $\alpha = 1000$ this function does not get near its peak till about $q = 0.002$. A look at figure (4.9) shows that the position error does not exceed 0.0005 (half a millimeter). At these minute levels, the error is not enough to activate the nonlinear function for this value of α. However, when α is increased to 100,000, these errors do indeed activate the nonlinear term, causing an increased proportional gain on the system, rendering it oscillatory. Thus depending on the accuracy required, this controller may or may not be tunable as is by a designer wishing to use it with force control. The only parameters of the discontinuous control system that can be altered are the anti-stiction force applied and the position error at which it stops getting applied. This means that the nonlinear compensator will always be activated at errors very close to zero, and so oscillatory behavior of the dynamic system will persist.

4.4 Experiments

This section will describe the experimental setup, and then present how well the control schemes performed with constrained motion experiments.

4.4.1 Experimental setup

The trajectory of the manipulator was the same as that for the one used in the simulation. The end effector was initially positioned in contact with the surface. It was then moved in a straight line, while maintaining a certain force on the surface. Data from the force sensor on the end effector was found to be extremely noisy, and hence a second order low pass Butterworth filter had to be used on it. At the tip of the end effector was a circular disk in place of the gripper. The disk provided the contact interface between the end effector and the surface. The disk is able to rotate, in effect creating a 3 DOF system. The rotation on the wrist however was only used to maintain the wrist's absolute position while the two axes were moving. Its controller is independent to the rest of the system. A block diagram of the system with the independent wrist controller is shown if fig. 4.14. This is necessary for knowing that the force being read is actually the contact force of the x-axis and the surface. If this scheme were not present (say if the orientation of the disk was fixed), the forces read (X and Y in the this case) would have to be resolved to find the contact force. However, while sliding, the force that the X axis encounters will also include disturbances due to friction. These disturbances do not constitute to the contact force and will produce erroneous information.

4.4.2 Discussion and Results

A discussion will be made regarding the nature of the experimental setup and how it affected these experiments. This will provide a better appreciation of the results.

The plots for the experimental results are contained in figures (4.15) through (4.24). The position error and force regulation are plotted for each experiment with real time data taken at 3 msec. intervals.

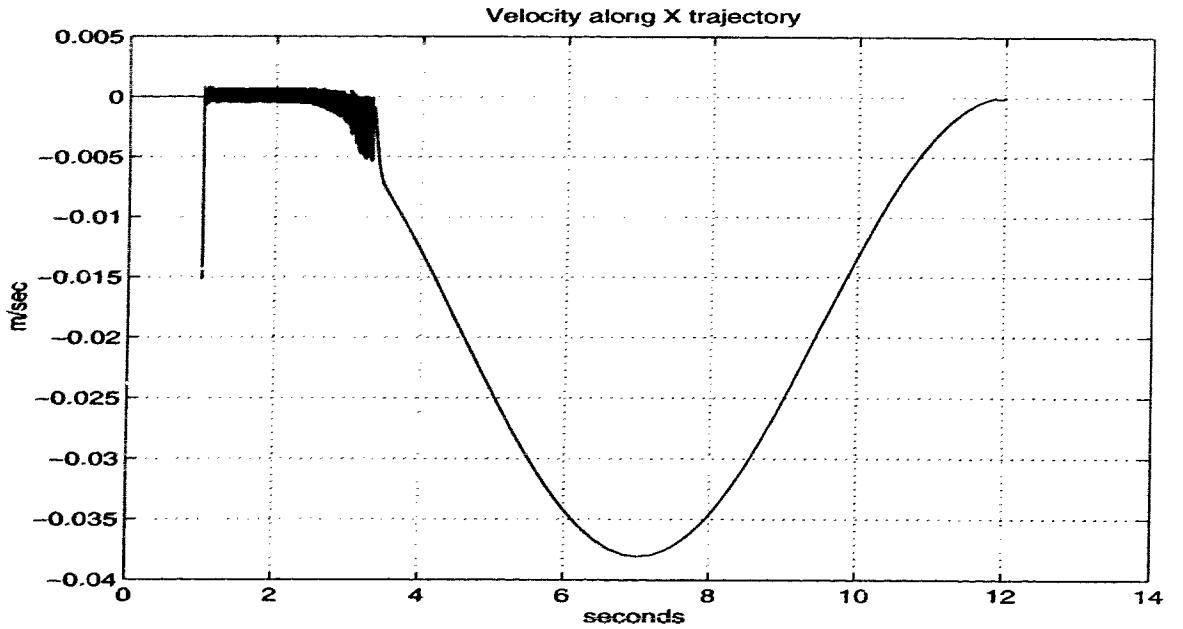

B: Velocity profile

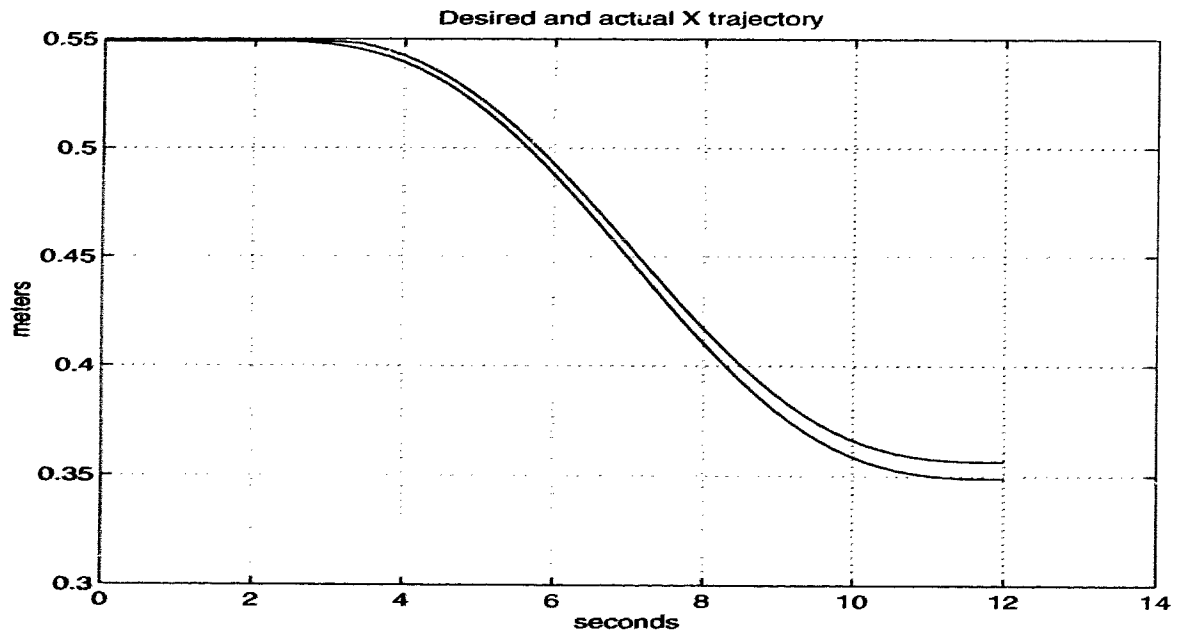

A: Position trajectory

Figure 4.4: Simulations of PD controller for constrained robot motion. A: Position Profile, B: Velocity Profile.

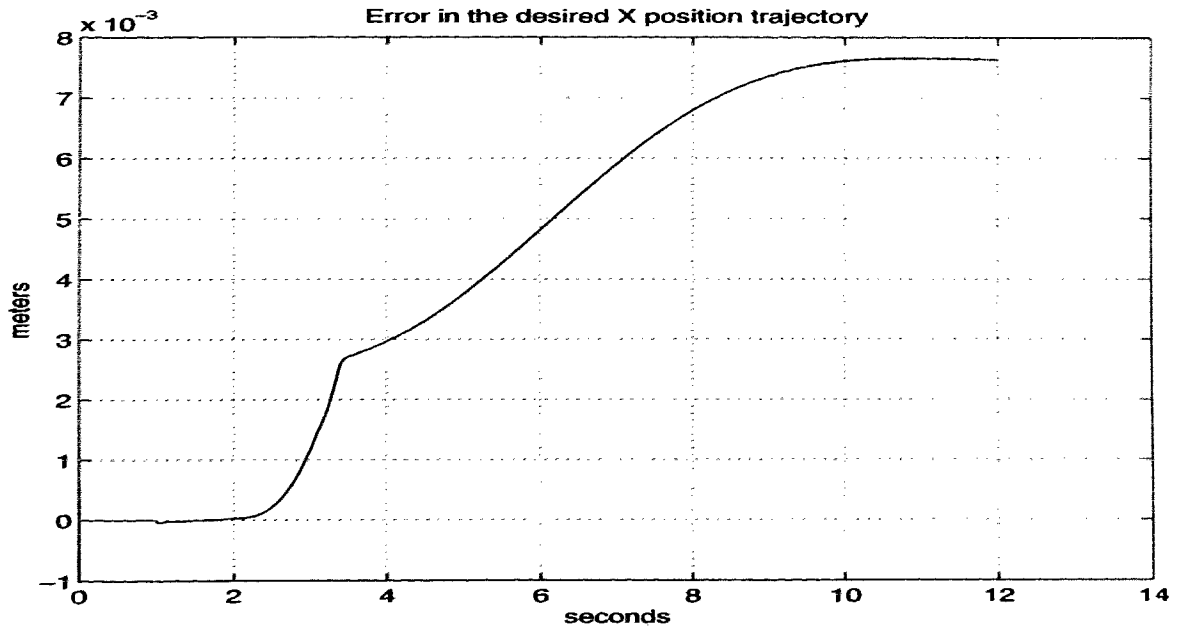

D: Position tracking error

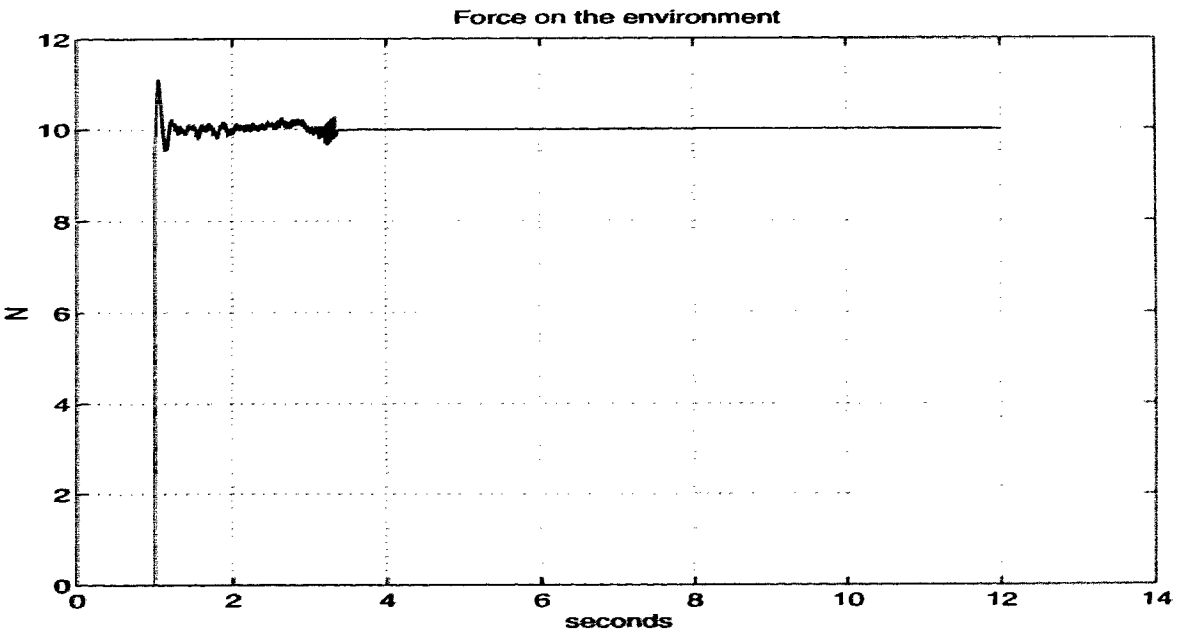

C: Regulated force

Figure 4.5: Simulations of PD controller for constrained robot motion. C: Force Profile, D: Position Error.

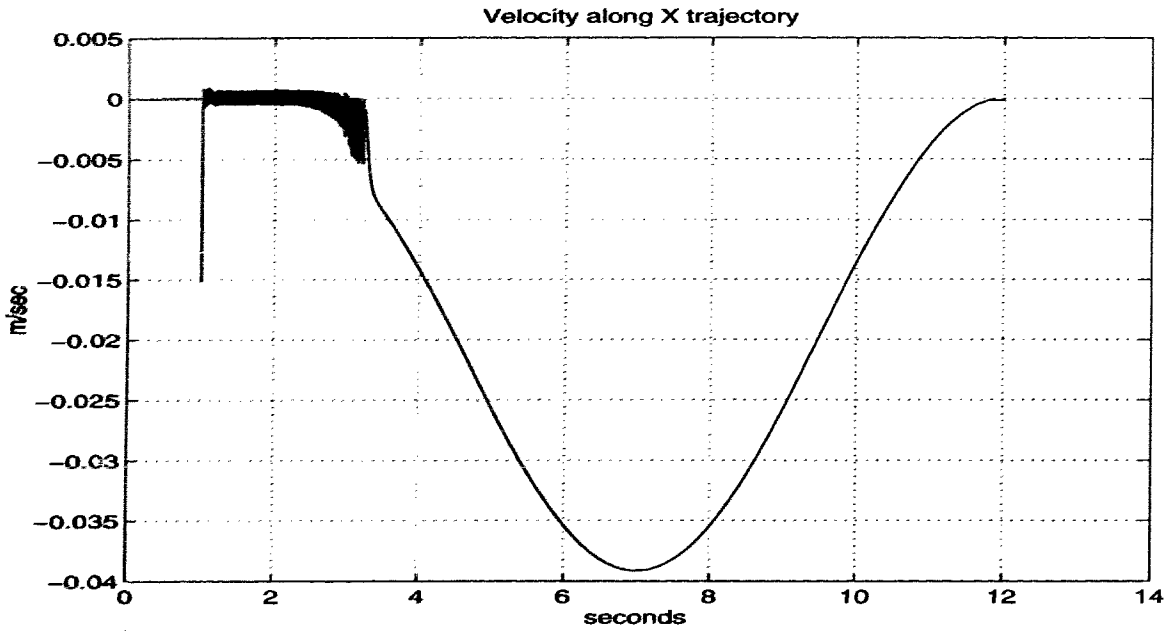

B: Velocity profile

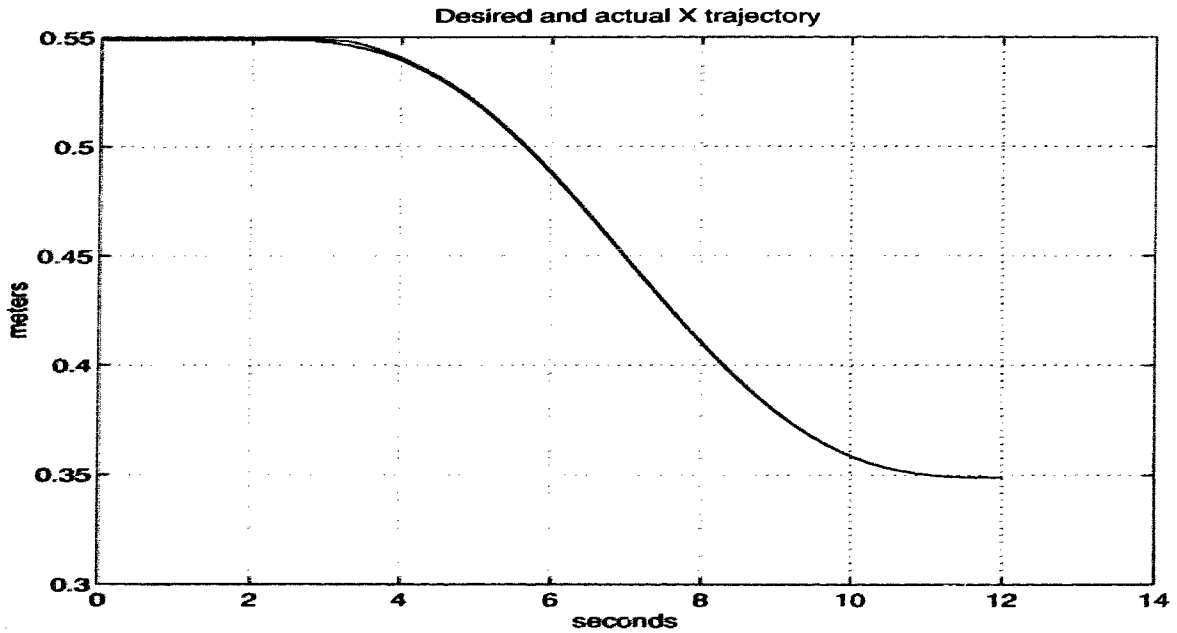

A: Position trajectory

Figure 4.6: Simulations of PID controller for constrained robot motion. A: Position Profile, B: Velocity Profile.

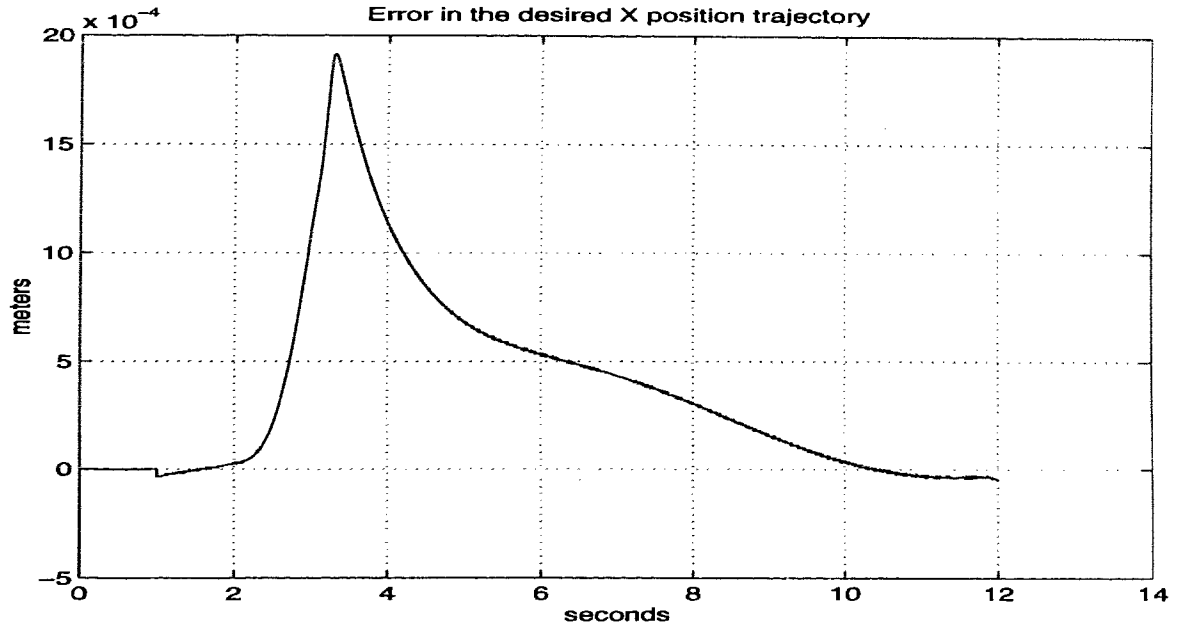

D: Position tracking error

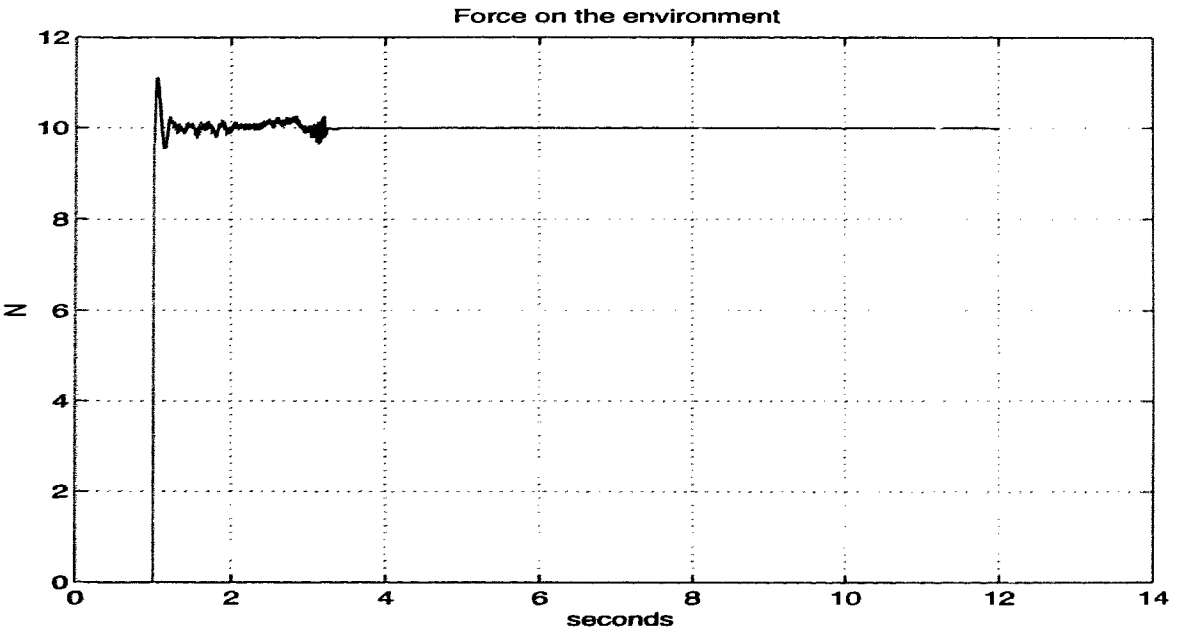

C: Regulated force

Figure 4.7: Simulations of PID controller for constrained robot motion. C: Force Profile, D: Position Error.

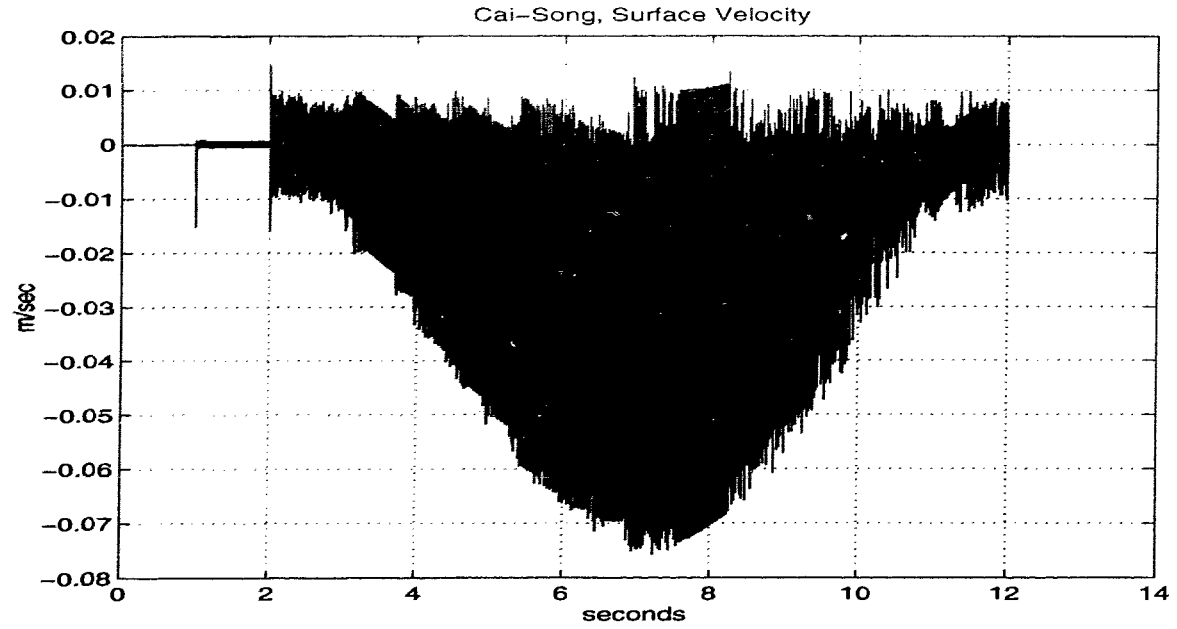

B: Velocity profile

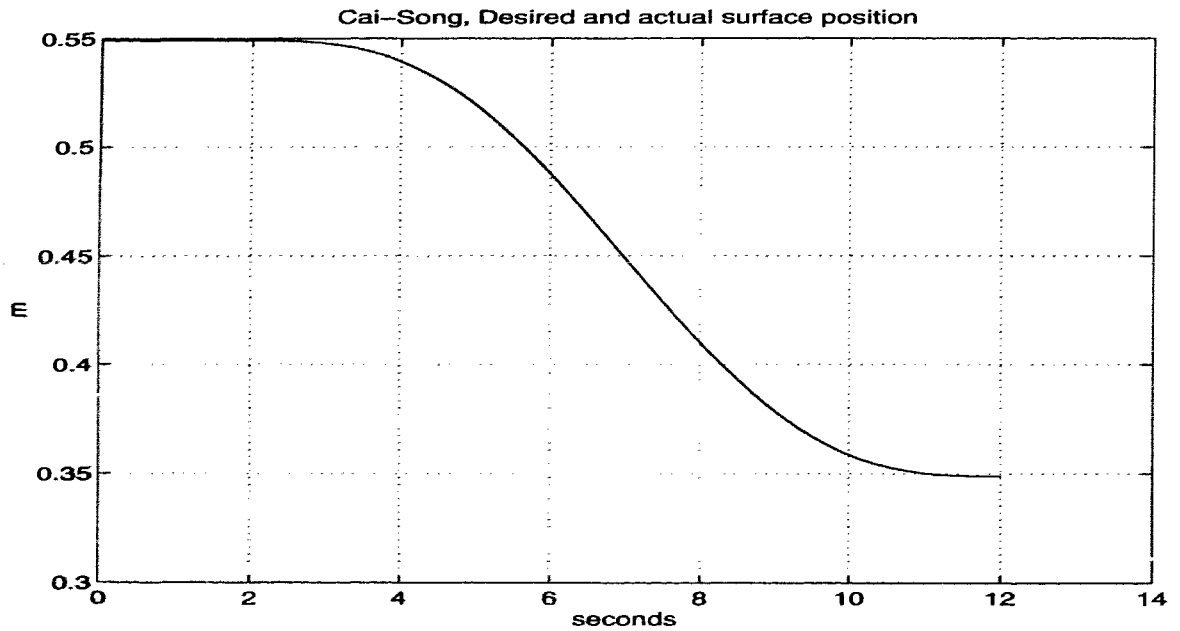

A: Position trajectory

Figure 4.8: Simulations of smooth nonlinear control system for constrained robot motion. $\alpha = 100000$. A: Position Profile. B: Velocity Profile.

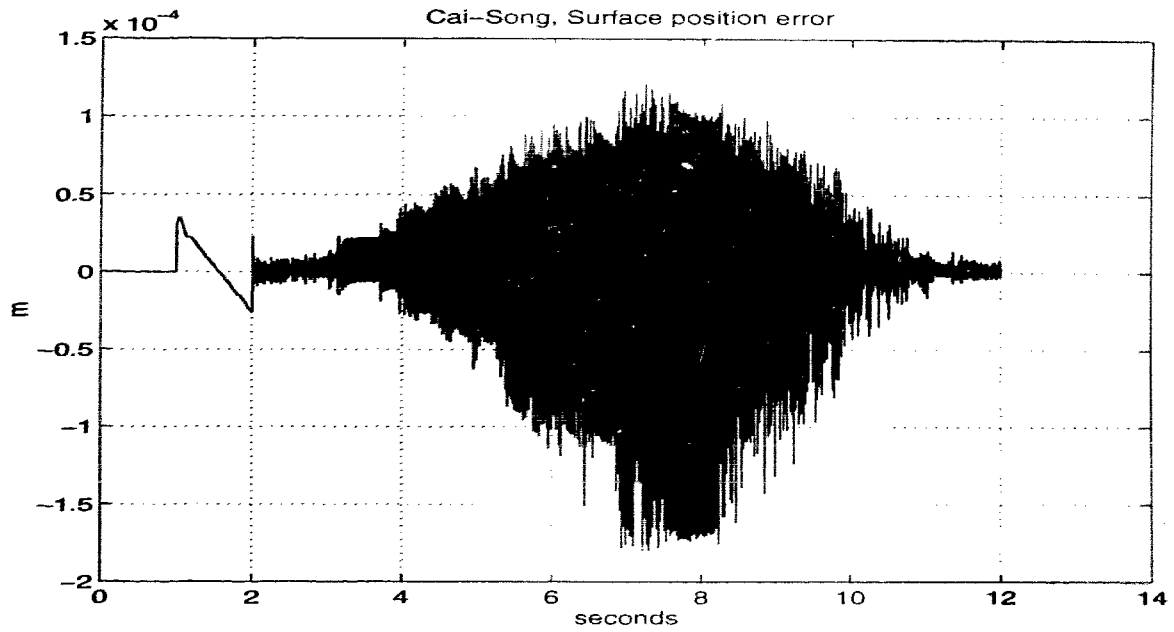

D: Position tracking error

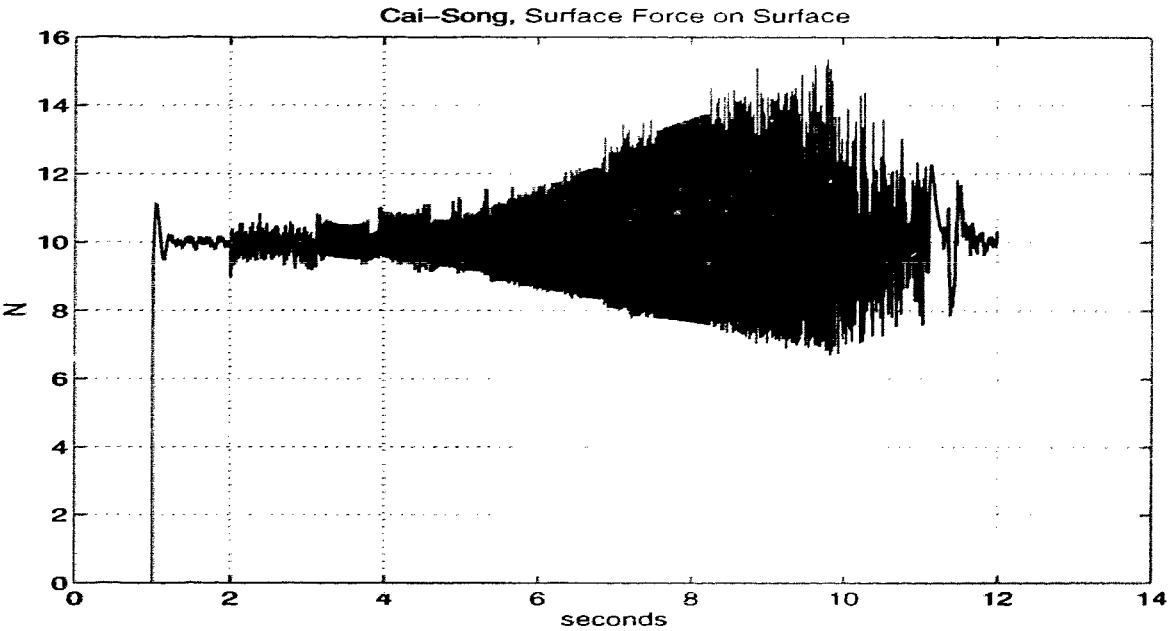

C: Regulated force

Figure 4.9: Simulations of smooth nonlinear control system for constrained robot motion. $\alpha = 100000$. C: Force Profile, D: Position Error.

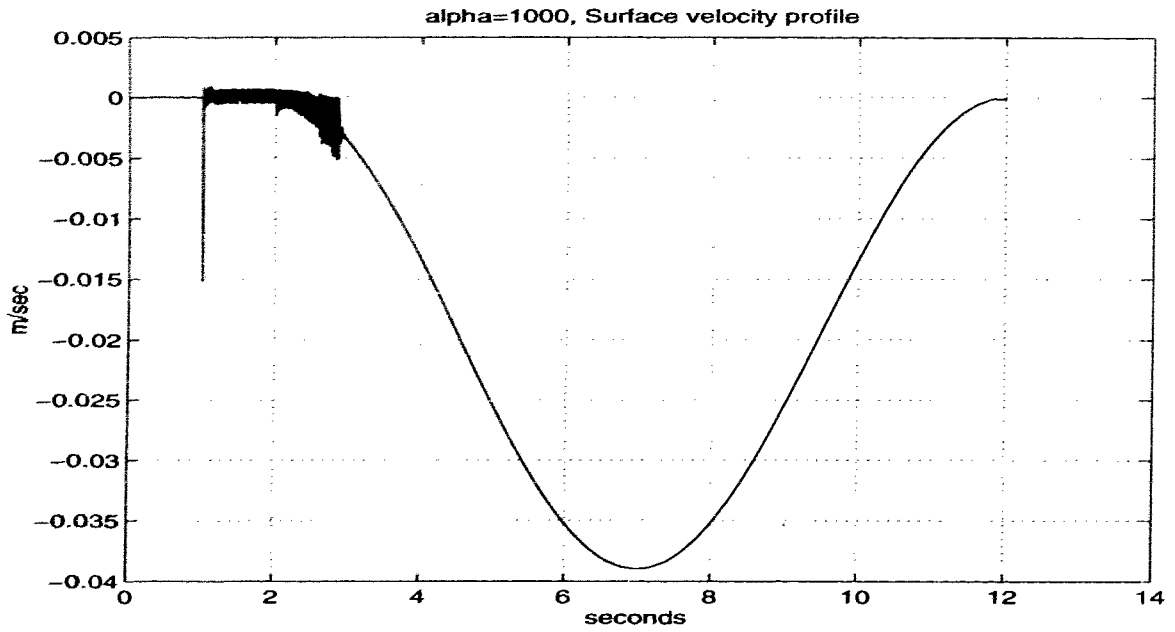

B: Velocity profile

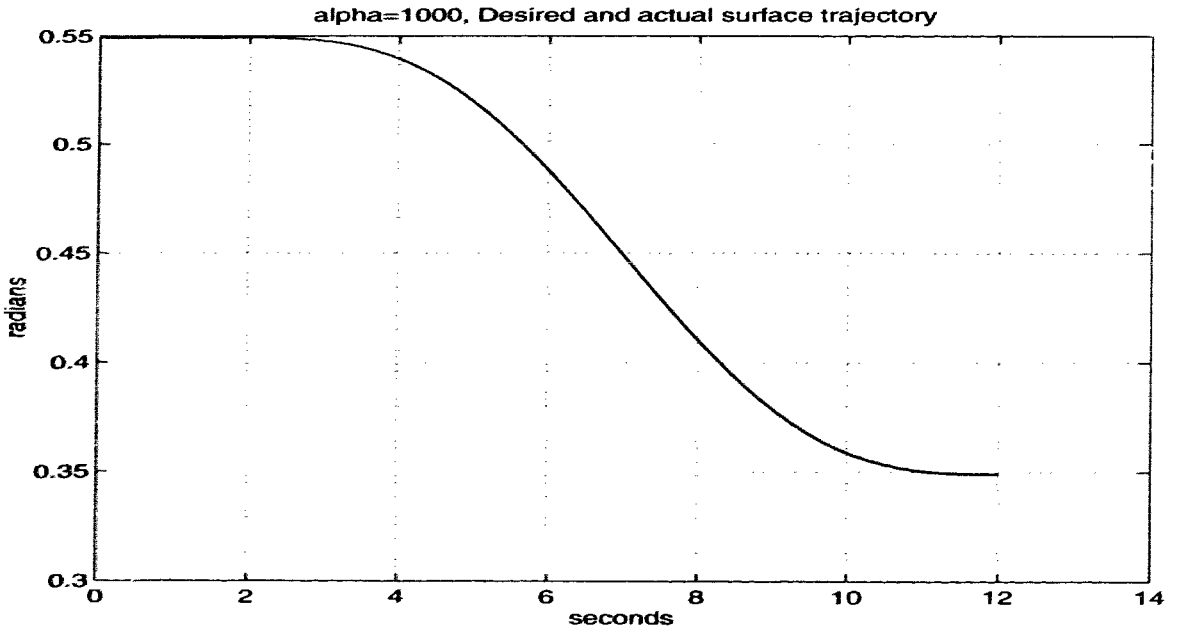

A: Position trajectory

Figure 4.10: Simulations of smooth nonlinear control system for constrained robot motion. $\alpha = 1000$. A: Position Profile, B: Velocity Profile.

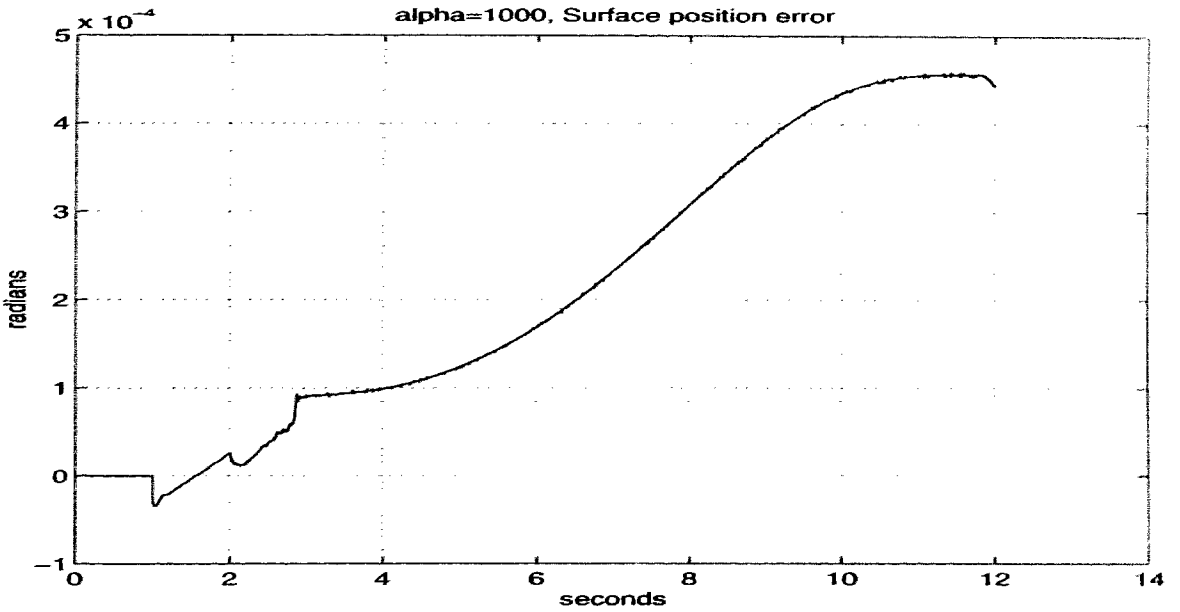

D: Position tracking error

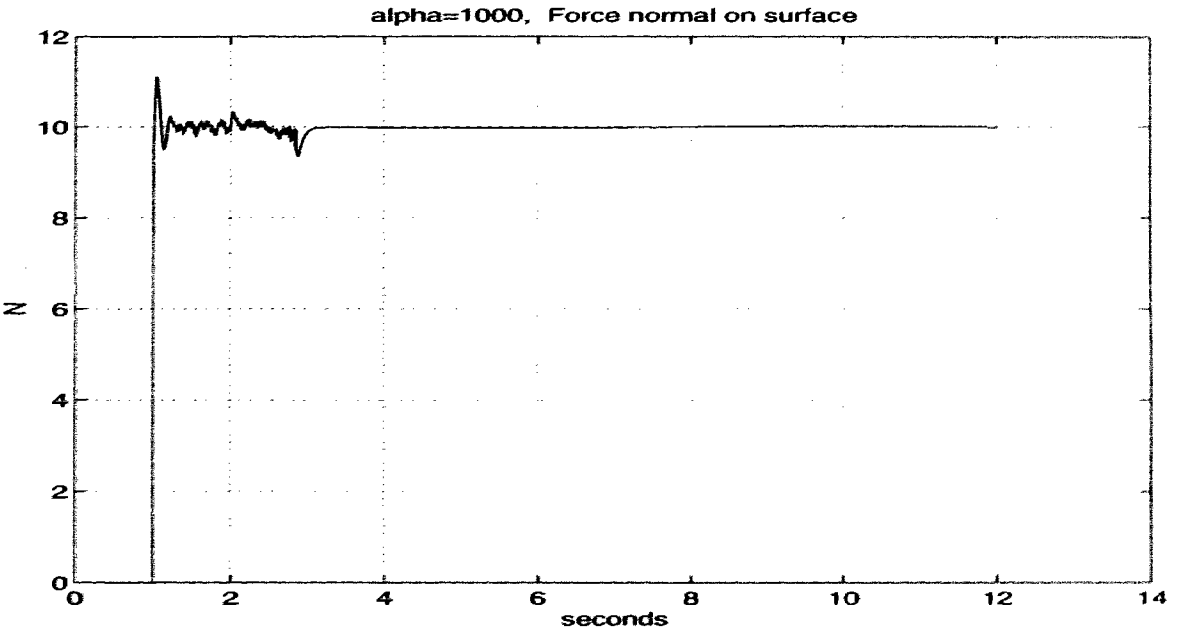

C: Regulated force

Figure 4.11: Simulations of smooth nonlinear control system for constrained robot motion. $\alpha = 1000$. C: Force Profile, D: Position Error.

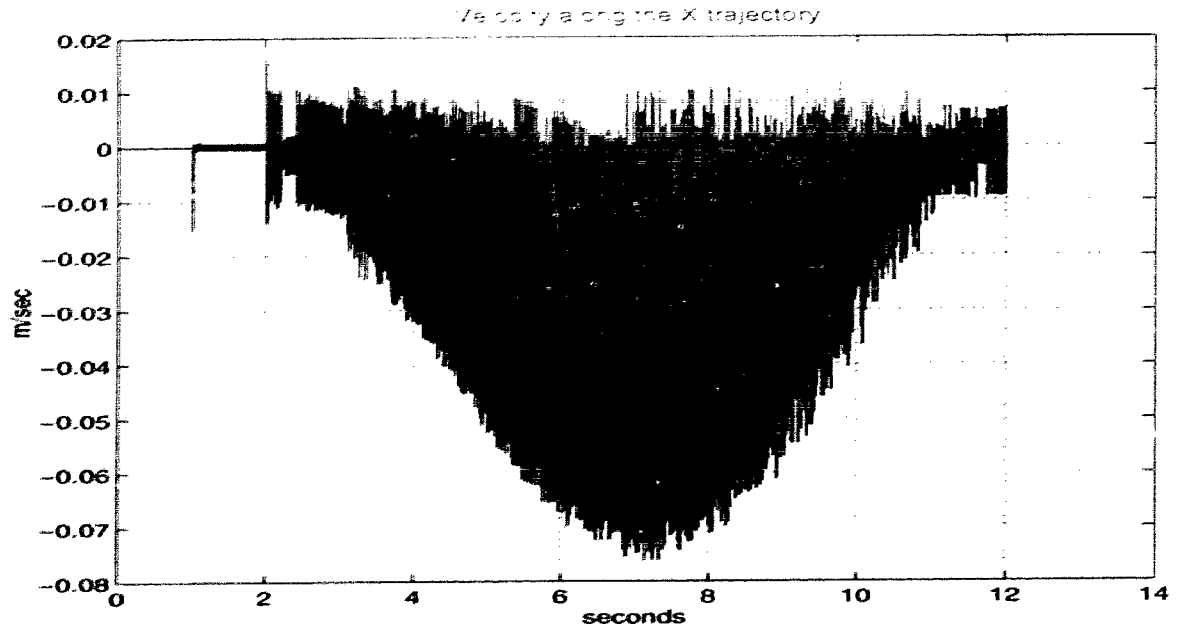

B: Velocity profile

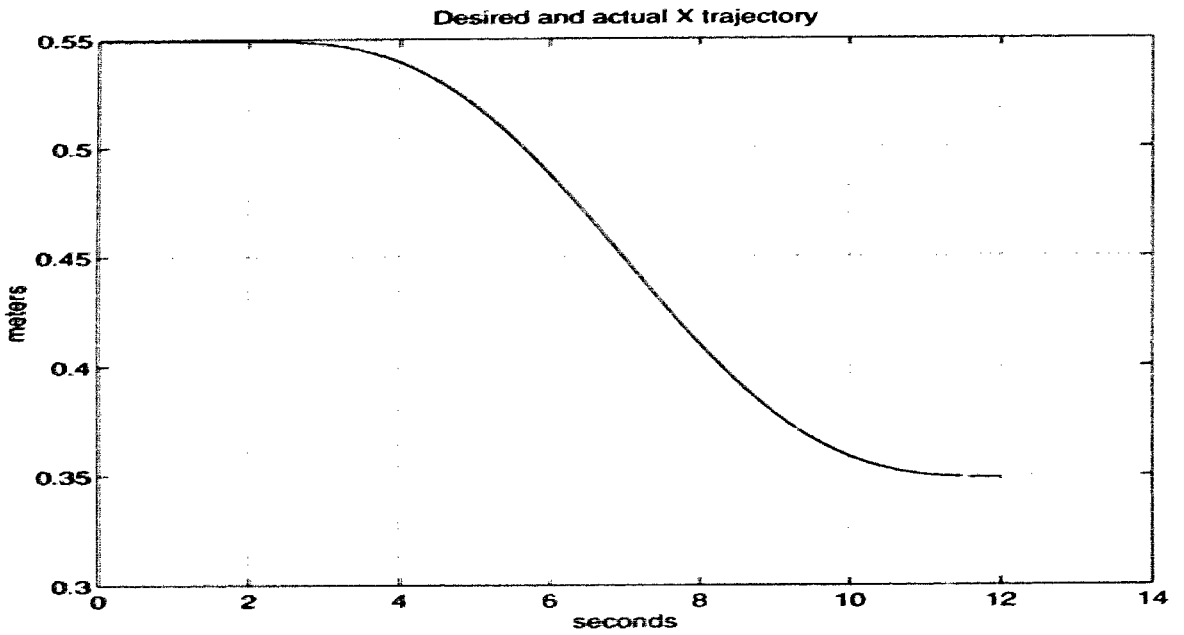

A: Position trajectory

Figure 4.12: Simulations of discontinuous controller for constrained robot motion. A: Position Profile, B: Velocity Profile.

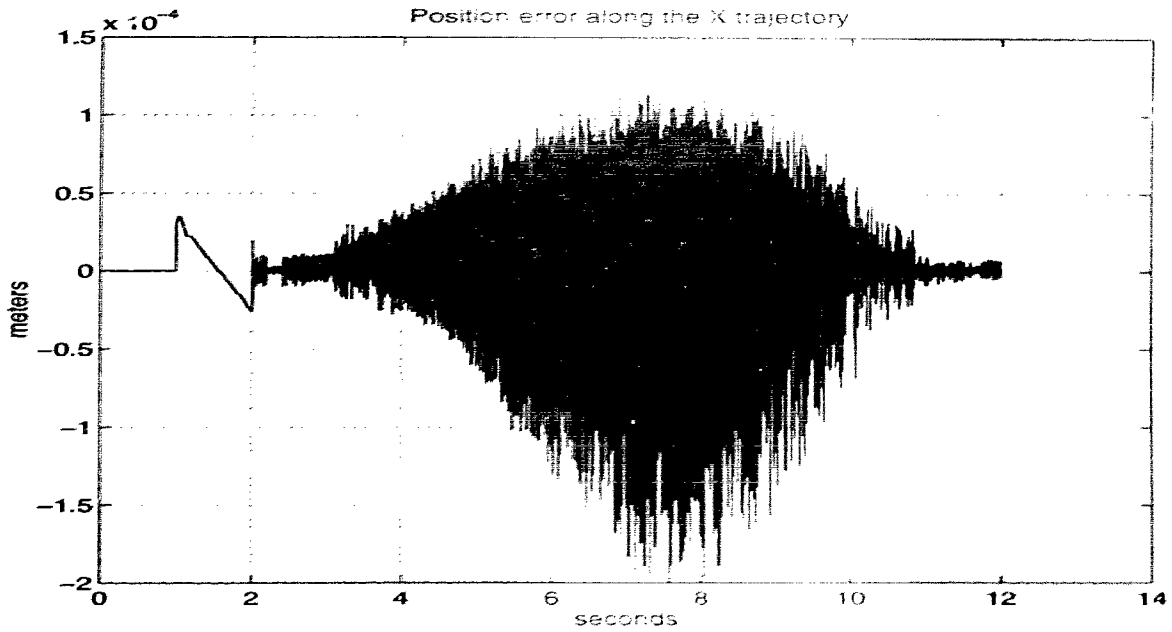

D: Position tracking error

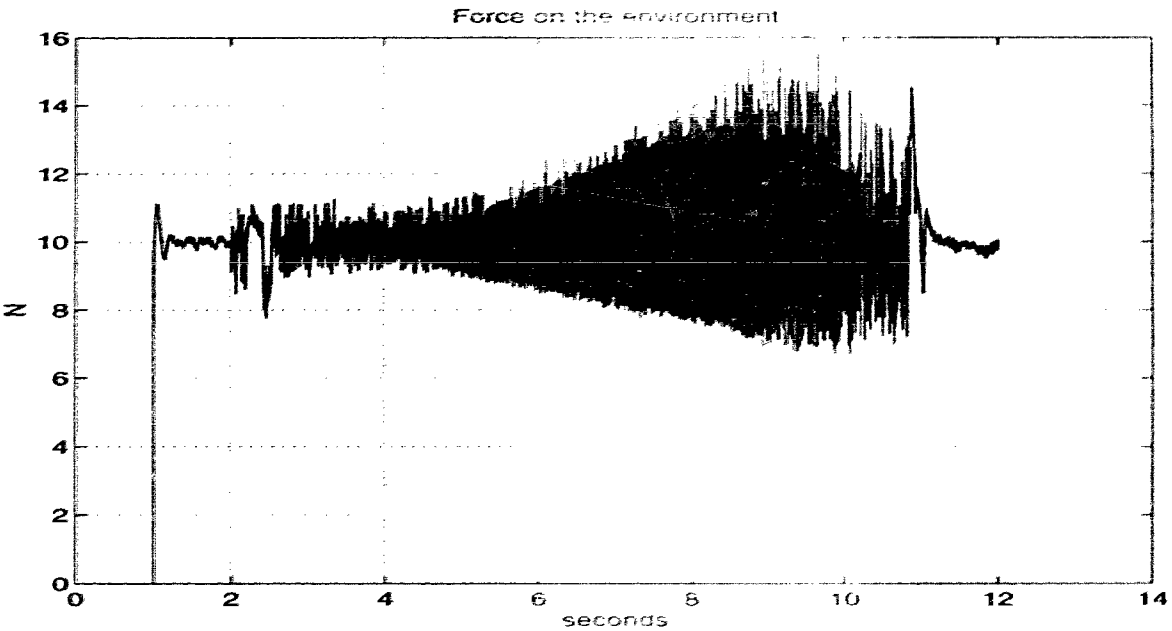

C: Regulated force

Figure 4.13: Simulations of discontinuous controller for constrained robot motion. C: Force Profile, D: Position Error.

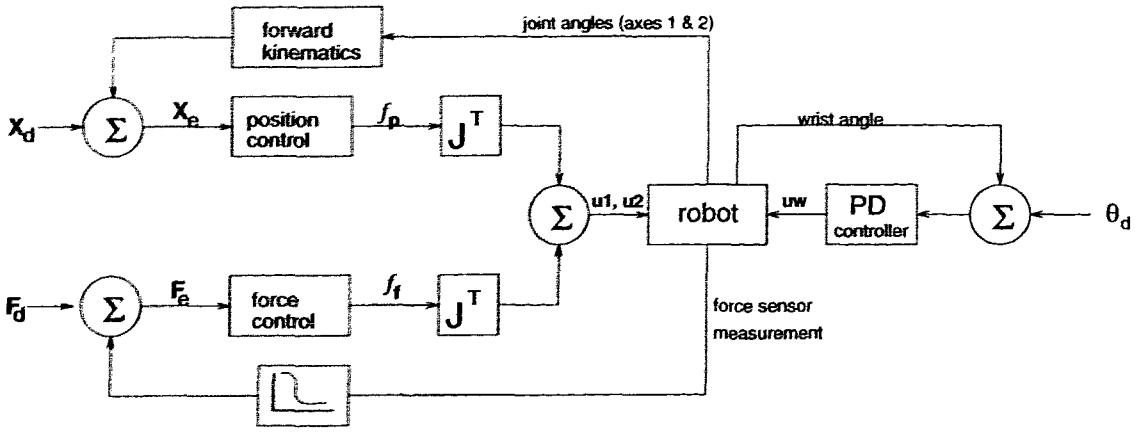

Figure 4.14: Block diagram of the controller with independent wrist correction.

The plots for each experiment reveal poor force regulation. The deficiencies with force regulation stem from the independent control scheme implemented to regulate the absolute position of the wrist. As the end effector is being pulled along the surface, the control system regulating the wrist attempts to correct the position of the wrist, relative to the joint angles of the 2 links, in an attempt to maintain an absolute direction on the wrist. As the wrist corrects its position while it is in contact with the surface, a resultant torque is generated which is read by the force sensor. The force sensor is unable to determine the cause of this disturbance, and assumes that it is pressing too hard. This disturbance causes the force regulator to be unable to properly interpret the contact force coming from the force sensor. As a result, the end effector has a tendency to prematurely lose contact with the surface. To illustrate this, the position data was taken at the wrist while the manipulator was in motion and shown in figure (4.16).

It is also worth pointing out that when there is no contact with the surface, position regulation is much improved due to the lack of surface friction working against motion. The same concept applies when the magnitude of the contact force is smaller. Since the opposition due to friction is proportional to the normal force, a trajectory that experiences a smaller contact force will exhibit better position tracking characteristics. Thus for trajectories that exhibited poor force regulation, it is not unexpected to find good position tracking results.

The changes in control gains for the linear control systems were too inconsistent to be correlated in any way. PD control shows almost identical tracking for the different proportional gains. It is to be expected that at the very least. the initial error due to stiction would be reduced somewhat by the increase in proportional gain. This was not the case and is believed to be due to inconsistencies in the regulating force. The force signal that is presented here is low-pass filtered. The actual force signal contains much more noise, thus the force reading may not be very accurate. To illustrate this, the unfiltered force signal for the PD controller of figure (4.15) is plotted (figure 4.16). The PD controller with a higher gain is plotted in figure (4.17); a comparison with figure (4.15) will reveal little difference in the tracking accuracy. The response of the PID controller reveals errors of a similar magnitude to that of the PD controlled manipulator. Comparing figures (4.18) and (4.19) suggests that a higher integral gain causes a limit cycle t occur. It is also apparent that the startup error due to stiction diminishes when the integral error is increased.

For the nonlinear controllers, changes in the nonlinear parameters had more resounding effects than merely changing the control gains. Changes in the parameter α for the smooth nonlinear controller can be seen to affect the system through figures (4.20) and (4.21). A nonlinear function ($tanh(\alpha q)$) which is too steep about the origin will instigate chatter in the force regulation. The tracking error when $\alpha = 500$ is also much superior. The steep slope of the nonlinear function about the origin implies a large proportional gain when the position error is small. This result is consistent with the simulations, which exhibited similar oscillatory behavior for functions with large values for α. The discontinuous controller inherently displayed poor performance. Not surprisingly since the control output when the position error is small, is always large enough to overcome the stiction. This can be interpreted as the smooth nonlinear function about the origin with an α of ∞. The discontinuous controller continuously exhibited chattering. The parameters investigated were the effect of the anti-stiction torque level and the artificial zero bound. The chattering increased somewhat with an increase in the anti-stiction torque, however it was found that the artificial zero bound could not be made too small (see figures 4.22 to 4.24). In changing the error tolerance from 0.1 millimeters to 0.01 millimeters, the chattering against the surface

became so hard that it consistently triggered an emergency stop programmed into the control routine to prevent the end effector from being damaged by contact force. This is illustrated in figure (4.24), where one can see the control routine prematurely coming to an end.

One may conclude then that the smooth continuous nonlinear controller is advantageous as a controller for constrained motion due to its flexibility. The ability to change the anti stiction torque level ($\tau_m stk$) and the slope of the nonlinear function about the origin (by changing the value for α) means a designer can fine tune this system to a greater level than the other control systems. It was stated that due to restraints with the 4 DOF system the conclusions regarding the linear controllers are vague at best. However, it is possible to use the smooth nonlinear controller as a PD control system (setting τ_{mstk} to zero), which implies that it is superior to just a PD controller by itself. While it is difficult to judge the performance of the PID relative to the others, it was noticed that a large enough integral gain would instigate a limit cycle. The PID does offer an extra degree of freedom over the PD controller in tuning parameters through its integrator. However, the tunable parameters of the smooth nonlinear controller (steepness of the nonlinear function about the origin and the stiction level) are believed to be more effective in creating accurate and stable force/position regulation.

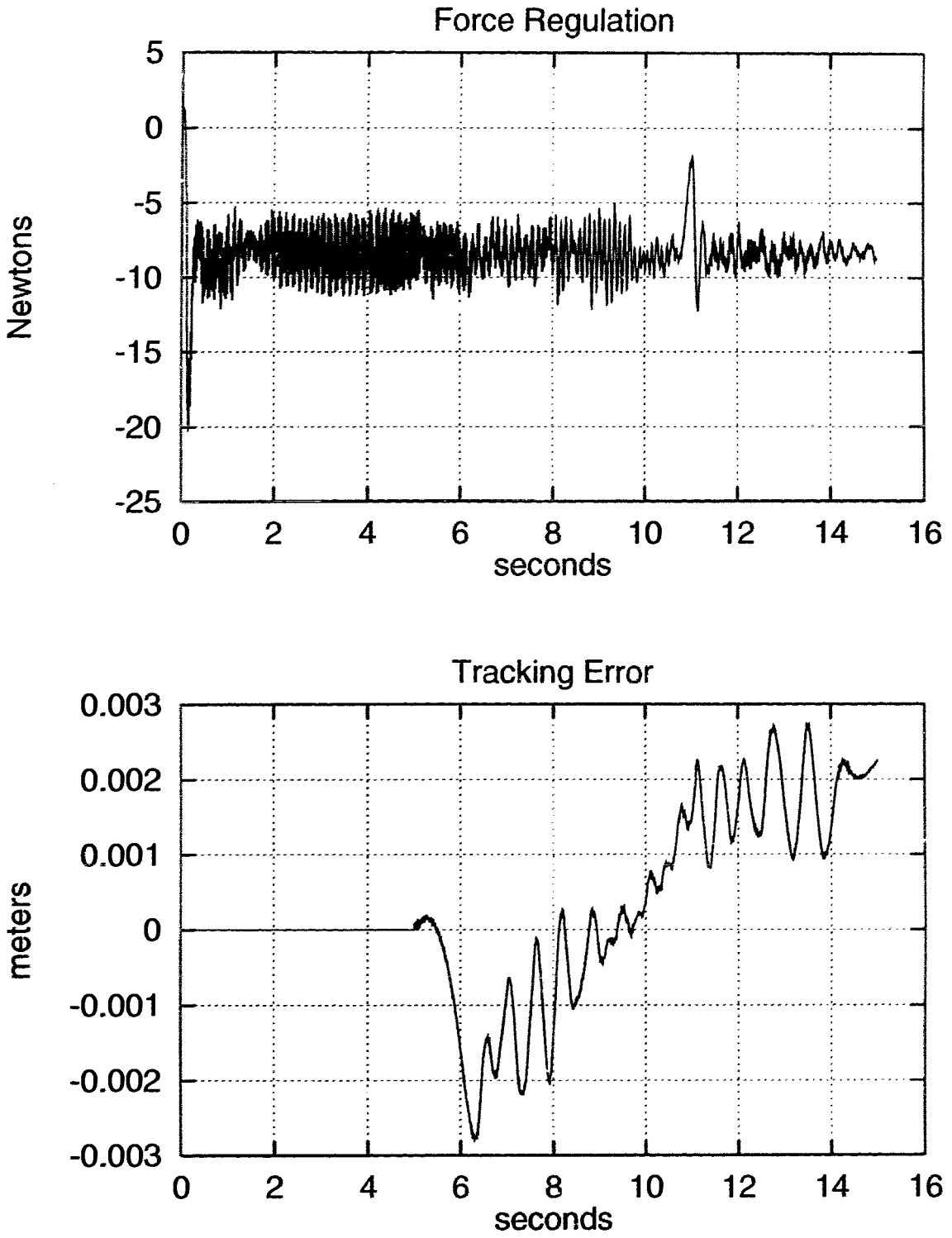

Figure 4.15: Experimental results: PD position control. Kp = 150, Kd = 4

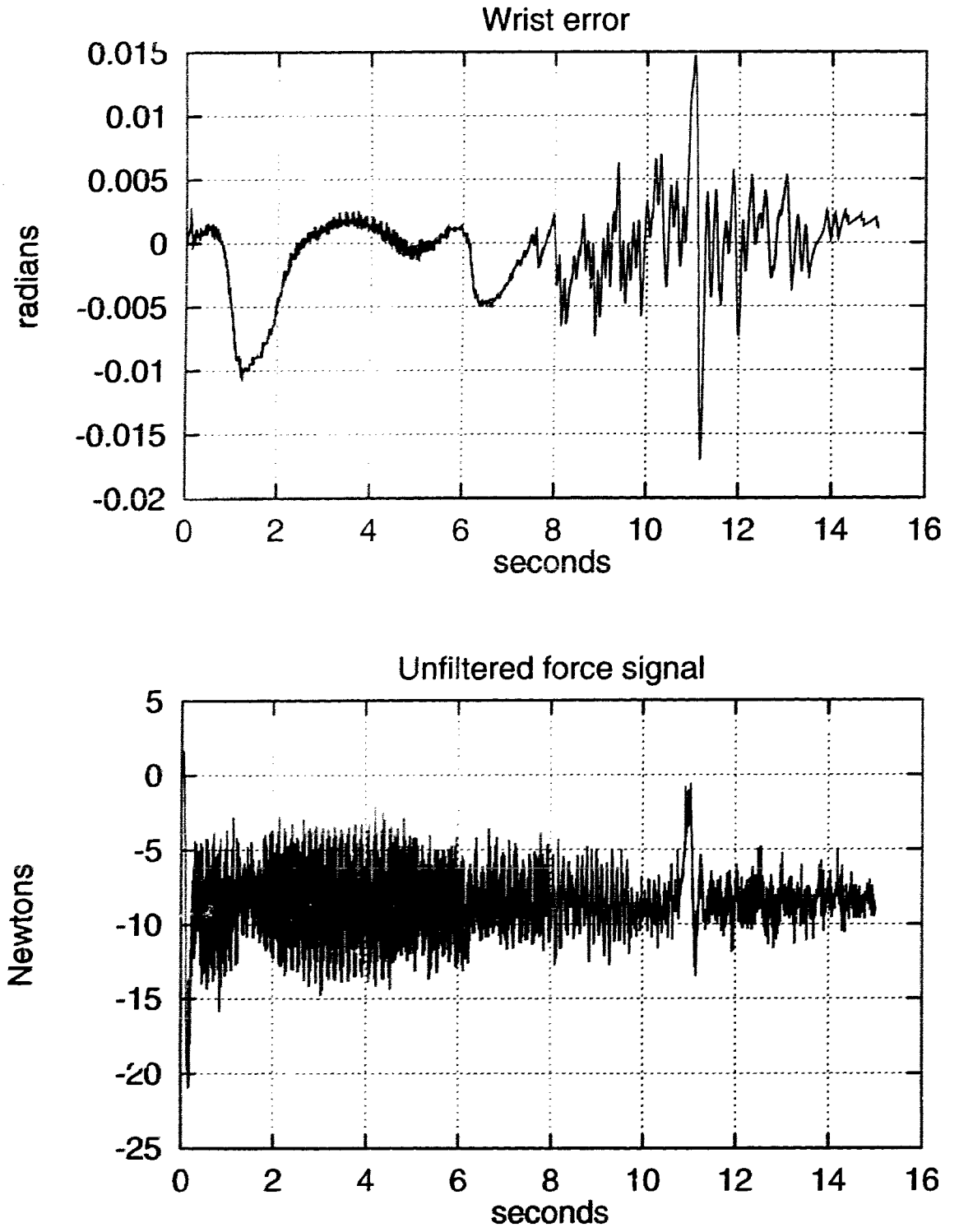

Figure 4.16: Experimental results: PD position control. Kp = 150, Kd = 4

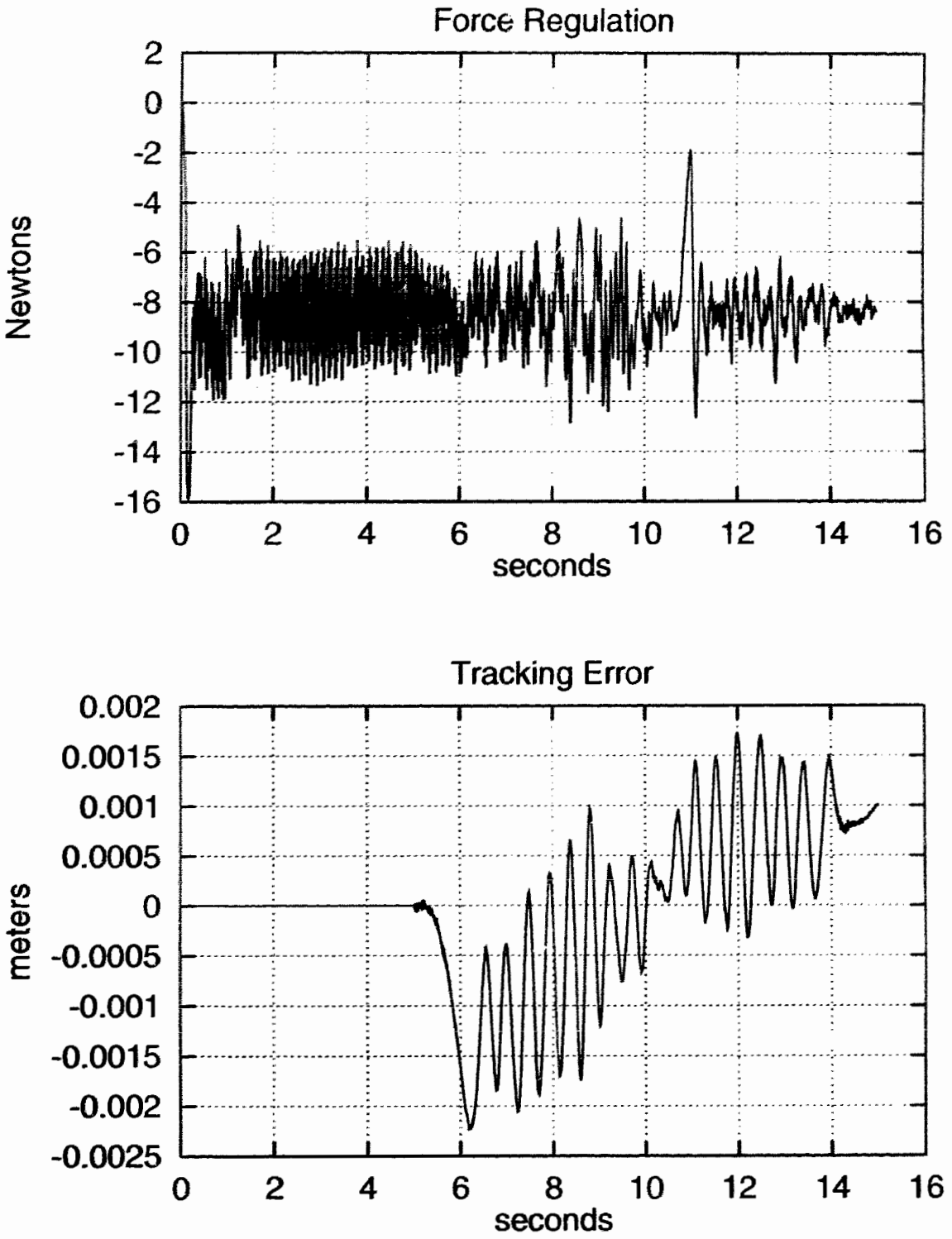

Figure 4.17: Experimental results: PD position control. Kp = 250, Kd = 4

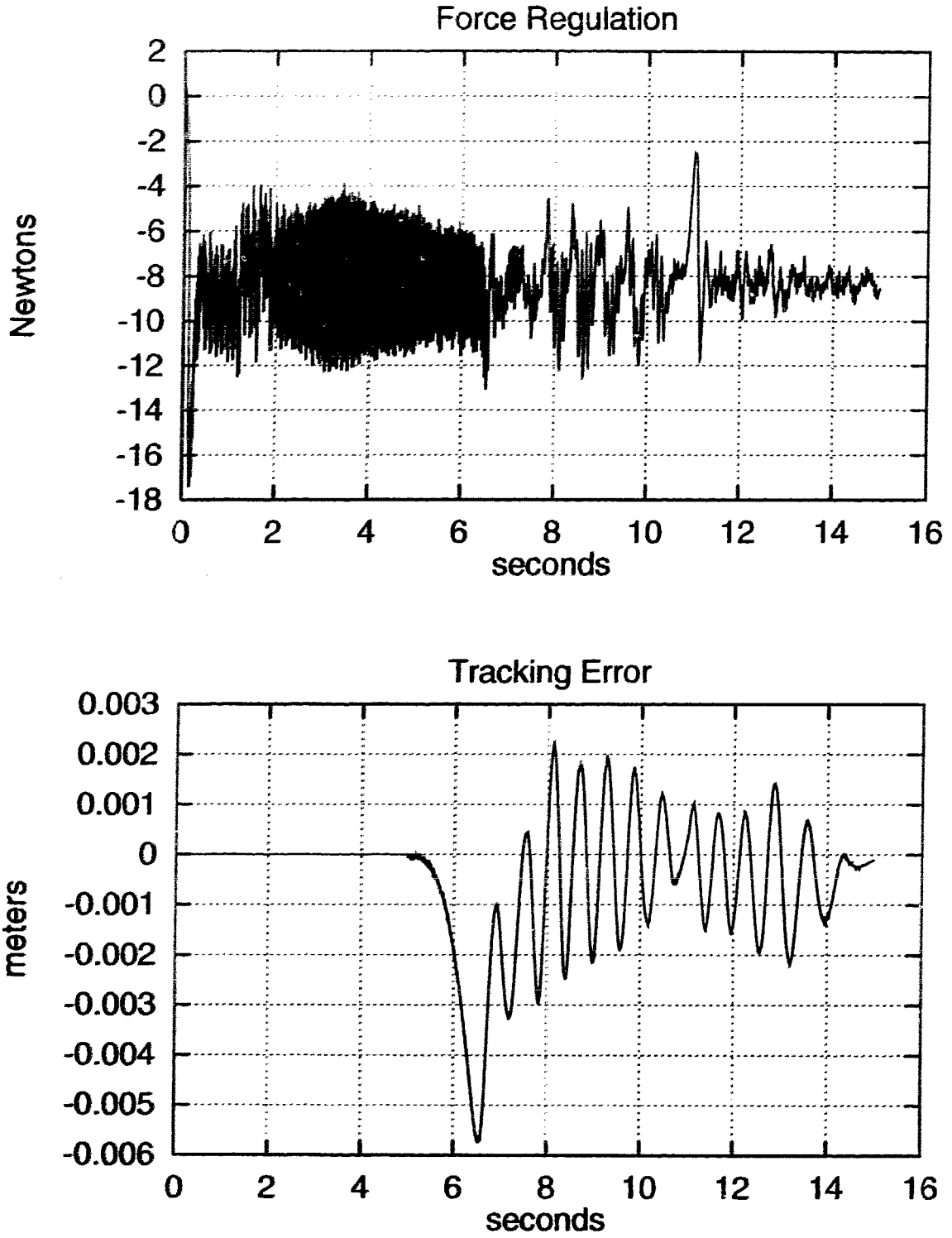

Figure 4.18: Experimental results: PID control. Kp = 150, Ki = 200, Kd = 4

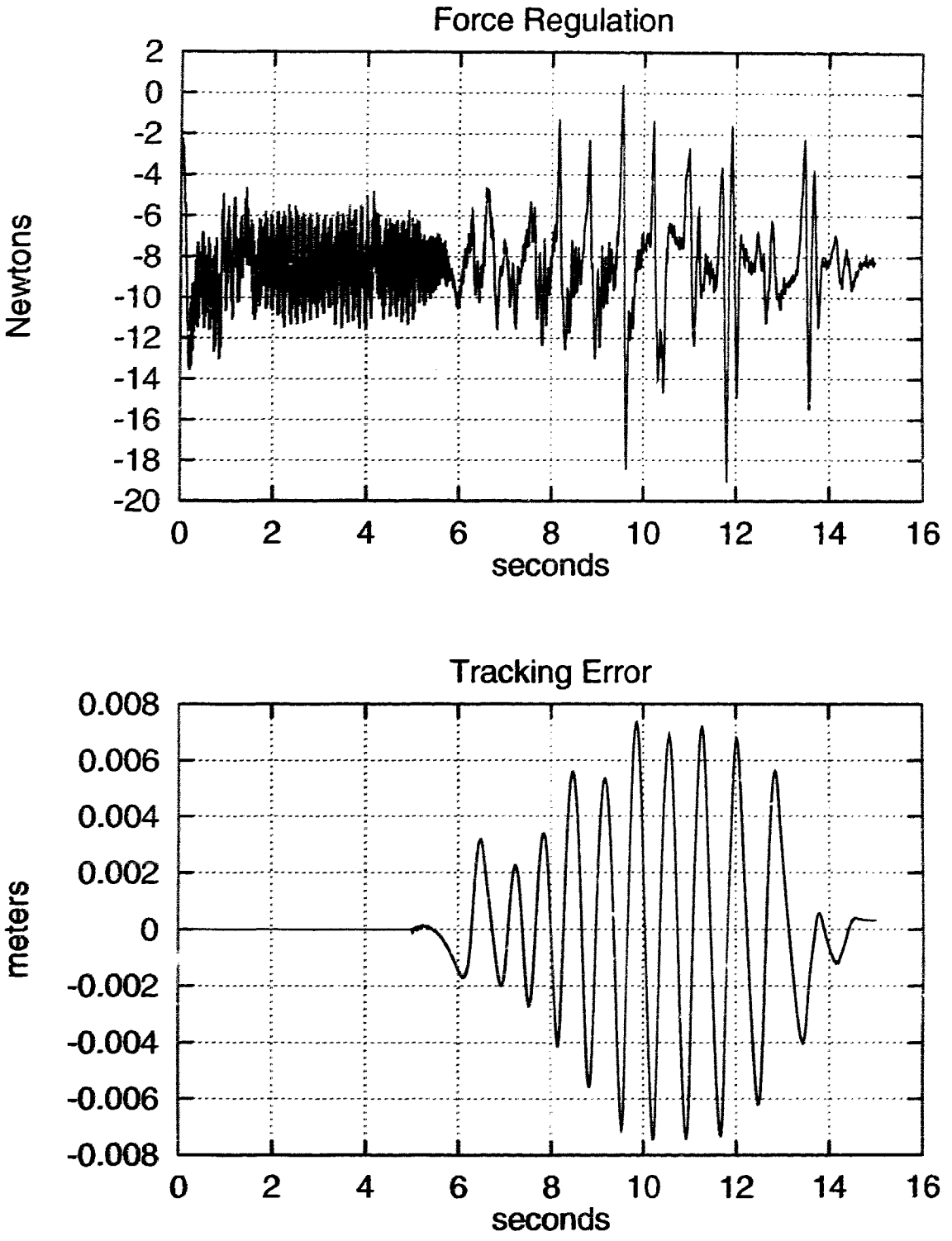

Figure 4.19: Experimental results: PID control. Kp = 150, Ki = 300, Kd = 4

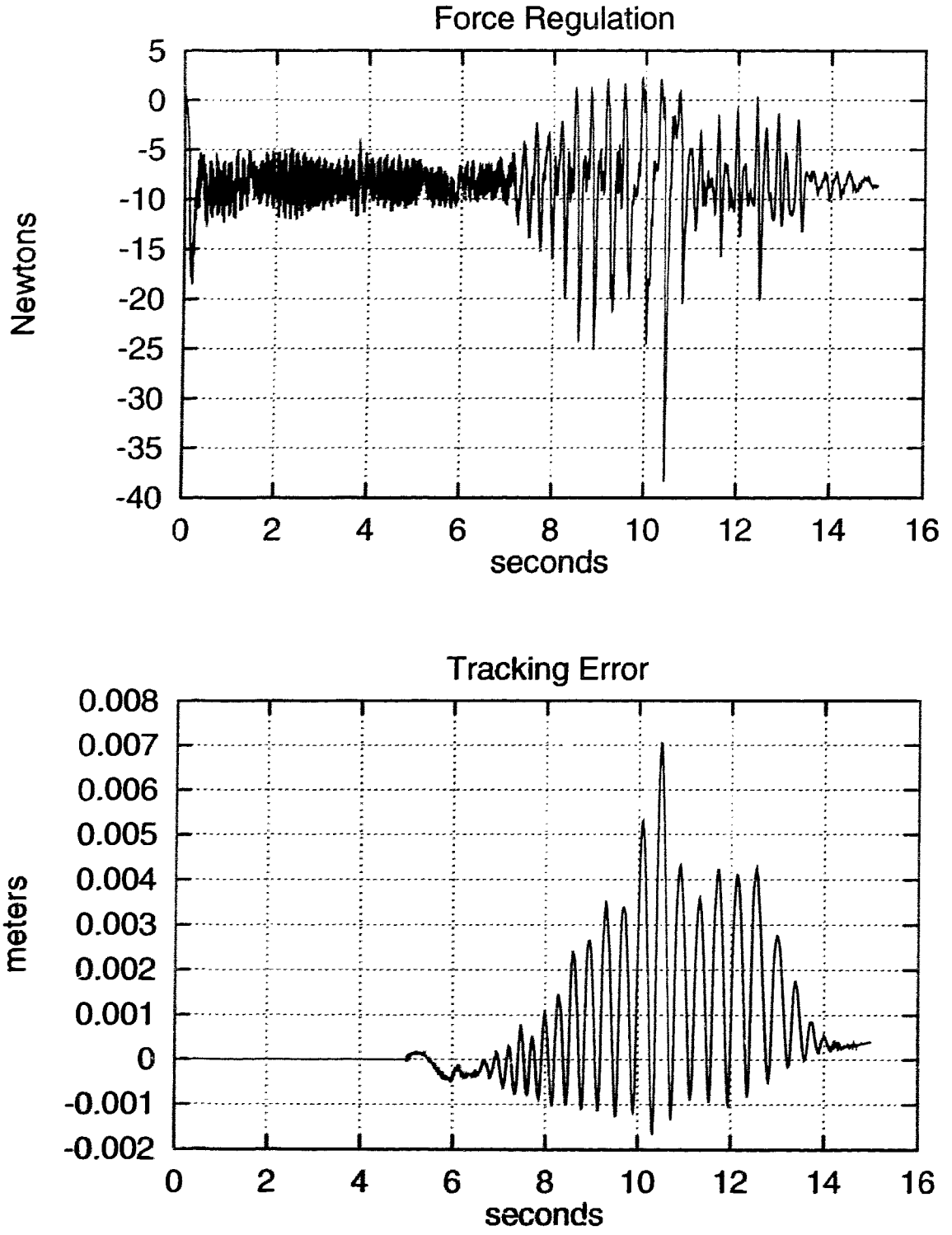

Figure 4.20: Experimental results: Smooth nonlinear control. $\alpha = 1000$

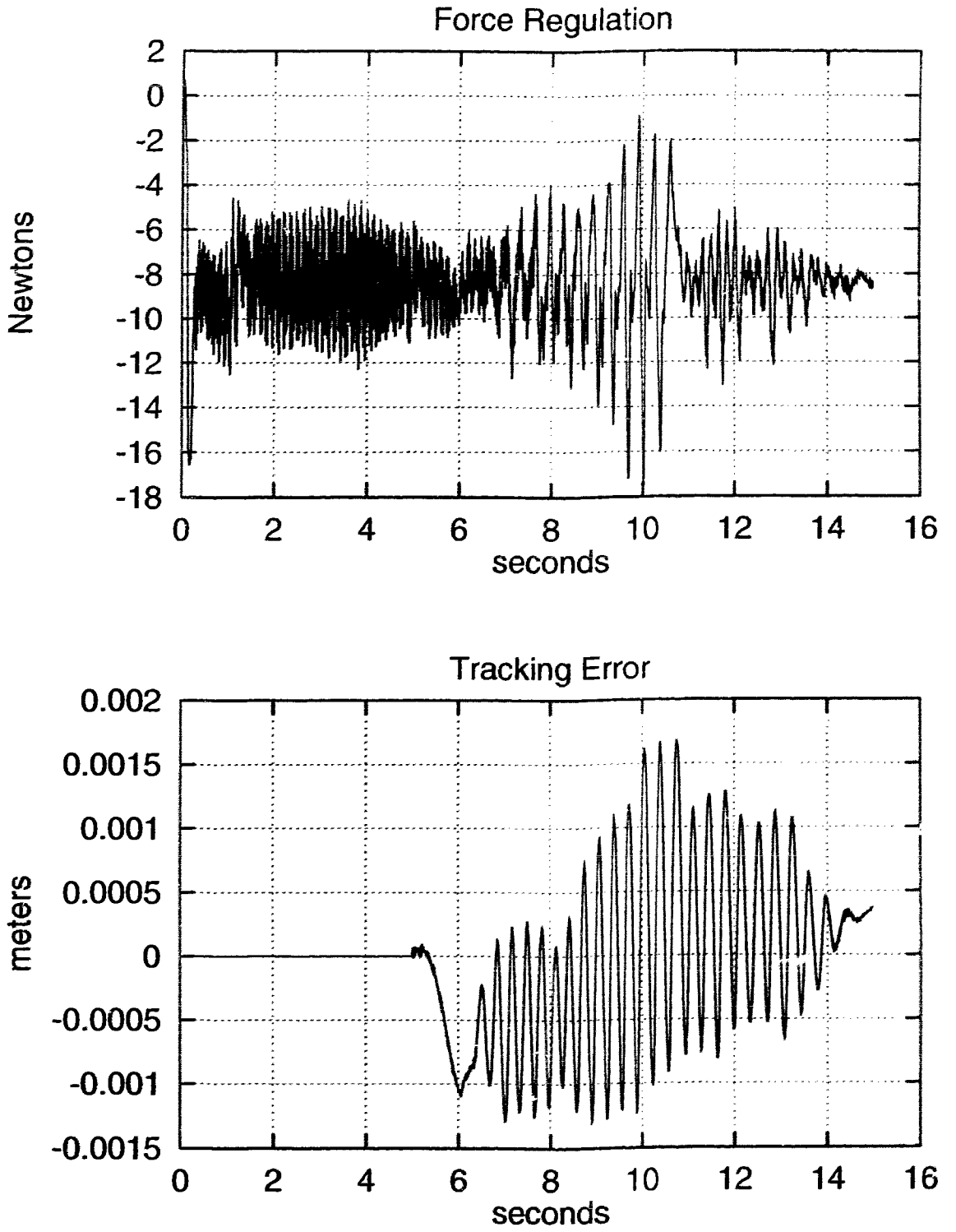

Figure 4.21: Experimental results: Smooth nonlinear control. $\alpha = 500$

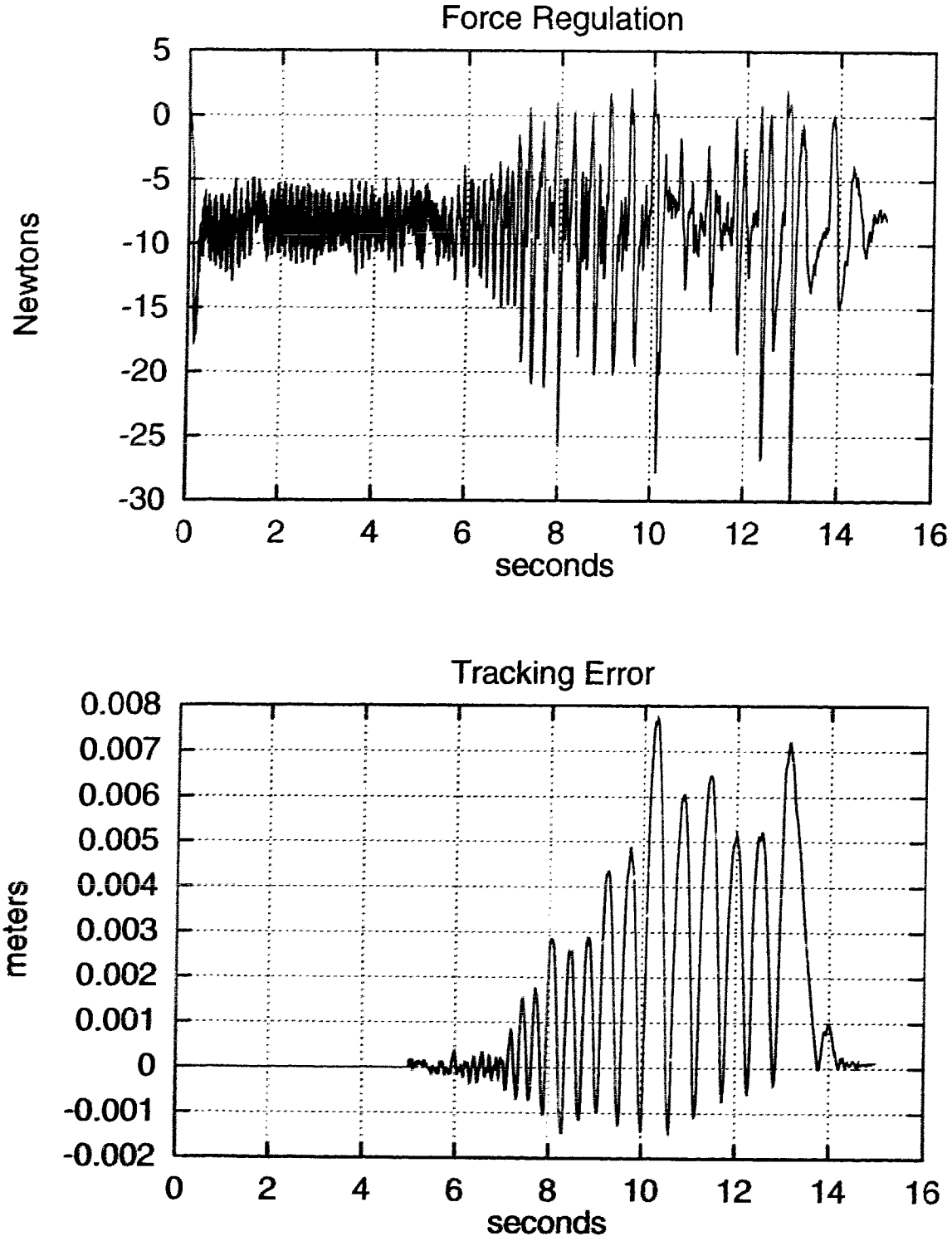

Figure 4.22: Experimental results: Discontinuous control. $\tau_{mstk} = 0.75$N, 0.1mm tolerance

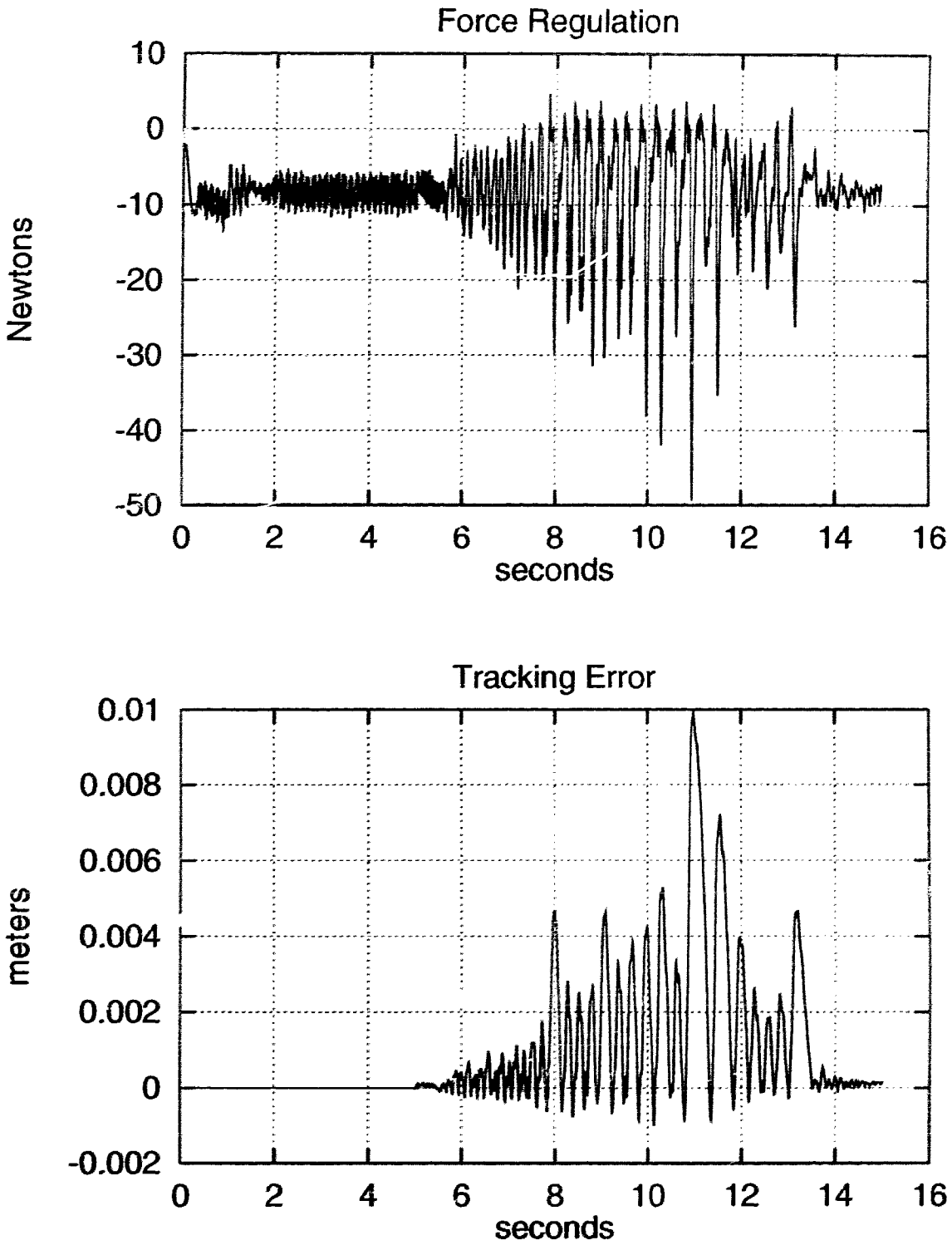

Figure 4.23: Experimental results: Discontinuous control. $\tau_{msik} = 1.5$N, 0.1mm tolerance

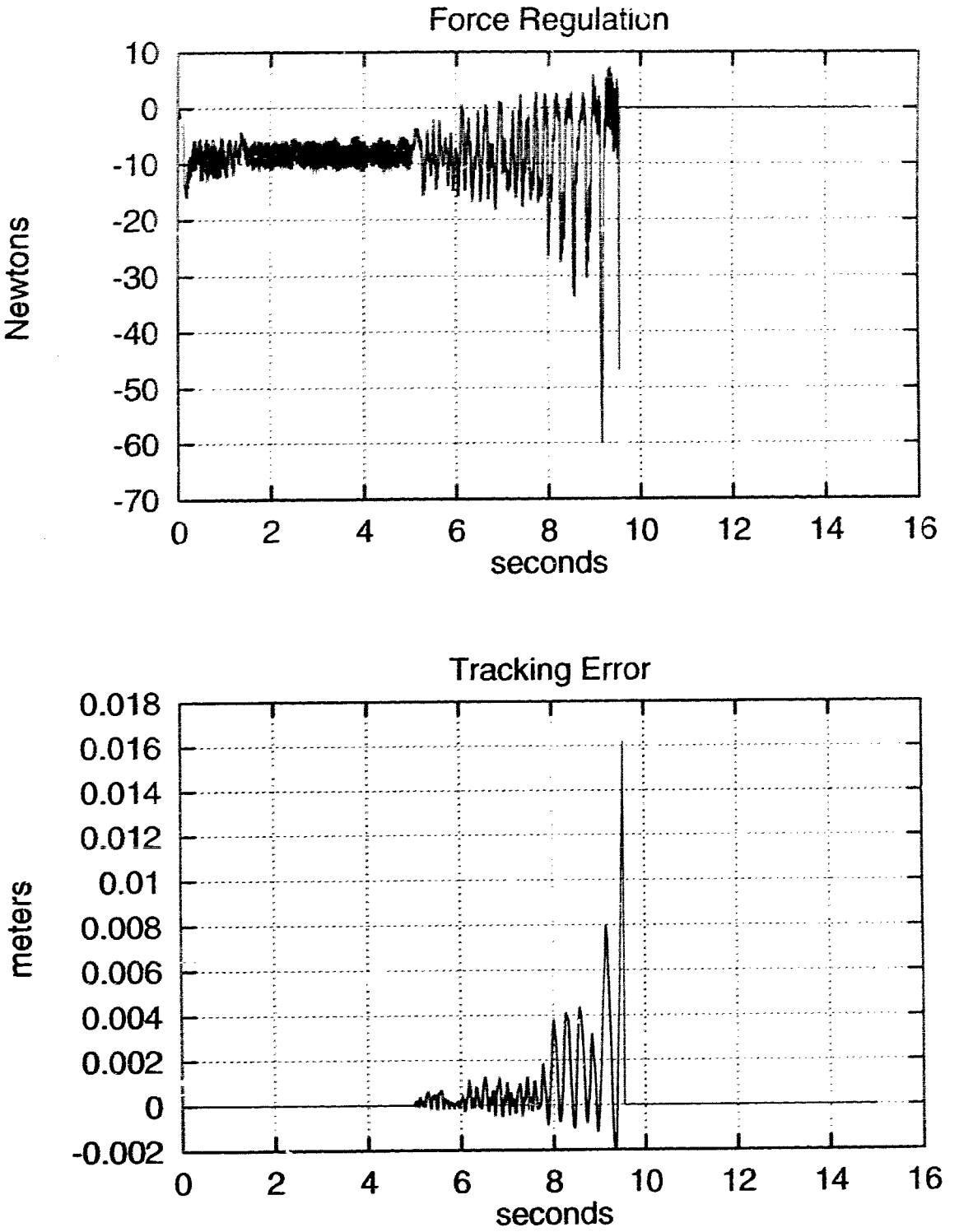

Figure 4.24: Experimental results: Discontinuous control. $\tau_{mstk} = 0.75$N, 0.01mm tolerance

Chapter 5

Conclusions and Future Work

Different control systems for the purpose of low velocity friction compensation were investigated. The control schemes were then examined when used inside of a hybrid control scheme. In the process, the manipulator was upgraded from a two degree of freedom planar type system to a four degree of freedom SCARA type assembly cell, in order to give the mechanism more functionality. The control methods investigated consisted of two linear (PD and PID) and two nonlinear controllers. One nonlinear controller was discontinuous and piecewise linear, while the other was smooth and satisfied a Lipschitz condition. The details of stability proofs for the nonlinear controllers were presented. Lyapunov's direct method was used for the Lipschitz control while a modified version of the direct method was used for the discontinuous controller.

The investigation of the control systems when undergoing free motion produced some interesting observations. The attempt at constrained motion was rather problematic. A thorough re-analysis of the constraint dynamics was not conducted, and the mechanical configuration did not lend itself kindly to performing constrained motion.

Simulations carried out in the earlier part of this work proved the existence of multiple stable equilibrium points as illustrated by Hahn [16]. The friction model used to model joint friction included viscous friction, as well as an artificial zero for numeric stability as proposed by Karnop [14]. PID control was simulated to reveal the existence of limit cycles which were shown to be stable or unstable depending on the size of the integral gain. All control systems were ported to the two DOF

manipulator to investigate their performance on a typical mechanism. The nonlinear controllers proved to provide better tracking results, albeit in a much more oscillatory fashion. PID control proved to be the superior linear control and was comparable to its nonlinear counterparts in terms of positioning errors. The amplitude of its limit cycles was smaller than the accuracy of the PD control. The smooth nonlinear controller proposed by Cai [9] was shown to be theoretically capable of providing a bound on the steady state error. This bound was not realized with the experiments due to the bandwidth of the mechanical system being too small.

The proof of stability for the discontinuous controller is rather inelegant. The vague notion of the dini-derivative is used to compensate for a system that does not satisfy a Lipschitz condition. An alternative proof may be constructed using work published only recently by Paden [29], [30]. Another alternative however would be to almagate both control systems into one, taking the best features of each. What this means is that one could devise a new control system, which would be identical to the discontinuous controller, except use a smooth hyperbolic tangent function about the origin as opposed to the signum function. This would retain the less oscillatory response of the discontinuous controller, while facilitating the stability proofs by providing a system free of discontinuities. The *tanh()* function also provides a designer with another parameter to tune when designing a control system; one can look at it as an extra degree of control in the system design. A description of this controller is presented in figure 5.1. The stability of this proposed control method should not be difficult to prove using the previous methods based on Lyapunov. A full investigation of this controller could be the basis for future work.

Each of the control systems were tested as tools for controlling a manipulator in constrained motion as part of a hybrid control system. The simulations and experiments provided several conclusions on their adaptability to such a scheme. Force control does not perform well in the presence of high proportional gain. The nature of the nonlinear control system puts a fairly high gain at a small position error. The discontinuous controller has no modification for this and so inherently performs poorly at force regulation. The α parameter with the smooth controller however may be modified, providing a more stable force control. PID control may be superior to the PD

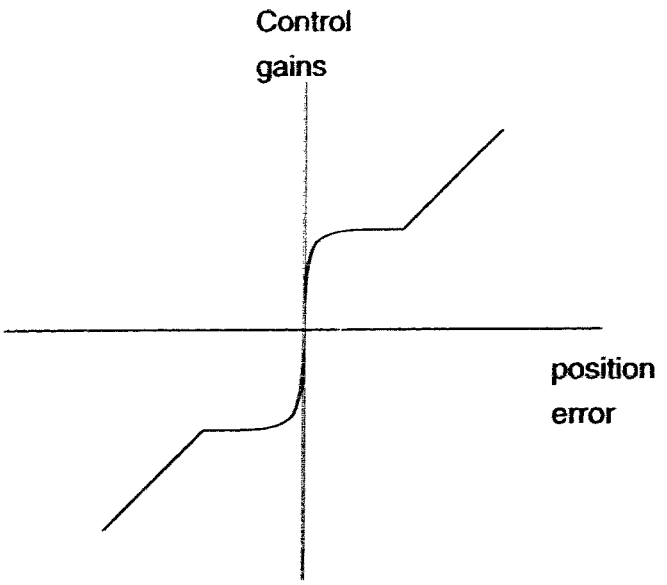

Figure 5.1: Alternative Control System

system for constrained motion. However, the existence of a limit cycle was observed while using PID control with a high integral gain to follow a trajectory with the end effector in contact with a surface. It was concluded that the parameters available for tuning on the smooth nonlinear controller provided more effective results than an integrator in this system.

To provide a completed picture for an overall system to provide force guided assembly in a manufacturing environment, these control systems provide solutions for the lowest level. To allow force guided assembly, some form of force interpretation and reasoning is required from a control standpoint. To this effect, a higher level controller is needed to act on top of these low level systems. This supervisory structure will make higher level decisions such as trajectory planning and generation, force interpretation, obstacle avoidance, and so forth. This seems fitting to be the topic of another research project. Emerging technologies such as neural systems, fuzzy systems, and petri nets seem fitting for this type of application. Another application which involves taking these low level systems further and making them more functional in a real world environment would be coordinated control. For many tasks, it is beneficial to have more than one manipulator handle an object, such as lifting a heavy object, or when a grasp

by one manipulator is infeasible. A brief study with several references is outlined in [31].

Appendix A

Details of nonlinear analyses such as Lyapunov

A.1 Smooth Nonlinear Controller

The system (2.15),

$$I\ddot{q} = -k_d\dot{q} - k_p q - \tau_c(q) + \tau_f$$

is globally asymptotically stable with the nonlinear term given by (2.13),

$$\tau_c(q) = \tau_{mstk}\tanh(\alpha q).$$

To show this, a Lyapunov function candidate is selected as follows:

$$V = \frac{1}{2}I\dot{q}^2 + \frac{1}{2}k_p q^2 + \frac{\tau_{stk}}{\alpha}\ln(\frac{e^{\alpha q} + e^{-\alpha q}}{2}) \tag{A.1}$$

which is positive definite and differentiable. In order to show stability, it is necessary to show that $\dot{V} < 0 \;\; \forall \dot{q} \neq 0$ [32]. Its derivative, by substituting the system dynamics (2.15) into (A.1) can be written as:

$$\begin{aligned}
\dot{V} &= I\dot{q}\ddot{q} + \frac{1}{2}\dot{I}\dot{q}^2 + k_p q\dot{q} + \tau_{stk}\tanh(\alpha q)\dot{q} && \text{(A.2)}\\
&= -k_d\dot{q}^2 + \dot{q}\tau_f && \text{(A.3)}\\
&= -k_d\dot{q}^2 - \dot{q}\cdot sgn(\dot{q})\tau_{slp} - (1 - \|sgn(\dot{q})\|)\tau_{stk} && \text{(A.4)}\\
&= -k_d\dot{q}^2 - \|\dot{q}\|\tau_{slp} \leq 0 && \text{(A.5)}
\end{aligned}$$

For a 1DOF system, there are no coriolis terms and the inertial component of the dynamics is time invariant ($\dot{I} = 0$). Equation (A.5) and inequality arises from the definition of τ_f and the fact that for any q, there exists the relationship $q \cdot sgn(q) \geq 0$. $\dot{V} = 0$ only when $\dot{q} = 0$. By La Salle's theorem, which extends Lyapunov's Direct Method to include the inequality, the system is globally asymptotically stable [20] [33]. The concept of the invariant set used with La Salle's theorem is used again to reveal the bounds on the error. It is known that the steady state solution of $\dot{V}$ will converge to a value within the largest invariant set, thus the invariant set will provide the bounds on the steady state error.

Let E be the invariant set, and substitute the conditions therein into the system dynamics. Using the inequality $\tau_{stk} \leq \tau_{mstk}$, we get:

$$\begin{aligned} E &= \{q \in R | \ \ddot{q} = \dot{q} = 0\} \\ &= \{q \in R | \ k_p \|q\| + \tau_{mstk} \tanh(\alpha \|q\|) \leq \tau_{stk}\} \end{aligned} \tag{A.6}$$

The two arguments on the left of the inequality in (A.6) are always greater than or equal to 0, then we have:

$$\tau_{mstk} \tanh(\alpha \|q\|) \leq \tau_{stk} \tag{A.7}$$

Solving (A.7) we can have the following bound on q inside the invariant set, indicating the bounds on the steady state error:

$$q \leq \frac{1}{2\alpha} \ln(1 + 2 \cdot \frac{\tau_{mstk}}{\alpha}) \tag{A.8}$$

A.2 Discontinuous Nonlinear Controller

It can be seen from eq. (2.20)

$$V = \frac{1}{2} I \dot{q}^2 + \frac{1}{2} k_p q^2 + g(q)$$

and figure (2.6) that this energy function is positive definite as well as decrescent for trajectories outside the region of discontinuity. A decrescent function $V(t, x)$ is one which is bounded for each x as t increases [32].

Using the 1DOF dynamic model of the distal link defined in eq.(2.6) and the controller of eq's. (2.18) and (2.19) and figure 2.5, the derivative of the energy function of eq.(2.20) along the solution trajectory can be written as:

$$\begin{aligned} \dot{V} &= I\dot{q}\ddot{q} + k_p q\dot{q} + \dot{g}(q)\dot{q} \\ I\ddot{q} &= \tau - \tau_f \\ \dot{V} &= \dot{q}(\tau - \tau_f) + k_p q\dot{q} + \dot{g}(q)\dot{q} \end{aligned} \tag{A.9}$$

From eqs.(2.1) - (2.2), (2.18), and the fact that outside the discontinuity τ_{stk} is zero, this can be written as:

$$\dot{V} = -k_d\dot{q}^2 - \dot{q}\,\tau_{slp}(\dot{q}) + \dot{q}(\dot{g}(q) - k_p q_c) \tag{A.10}$$

From eq.(2.19) and eq.(2.21) we see that $k_p q_c = \dot{g}(q)$ except when $q = 0$, where $\dot{g}(q)$ is undefined. eq.(A.10) becomes:

$$\dot{V} = -k_d\dot{q}^2 - \dot{q}\tau_{slp}(\dot{q}) \leq 0 \tag{A.11}$$

For the trajectories within the region of discontinuity, the notion of the 'Dini-Derivative' [21] is used. These are the limiting values of $\dot{V}$ on both sides of the discontinuous region, and denoted $D * \dot{V}(\cdot)$, and can have any of four values. The values are labeled as the upper right $D^+f(.)$, lower right $D_+f(.)$, upper left $D^-f(.)$, and lower left $D_-f(.)$ derivatives. They are defined as follows ([22] pp. 188-189),

$$\begin{aligned} D^+f(q) &= \lim_{q\to q_0^+} \sup \frac{f(q) - f(q_0)}{q - q_0} \\ D_+f(q) &= \lim_{q\to q_0^+} \inf \frac{f(q) - f(q_0)}{q - q_0} \\ D^-f(q) &= \lim_{q\to q_0^-} \sup \frac{f(q) - f(q_0)}{q - q_0} \\ D_-f(q) &= \lim_{q\to q_0^-} \inf \frac{f(q) - f(q_0)}{q - q_0} \end{aligned}$$

For any point on the trajectory where $\dot{V}$ exists, the four possible dini-derivatives have a common value equal to that of the regular derivative [21] [22]. Since V is

continuous and $\dot{V}$ is negative semi definite (n.s.d.) outside of the discontinuous region, the dini-derivatives are also n.s.d. for points within the region. The dini-derivatives are therefore n.s.d. over the entire trajectory, and from eq.(A.11), $\dot{V} = 0$ implies $\dot{q}$=0 which is the q axis. No complete trajectories can be contained there, so $D * \dot{V}(\cdot)$ is negative definite over the entire trajectory, implying global asymptotic stability.

Appendix B

Introduction to Constraint Dynamics for Robots.

The method proposed by many authors involve variational methods for dynamics. The treatment presented here will not be exhaustive, but will serve to introduce some of the underlying principles associated with the dynamics of a constrained robot. Readers who wish a more complete treatment of constrained dynamics, are referred to several papers by McClamroch [25], [23], [34], and others [26], [35], [36] in addition to any good text on dynamics [37], [38].

A manipulator that has its end effector in contact with a rigid surface is constrained to move in certain directions. For example, in fig. (4.3), the manipulator is constrained to move along the Y axis. These constraints may be formulated as constraint equations $\mathbf{\Phi}$. Constraint equations which may be written in the form of

$$\mathbf{\Phi}(\mathbf{x}, \mathbf{t}) = \mathbf{0}$$

are referred to as *holonomic constraints.* Constraints imposed on manipulators which restrict their motion within their workspace are holonomic. e.g. in fig. (4.3), there exists a constraint in cartesian coordinates of the form $y = 4$, or alternatively $y-4 = 0$, assuming that the barrier was at that position on the Y axis.

If we consider the surface to be frictionless, the work done by the surface on the end effector of the manipulator is zero. If we consider the force on the end effector

as comprising of the applied force $\mathbf{F^A}$ and the constraint force $\mathbf{F^C}$, then a virtual displacement $\delta\ \boldsymbol{x}$ causes virtual work to be done δW^A and δW^C. This virtual displacement must be *kinematically admissible*, which implies tangent to the constraint surface. Thus

$$\frac{\partial}{\partial \mathbf{x}}\mathbf{\Phi}(\mathbf{x},\mathbf{t})\delta\mathbf{x} = \mathbf{0} \tag{B.1}$$

Since it has been assumed that the contact surface is frictionless, the work done by the constraint force is zero (a *workless constraint*). Thus

$$\delta\mathbf{x}^{\mathbf{T}}\mathbf{F^C} = \mathbf{0} \tag{B.2}$$

The discussion will commence with the *Lagrange Multiplier Theorem* which will define a Lagrange multiplier. The proof of this theorem can be found in [37] pp. 121-123.

Let $\mathbf{b}$ be a vector in R^n and $\mathbf{A}$ be an $m \times n$ matrix. If there exists a nonzero vector $\{\mathbf{s} \in R^n\}$ such that $\mathbf{s^T b} = 0$, and $\mathbf{As} = 0$, then there also exists a vector $\{\boldsymbol{\lambda} \in R^m\}$ called a *Lagrange multiplier*, such that

$$\mathbf{s^T b} + \mathbf{s^T A^T}\lambda = \mathbf{0} \tag{B.3}$$

This implies that

$$\mathbf{b} + \mathbf{A^T}\lambda = \mathbf{0} \tag{B.4}$$

And if $\mathbf{A}$ is nonsingular, then $\boldsymbol{\lambda}$ is unique.

Applying this to the principle of virtual work, the sum of equations (B.1) and (B.2) can be interpreted in the same form as eq.(B.3). Identifying $\mathbf{s}$ with $\delta\mathbf{x}$, $\mathbf{b}$ with $\mathbf{F^c}$, and $\mathbf{A}$ with $\frac{\partial}{\partial \mathbf{x}}\mathbf{\Phi}(\mathbf{x},\mathbf{t})$, the workless constraint can be written as

$$\delta\mathbf{x^T F^c} + \delta\mathbf{x^T}\frac{\partial}{\partial \mathbf{x}}\mathbf{\Phi}(\mathbf{x},\mathbf{t})^{\mathbf{T}}\lambda = \mathbf{0} \tag{B.5}$$

and thus

$$\mathbf{F^c} = -\frac{\partial}{\partial \mathbf{x}}\mathbf{\Phi}(\mathbf{x},\mathbf{t})^{\mathbf{T}}\lambda \tag{B.6}$$

This development of the formulation for the constrained forces at the end effector allows us to proceed in defining the dynamic model. Taking the model in eq.(2.4)

defining a planar manipulator. all that needs to be done is to transform the equation into an equivalent in the task space and add the component that corresponds to the constraint forces at the end effector. In the joint space, the dynamic equation is

$$\mathbf{I}(\mathbf{q})\ddot{\mathbf{q}} + \mathbf{C}(\mathbf{q}, \dot{\mathbf{q}}) + \tau_f = \tau$$

where τ_f defines the joint torques felt by the constraint forces on the end effector as defined in eq(B.6).

Using the manipulator Jacobian $\mathbf{J}$ and commencing with expressions for the instantaneous velocity and accelerations, $\dot{\mathbf{x}} = \mathbf{J}\dot{\mathbf{q}}$ and $\ddot{\mathbf{x}} = \dot{\mathbf{J}}\dot{\mathbf{q}} + \mathbf{J}\ddot{\mathbf{q}}$, the dynamic equation for the 2 DOF manipulator can be formulated as

$$\tilde{\tau} = \tilde{\mathbf{I}}(x)\ddot{\mathbf{x}} + \tilde{\mathbf{C}}(\mathbf{x}, \dot{\mathbf{x}})\dot{\mathbf{x}} + \mathbf{\Phi}^{\mathbf{T}}(\mathbf{x})\lambda \tag{B.7}$$

where

$$\tilde{\tau} = \mathbf{J}^{-\mathbf{T}}\tau$$

$$\tilde{\mathbf{I}} = \mathbf{J}^{-\mathbf{T}}\mathbf{I}\mathbf{J}^{-1}$$

$$\tilde{\mathbf{C}} = \mathbf{J}^{-\mathbf{T}}[\mathbf{C} - \mathbf{I}\mathbf{J}^{-1}\dot{\mathbf{J}}]\mathbf{J}^{-1}$$

A controller designed for this system is required to track some position vector $\mathbf{x}$ and a force vector by specifying a set of desired multipliers $\boldsymbol{\lambda}$. Once again, it should be emphasized that the above developments assume that there is no friction between the contacting surfaces. A reformulation of the above scheme that incorporates friction has only recently been proposed in the literature (Yao and Tomizuka [36]).

Bibliography

[1] J. D. Adams and S. Payandeh, "Experimental evaluation of low velocity friction compensation techniques in robotics," *Proc. of the IEEE Conf. on Systems, Man, and Cybernetics*, vol. 2, pp. 1705–1710, 1995.

[2] J. D. Adams and S. Payandeh, "On methods for low velocity friction compensation: Theory and experimental study," *Journal of Robotic Systems*, vol. 13, pp. 391–404, June 1996.

[3] J. Martins, J. Oden, and F. Simoes, "A study of static and kinetic friction," *International Journal of Engineering Science*, vol. 28, no. 1, pp. 29–92, 1990.

[4] S. W. Shaw, "On the dynamic response of a system with dry friction," *Journal of Sound and Vibration*, vol. 108, no. 2, pp. 305–325, 1986.

[5] B. Armstrong, "Friction: Experimental determination, modelling and compensation," *Proc. of the 1988 Int'l. Conf. on Robotics and Automation*, pp. 1422–1427, 1988.

[6] C. Johnson and R. Lorenz, "Experimental identification of friction and its compensation in precise, position controlled mechanisms," *IEEE Transactions on Industry Applications*, vol. 28, no. 6, pp. 1392–1398, 1992.

[7] J. H. Chin and C. C. Chen, "A study of stick slip motion and its influence on the cutting process," *International Journal of Mechanical Science*, vol. 35, no. 5, pp. 353–370, 1993.

[8] W. S. Newman, G. D. Glosser, J. H. Miller, and D. Rohn, "The effects of friction on space microgravity robots," *Proceedings of the IEEE Int. Conf. on Robotics and Automation*, vol. 2, pp. 1436–1441, 1992.

[9] L. Cai and G. Song, "A smooth robust nonlinear controller for robot manipulators with joint stick-slip friction," *Proc. of the IEEE Conf. on robotics and Automation*, pp. 449–454, 1993.

[10] C. Radcliffe, S. Southward, and C. MacCluer, "Robust nonlinear stick-slip friction compensation," *Journal of Dynamic Systems, Measurement, and Control*, vol. 113, pp. 639–644, December 1991.

[11] M. Ciliz and M. Tomizuka, "Modelling and compensation of frictional uncertainties in motion control: A neural network based approach," *Proceedings of the American Control Conference*, vol. 2, pp. 3269–3273, June 1995.

[12] E. Tung, G. Anwar, and M. Tomizuka, "Low velocity friction compensation and feedforward solution based on repetetive control," *Journal of Dynamic Systems, Measurement, and Control*, vol. 115, pp. 279–284, June 1993.

[13] B. Armstrong-Helouvry, P. Dupont, and C. Canudas de Wit, "A survey of models, analysis tools and compensation methods for the control of machines with friction," *Automatica*, vol. 30, pp. 1083–1138, June 1994.

[14] D. Karnopp, "Computer simulation of stick slip friction in mechanical dynamical systems.," *Journal of Dynamic Systems, Measurement and Control*, pp. 100–103, March 1985.

[15] M. W. Spong and M. Vidyasagar, *Robot Dynamics and Control*. John Wiley and Sons, N.Y., 1989.

[16] W. Hahn, *Stability of Motion*. Springer-Verlag, 1967.

[17] C. Canudas de Wit, P. Noel, A. Aubin, and B. Brogliado, "Adaptive friction compensation in robot manipulators: Low velocities," *Int'l Journal of Robotics Research*, vol. 10, no. 3, pp. 189–199, 1991.

[18] C. Radcliffe and S. Southward, "A property of stick-slip friction models which promotes limit cycle generation," *IEEE American Control Conference*, vol. 2, pp. 1198–1203, 1990.

[19] J. Holtzman, *Nonlinear System Theory: A functional Anlysis Approach*. Prentice-Hall, Inc., 1970.

[20] J. J. Craig, *Adaptive Control of Mechanical Manipulators*. Addison-Wesley, 1988.

[21] N. Rouche, P. Habets, and N. Laloy, *Stability Theory by Lyapunov's Direct Method*. Springer-Verlag, New York, 1977.

[22] E. MacShane, *Integration*. Princeton University Press, 1944.

[23] N. Harris Mcclamroch and D. Wang, "Feedback stabilization and tracking of constrained robots," *IEEE Transactions on Automatic Control*, vol. 33, pp. 419-426, May 1988.

[24] S. D. Eppinger and W. P. Seering, "Introduction to dynamic models for robot force control," *IEEE Control Systems Magazine*, vol. 7, pp. 48-52, April 1987.

[25] N. Harris Mcclamroch, "Singular systems of differential equations for constrained robot systems," *Proc. of the IEEE Int'l Conf. on Robotics and Automation*, pp. 21–28, April 1986.

[26] R. K. Kankaanranta and H. N. Koivo, "Stability analysis of position - force control using linearized cartesian space model," *IFAC Symposium on Robot Control*, pp. 249–254, 1988.

[27] J. J. Craig, *Introduction to Robotics: Mechanics and Control*. Wiley, 1986.

[28] T. Baumeister, E. Avallone, and T. Baumeister III, *Mark's Standard Handbook for Mechanical Engineers*. New York: McGraw Hill Inc., 8 ed., 1978.

[29] D. Shevitz and B. Paden, "Lyapunov stability theory of nonsmooth systems," *IEEE Transactions on Automatic Control*, vol. 39, pp. 1910-1914, September 1994.

[30] B. Paden and S. Sastry, "A calculus for compting filipov's differential inclusion with application to the variable structure control of robot manipulators," *IEEE Transactions on Circuits and Systems*, vol. 34, pp. 73–82, January 1987.

[31] J. Adams, "Study of coordinated control of mechanical fingers," tech. rep., Experimental Robotics Lab, School of Engineering Science, Simon Fraser University, Burnaby, British Columbia, Canada, April 1995.

[32] M. Vidyasagar, *Nonlinear Sysytems Analysis.* Englewod Cliffs, New Jersey: Prentice-Hall, Inc., 1978.

[33] J. La Salle and S. Lefschetz, *Stability by Liapunov's Direct Method.* London: Academic Press Inc., 1961.

[34] D. Wang and N. Harris McClamroch, "Position/force control design for constrained mechanical systems: Lyapunov's direct method," *Proceedings of the 28 IEEE Conference on Decision and Control*, pp. 1665–1669, December 1989.

[35] M. M. Bridges, J. Cai, D. M. Dawson, and M. T. Grabbe, "Experimental results for a robust position and force controller implemented on a direct drive robot," *Robotica*, vol. 13, pp. 11–18, 1995.

[36] B. Yao and M. Tomizuka, "Adaptive control of robot manipulation in constrained motion - controller design," *Journal of Dynamic Systems, Measurement, and Control*, vol. 117, pp. 320–328, September 1995.

[37] E. J. Haug, *Intermediate Dynamics.* Englewood Cliffs, New Jersey: Prentice Hall, 1992.

[38] D. T. Greenwood, *Principles of Dynamics.* Englewood Cliffs, New Jersey: Prentice Hall , Inc., 2 ed., 1988.

[39] PITTMAN, Harleysville, PA, *Bulletin: ELCOM, Pittman Brushless DC Servo Motors*, March 1989. series 5100 - 50mm square cross section.

[40] PITTMAN, Harleysville, PA, *Bulletin: Lo-Cog DC Servo Motors and Gearmotors*, March 1992. series 8000 motors.

[41] Spectrum Signal Processing Inc., Burnaby, B.C. Canada, V5A 4V7, *TMS320C30 Processor Board User's Manual / Technical Reference Manual*, 1991.

[42] Integrated Motions Incorporated, *DS-2 Controller / Data Acqisition Module*, 758 Gilman St., Berkely, California 94710 1992.